Charles University in Prague
Faculty of Mathematics and Physics

DIPLOMA THESIS

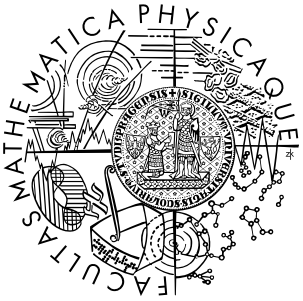

Barbora Benešová

Models of Specific Shape-Memory Materials

Supervisor: prof. Ing. Tomáš Roubíček, DrSc,
Mathematical Institute of Charles University

Branch of study: Physics, Mathematical and Computer Modelling
in Physics and Technology

2008

It is a pleasant duty to thank prof. Roubíček for supervising my thesis and always trying to help out with problems and questions that arose while writing it. Also a warm thank you goes to my consultant Dr. Kružík for giving me advice throughout the work on my thesis as well as for careful reading of its final version. Moreover I am thankful to my consultant Ing. Landa and also to Ing. Seiner for discussion regarding physical questions.

I acknowledge the support of the Jindřich Nečas Center for Mathematical Modeling, project LC06052 financed by MŠMT.

Last but not least I thank my parents for their support throughout the years of my study and my partner for his unwavering love and support.

I hereby declare, that I have written this diploma thesis independently using no other than cited references. I give my consent to this work being available on loan.

Prague August 8, 2008 Barbora Benešová

Contents

Název práce: Modelování speciálních materiálů s tvarovou pamětí
Autor: Bc. Barbora Benešová
Katedra (ústav): Ústav teoretické fyziky
Vedoucí diplomové práce: prof. Ing. Tomáš Roubíček, DrSc, Matematický ústav Univerzity Karlovy
e-mail vedoucího: roubicek@karlin.mff.cuni.cz
Abstrakt: Tato diplomová práce je zaměřena na studium tzv. látek s tvarovou pamětí. Tomuto problému se věnuje komplexně od představení fyzikálních podstaty jevů jež činí tyto látky speciálními a představí možnosti modelování chování těchto látek při zatěžovaní. Speciálně se věnuje studiu evoluce v kvazistatisckém přiblížení, v rámci kterého představí efektivní model pro popis látky s pamětí tvaru. Tento model je dále zkoumán po stránce matematické analýzy a je představena teorie zaručující existenci tzv. energetického řešení kvazistatické evoluce. Oproti předchozím pracím rozšiřuje matematickou teorii o případ časově proměnných Dirichletových okrajových podmínek. V neposlední řadě jsou též prezentovány výsledky simulací vycházející s představeného modelu a aplikovné pro případ látky tvarovou pamětí $NiTi$ vyskytujíci se v austenitu a též v R-fázi. Poprvé pro případ látek s tvarovou pamětí je implementována tzv. dvojstranná energetická nerovnost, která představuje možný přístup ke globální optimalizaci v rámci rychlostně nezávislých procesů.
Klíčová slova: Látky s pamětí tvaru, $NiTi$, R-fáze, mechanika kontinua, rychlostně nezávislé procesy, energetické řešení.

Title: Models of specific shape-memory materials
Author: Bc. Barbora Benešová
Department: Department of theoretical physics
Supervisor: prof. Ing. Tomáš Roubíček, DrSc, Mathematical Institute of the Charles University
Supervisor's e-mail address: roubicek@karlin.mff.cuni.cz
Abstract: This diploma thesis is concerned with the study of so called shape memory materials. It handles the subject in great complexity, starting from the physical background of effects that distinguish these materials from others. In addition it introduces the reader into possibilities of modelling such materials in the framework of continuum mechanics. Especially in the approximation of quasi-static processes an effective model describing the evolution of a shape memory specimen is presented. This model is further studied from the viewpoint of mathematical analysis and a mathematical theory assuring the existence of a so called energetic solution of quasi-static evolution is shown. In addition to previous works this thesis handles also the case of time-dependent Dirichlet boundary conditions. Not unimportant are results of simulations relying on the models presented predicting the behaviour of a specimen of the shape memory alloy $NiTi$ in austenite or R-phase under loading. For the first time in the framework of modelling shape memory alloys the double-sided energy inequality, which represents a possible approach to global optimization for rate-independent processes, has been implemented.
Keywords: Shape memory alloys, $NiTi$, R-phase, continuum mechanics, rate-independent processes, energetic solution.

Nomenclature

$C(\Omega)$	the space of continuous functions on Ω equipped with the norm $\|u\| = \max_{x\in\bar{\Omega}} \|u(x)\|$
$C^k(\Omega)$	the space of functions that have continuous derivatives up to the order k on Ω
$C(\bar{\Omega}, V)$	the space of continuous functions on Ω with values in some Banach space V equipped with the norm $\|u\| = \max_{x\in\bar{\Omega}} \|u(x)\|_V$
$C([0,T], V)$	the space of continuous functions on $[0,T]$ with values in some Banach space V equipped with the the norm $\|u\| = \max_{t\in[0,T]} \|u(t)\|_V$
$\mathbb{I}$	the identity matrix
$L^p(\bar{\Omega}, \mathbb{R}^n)$	the space of p-integrable (vectorial for $n>1$) functions on Ω equipped with the norm $\|u\| = \left(\int_\Omega \|u(x)\|^p \mathrm{d}x\right)^{1/p}$
$L^p(\Omega, \mathbb{R}^{n\times m})$	the space of p-integrable matrix functions on Ω
$L^p(\Omega, V)$	the space of p-integrable functions on Ω with values in some Banach space V equipped with the norm $\|u\| = \left(\int_\Omega \|u(x)\|_V^p \mathrm{d}x\right)^{1/p}$
$L^p([0,T], V)$	the space of p-integrable matrix functions on $[0,T]$ with values in some Banach space V equipped with the norm $\|u\| = \left(\int_0^T \|u(t)\|_V^p \mathrm{d}x\right)^{1/p}$
M	the number of martensitic variants
$\mathcal{M}(\mathbb{R}^{n\times m})$	the space of Radon measures on $\mathbb{R}^{n\times m}$
p'	the conjugate exponent to some $p \in [1,\infty]$, namely $p' = \frac{p}{p-1}$
p^*	the exponent in the embedding $W^{1,p}(\Omega) \hookrightarrow L^{p^*}(\Omega)$, namely $p^* = \frac{np}{n-p}$ if $\Omega \subset \mathbb{R}^n$ and $p < n$, p^* is anything in $[1,\infty)$ if $p = n$ and $p^* = \infty$ if $p > n$
$p^\sharp$	the exponent in the trace operator $u \to u_{\|\Gamma} : W^{1,p}(\Omega) \to L^{p^\sharp}(\Gamma)$, namely $p^\sharp = \frac{np-p}{n-p}$ if $\Omega \subset \mathbb{R}^n$ and $p < n$, $p^\sharp$ is anything in $[1,\infty)$ if $p = n$ and $p^\sharp = \infty$ if $p > n$
$W^{1,p}(\Omega, \mathbb{R}^n)$	the Sobolev space of p-integrable (vectorial for $n>1$) functions on Ω whose distributional derivatives are also p-integrable equipped with the norm $\|u\| = \left(\int_\Omega \|u(x)\|^p + \|\nabla u(x)\|^p \mathrm{d}x\right)^{1/p}$
$W^{1,p}(\Omega, \mathbb{R}^{n\times m})$	the Sobolev space of p-integrable matrix functions on Ω whose distributional derivatives are also p-integrable

$W^{1,p}(\Omega, V)$	the Sobolev space of p-integrable functions on Ω whose distributional derivatives are also p-integrable with values in a Banach space V equipped with the norm $\|u\| = \left(\int_\Omega \|u(x)\|_V^p + \|\nabla u(x)\|_V^p \mathrm{d}x\right)^{1/p}$
$W^{1,p}([0,T], V)$	the Sobolev space of p-integrable functions on $[0,T]$ whose distributional derivatives are also p-integrable with values in a Banach space V equipped with the norm $\|u\| = \left(\int_0^T \|u(t)\|_V^p + \|\nabla u(t)\|_V^p \mathrm{d}t\right)^{1/p}$
$W^{\alpha,p}(\Omega, \mathbb{R}^n)$	the Sobolev space of p-integrable (vectorial for $n>1$) functions on Ω having fractional derivatives
Γ	the boundary of the domain Ω
Γ_D	the part of the boundary of the domain Ω where Dirichlet boundary conditions are prescribed
Γ_N	the part of the boundary of the domain Ω where Neumann boundary conditions are prescribed
Ω	a bounded, connected Lipschitz domain
$\bar{\Omega}$	the closure of Ω
$\subset$	subset
$\hookrightarrow$	the continuous embedding
$\hookrightarrow\hookrightarrow$	the compact embedding
$\to$	strong convergence or mapping of elements into other ones
$\rightharpoonup$	weak convergence
$\overset{*}{\rightharpoonup}$	weak* convergence
$\otimes$	the tensorial product of two vectors
$\|\cdot\|$	the norm on a Banach space
$(\cdot,\cdot)$	the open interval
$[\cdot,\cdot]$	the closed interval

Preface

Shape memory alloys are so called smart materials exhibiting effect that distinguish them from other materials. Namely, the two most important ones are the *shape memory effect* which gave these materials their name and *pseudoelasticity*. Roughly speaking, the shape memory effects describes the ability of these materials to recover the shape they had prior to a mechanical deformation by heat supply. Pseudoelasticity on the hand refers to the ability to recover strains in the order of percent; or may also refer to the phenomenon of exhibit constant stress in a large area of strains.

It is these effects thanks to whom shape memory alloys have gained a lot of interest in engineering and development. New possibilities of applications such as dampers, actuators or applications in medicine just to mention some branches, were discovered in the past years. In addition to areas where these materials are used heavily, like peripheral vascular stents or dental braces, new application fields are under investigation.

But not only are shape memory alloys interesting for engineers, they are also attractive from the viewpoint of basic research and modelling as the applicability of the developed models is quite wide. Also in this work we are concerned with modelling of shape memory alloys within the framework of continuum mechanics following works [34], [35] or [60]. The model presented in the mentioned papers will be subject of this theses in the sense that it is analysed from the point of view of physics mathematics and numerics and extended as described in the next few paragraphs.

First of all the physical consistency of the model is investigated and it is shown in Chapter 1 that it may be derived from basic balances and the second law of thermodynamics if, of course, suitable constitutive relations are used. Also the causes of the special effects of shape-memory alloys are outlined.

The main cause is the existence of microstructure like the one shown e.g. in Figure 5.3. Although the existence of microstructure does not cause any physical difficulties from the point of view of mathematics it demands for an effective mathematical description. Such a description is given in Chapter 2 by means of so called *Young measures*. Moreover the existence of microstructure is mathematically connected to a broad area of non-convex minimization, some strategies will also be presented in Chapter 2.

From the point of view of mathematical research it is of course important to study the solvability of the system of equations that form a model of the behaviour of shape memory alloys. The concept of rate-independent processes introduced by Mielke ([43] or [44] to mention some source) is exploited and the existence of

solutions to the problem considering quasi-static evolution is shown in Chapter 3. Contrary to previous works where Dirichlet loads were omitted for simplicity here also time-dependent loads are taken into account. This of course demanded for a small albeit important change of strategy in defining and hence also proving existence of solutions. More is shown in great detail in Chapter 3.

Of course, if applicability of the model is at least a future goal the continuous model needs to be discretized and more preferably also implemented to allow for simulations that could be compared to experimental data to verify the strength of the model. Here we followed algorithms presented already in [33] or [35] but consider hard loading by a time-dependent Dirichlet boundary condition contrary to soft loading by applied forces. Also, a necessary condition for global optimization, the two-sided energy inequality (3.34), has been implemented - for the first time in the framework of shape memory alloys. Simulations suggest that it offers a helpful tool in global optimization as far as rate-independent processes are concerned. More can be read in Chapter 4 or Chapter 6.

In this work the alloy we shall perform simulations with was chosen to be $NiTi$ as it is being used far mostly in practice for instance the medical devices mentioned above are produced out of $NiTi$. Yet not enough is known to give a satisfactory description of representative parameters of $NiTi$. Simulated results obtained should be compared with experiments as soon as a bulk specimen of mono-crystalline $NiTi$ shall be produced. In more detail the simulations presented here consider the R-phase, the existence of which is a kind of speciality of $NiTi$. Namely, most shape memory alloys exhibit two phase the martensitic and austenitic (more information shall be given Chapter 1) but $NiTi$ can be found in martensite, austenite or R-phase. Though $NiTi$ is used in industry not much attention is paid to this third phase by engineers. The reason might be the small range of temperatures in which R-phase exists, but it also might be due to lack of knowledge if R-phase is considered. Still, the R-phase is interesting in the sense that after a phase transition into this phase a phase transition of the second order seems to be going on. However due to the limitations of the model presented this effect could not be studied in more detail and remains as a challenge for future work.

Chapter 1

Physical Background

Shape memory alloys are materials exhibiting special properties like the ability to recover their original form, after being deformed, only by heating. Due to their special character shape memory alloys have been object of study for several decades by now and the reader may find results known in e.g. the monographs [9], [53] or the lecture notes [49]. The most common effects of shape memory alloys are the following ones.

- *Shape memory effect*: The material is deformed at a temperature that is lower than θ_c being a critical temperature the meaning of which will become evident later. Then after being heated to a temperature higher than θ_c it recovers the original shape.
- *Pseudoelasticity*: If the material is exposed to loading at a temperature higher than θ_c it is deformed. Yet after removing the loads the material returns to its original shape which corresponds to an elastic response.
- *Quasiplasticity*: If the temperature is lower than the θ_c the material cannot recover its original shape after loading, even not for small loads.

These effects are dominantly caused by the fact that for the materials considered different crystalline structures are stable for different temperatures or loading conditions. To explain these effects in more detail first the crystalline structure shape memory alloys is described.

1.1 Crystalline structure

Shape memory alloys, as other crystals, consist of atoms that are arranged in crystal lattices described by a set of three linearly independent vectors $\{e_a\}$. A lattice is then called (cf. [53, pages 61-62])

$$L(e_a) = \{x \in \mathbb{R}^3, x = ne_a, n \in \mathbb{Z}\}. \tag{1.1}$$

The lattice type is usually identified by the group of symmetry of the lattice $G(e_a)$ which is defined as follows

$$G(e_a) = \{H \in Aut, L(He_a) = L(e_a)\}, \tag{1.2}$$

where *Aut* denotes the set of all tensors the determinant of which is positive.

In shape memory alloys two or more crystalline structures can be observed, or to be more specific at different temperatures (or loading conditions) the crystalline structure of the alloy is different. If the shape memory alloy exhibits only two crystalline structures then the more symmetric structure (i.e. the one for which $G(e_a)$ is bigger) is called the *austenitic* phase and the less symmetric one is referred to as the *martensitic* phase. If more than two crystalline structures are observed, as it is the case on for example *NiTi*, the least symmetric phase or all but the most symmetric phase might be called martensitic, depending on the current context.

If no loads are applied the austenitic phase is stable for temperatures higher than the critical temperature θ_c whereas the martensitic phase is stable for lower temperatures and at the critical temperature a phase transition between these two phases occurs. The phase transition however can also be induced by loading.

Although several models can be used to study the behaviour of shape memory alloys (cf. [57]) here we shall focus only on the so-called mesoscopic model which (among others) relies on continuum mechanics.

1.2 Framework of continuum mechanics

Continuum mechanics assumes[1] that the investigated body is exposed to an action of forces or displacements on the boundary which cause a mechanical response characterized by a vectorial function called *displacement*. The key ideas and notations shall be briefly repeated at this point for later use.

Assume having a body occupying the domain $\Omega \subset \mathbb{R}^3$ in the reference configuration[2]. Any smooth injective function $y(t) : \Omega \to \mathbb{R}^3$ such that $\det\nabla y(x,t) > 0$ is called a *deformation* of the body and $F(x,t) \equiv \nabla y(x,t)$ is called the *deformation gradient* of this deformation. In continuum mechanics describing solids however, the notion of *displacement* $u(x,t) = y(x,t) - x$ and *displacement gradient* $\nabla u(x,t) = F - \mathbb{I}$ is rather used.

Having established this notation we may concentrate on the question how the deformations described above are related to forces acting on the body. To do so denote $\Omega^y(t)$ the domain the material is occupying after the deformation $y(t)$ has been applied. Let $f^y(x^y,t) : \Omega^y(t) \to \mathbb{R}^3$ and $g^y(x^y,t) : \partial\Omega^y(t) \to \mathbb{R}^3$ denote the density of the body force and surface force acting on the body, respectively. The superscript "^{y}" was written here to indicate that $x^y \in \Omega^y(t)$ and the forces are defined in the deformed configuration.

It can be proved (see for example [20], originally proved by Cauchy) that there exists a tensor $T^y(t) : \Omega^y \to \mathbb{R}^{3\times3}_{\text{sym}}$, called *stress tensor*, such that Newton's Second

[1] For an introduction to continuum mechanics we refer to e.g. [20].

[2] Although more complicated definitions of a *reference configuration* could be possibly considered, here we shall agree to understand by reference configuration the stress-free configuration. In more clarity this is the configuration in which no loads are applied to the investigated body.

law can be rewritten as

$$\operatorname{div}(T^y(x^y,t)) + f^y(x^y,t) = \rho\dot{v}(x^y,t), \qquad \forall x^y \in \Omega^y \tag{1.3}$$

$$T^y(x^y,t)n = g^y(x^y,t). \qquad \forall x^y \in \Gamma_N^y \tag{1.4}$$

$$y(x,t) = y_0(x,t), \qquad \forall x \in \Gamma_D \tag{1.5}$$

where $\dot{v}$ is the material derivative of the velocity of the deformation. The symbols Γ_N and Γ_D denote in accord with the nomenclature used throughout this thesis the Neumann and Dirichlet part of the boundary of the domain Ω, respectively. In addition, we assume that $\partial\Omega = \Gamma_N \cup \Gamma_D \cup N$ where the measure in the sense of Lebesgue of N is zero and $\Gamma_D \cap \Gamma_N = \emptyset$.

Since in this work we are interested in quasi-static processes only, the velocity term shall be omitted.

1.2.1 Energy balance in the special case of non-dissipative processes

Let us now formulate the balance of the mechanical energy. To do so, we shall multiply the above equation (1.3) (with the velocity term already omitted) by the term $\frac{\partial y}{\partial t} - \frac{\partial \tilde{y}_0}{\partial t}$ and integrate by parts over Ω^y. Here $\tilde{y}_0$ is a suitable extension of the function y_0, defined on the Dirichlet boundary only, into the domain Ω^y. Under the assumption that all functions are sufficiently smooth this calculation yields

$$\begin{aligned}\int_{\Omega^y} T^y(x^y,t).\nabla\frac{\partial y}{\partial t}(x,t)\mathrm{d}x^y = &\int_{\Omega^y} f^y(x^y,t)\frac{\partial y}{\partial t}(x,t)\mathrm{d}x^y \\ &+ \int_{\Gamma_N^y} g^y(x^y,t)\frac{\partial y}{\partial t}(x,t)\mathrm{d}S^y + \langle\sigma, y_0(x,t)\rangle^y\,,\end{aligned} \tag{1.6}$$

where the symbol $\langle\sigma, y_0(x,t)\rangle^y$ denotes

$$\begin{aligned}\langle\sigma, y_0(x,t)\rangle^y = &\int_{\Omega^y} T^y(x^y,t).\nabla\frac{\partial \tilde{y}_0}{\partial t}(x,t)\mathrm{d}x^y - \int_{\Omega^y} f^y(x^y,t)\frac{\partial \tilde{y}_0}{\partial t}(x,t)\mathrm{d}x^y \\ &- \int_{\Gamma_N^y} g^y(x^y,t)\frac{\partial \tilde{y}_0}{\partial t}(x,t)\mathrm{d}S^y.\end{aligned} \tag{1.7}$$

In the energy balance, we may interpret the meaning of $\langle\sigma, y_0(x,t)\rangle^y$ as the effect of the hard load due to the Dirichlet boundary condition.

For further investigations we shall need also the balance of the total energy in the following form (cf. [39, pages 120-121])

$$\frac{1}{2}\int_{\bar{\Omega}} \dot{v}^2\mathrm{d}x^y + \int_{\Omega^y} \dot{e}\mathrm{d}x^y = \int_{\Omega^y} T^y(x^y,t).\nabla\frac{\partial y}{\partial t}(x,t)\mathrm{d}x^y, \tag{1.8}$$

where e is the density of the *internal energy*. Similarly as before the time derivative of the velocity shall be omitted since we are interested in quasi-static processes only.

Another, more useful, balance of the total internal is got by substituting the two previous equations into each other

$$\int_{\Omega^y} \dot{e}\mathrm{d}x^y = \int_{\Omega^y} f^y(x^y,t)\frac{\partial y}{\partial t}(x,t)\mathrm{d}x^y + \int_{\Gamma_N^y} g^y(x^y,t)\frac{\partial y}{\partial t}(x,t)\mathrm{d}S^y + \langle \sigma, y_0(x,t)\rangle^y . \tag{1.9}$$

Introducing furthermore the *Helmholtz free energy* ψ as

$$\psi = e - \theta\eta, \tag{1.10}$$

where θ is the temperature and η the entropy density, we get for the entropy production in the isothermal case (already rewritten into reference configuration using according transformation laws)

$$\chi \equiv \int_\Omega \theta\dot{\eta}\mathrm{d}x = \int_\Omega f\frac{\partial y}{\partial t}(x,t)\mathrm{d}x + \int_\Gamma g\frac{\partial y}{\partial t}(x,t)\mathrm{d}S + \langle \sigma, y_0(x,t)\rangle - \int_\Omega \dot{\psi}\mathrm{d}x. \tag{1.11}$$

Due to the second law of thermodynamics χ, being the total entropy production multiplied by temperature, has to be non-negative. In the special case of non-dissipative processes treated in this subsection we may even assume that the entropy production is equal to zero. When integrating the above equation in time from t_1 to t_2 setting the entropy production to zero and defining the *Gibbs free energy* as

$$G(t,y(t)) = \int_\Omega \psi\mathrm{d}x - \int_\Omega y(t,x)f\mathrm{d}x - \int_{\Gamma_N} y(t,x)g\mathrm{d}S, \tag{1.12}$$

we may rewrite eq. (1.11) as

$$\begin{aligned} G(t_2,y(t_2)) - G(t_1,y(t_1)) = &- \int_{t_1}^{t_2}\left(\int_\Omega y(x)\frac{\partial f}{\partial t}\mathrm{d}x + \int_{\Gamma_N} y(x)\frac{\partial g}{\partial t}\mathrm{d}S\right)\mathrm{d}t \\ &+ \int_{t_1}^{t_2}\langle \sigma, y_0(x,t)\rangle\,\mathrm{d}t. \end{aligned} \tag{1.13}$$

This equation essentially means that the change of the Gibbs free energy during the loading process is balanced by the work of external forces.

We shall now exploit the concept of quasi-static processes once again to see which states, represented by the deformation $y(t)$, might be defined as stable. Recall, that we call a process quasi-static if at fixed times differing by a time increment Δt the system can be supposed to be in equilibrium. In each step the system is deviated (a little bit) from equilibrium and within this (small) time increment it returns to another equilibrial state again (see e.g. [13, pages 95-98]). This corresponds to the view that the process happens infinitely slowly. In total abstraction this time increments tend to zero so that we may assume that the system is in equilibrium at any time t.

Furthermore let us use the the so called *postulate of realizability*, which states that *as soon as a process can occur from the view of thermodynamics, it will occur* (formulated in [37]). In our case a process can occur from the view of thermodynamics if the entropy production during this process is non-negative. We will then say that a state is stable for the time increment Δt if no other

deformation can be reached during this time interval such that the entropy is not decreased. A condition for a state, represented by $y(t)$, to be stable is then

$$G(t, y(t)) \leq G(t, \bar{y}(t)), \tag{1.14}$$

To see this suppose that the state represented by $y(t)$ is stable but (1.14) does not hold. Then as $y(t)$ is stable it has to hold

$$\begin{aligned} -(G(t+\tau, y(t+\tau)) - G(t, y(t))) - \int_t^{t+\tau} \left(\int_\Omega y(x) \frac{\partial f}{\partial t} \mathrm{d}x + \int_{\Gamma_N} y(x) \frac{\partial g}{\partial t} \mathrm{d}S \right) \mathrm{d}t \\ + \int_t^{t+\tau} \langle \sigma, y_0(x,t) \rangle \, \mathrm{d}t < 0, \end{aligned} \tag{1.15}$$

for any τ smaller than Δt. We already mentioned that in total abstraction the time increment may tend to zero. When setting $y(t+\tau) = \bar{y}$ for which (1.14) is not satisfied and choosing τ sufficiently small this yields that

$$G(t+\tau, y(t+\tau)) < G(t, y(t)), \tag{1.16}$$

a contradiction.

This result of stability can also be reached by a different method. Assume that the studied material is hyper-elastic i.e. there exist a function $W(t, \theta) : \Omega \times \mathbb{R}^{3\times 3}_{\mathrm{sym}} \to \mathbb{R}$ such that $\hat{T} = \frac{\partial W}{\partial F}(x, F, t, \theta)$ (cf. e.g. [51, page 206]) for all times, all temperatures θ and all tensors F, where $\hat{T}$ denotes the Piola-Kirchhoff transformation of T^y. The function W is in such a case referred to as the stored energy density. Moreover assume that the stored energy density and temperature do not depend explicitly on time. Then the energy balance (1.6) may be rewritten in the reference configuration as

$$\begin{aligned} \frac{\mathrm{d}}{\mathrm{dt}} \int_\Omega W(x, F, \theta) \mathrm{d}x = \int_\Omega f(x,t) \frac{\partial y}{\partial t}(x,t) \mathrm{d}x \\ + \int_{\Gamma_N} g(x,t) \frac{\partial y}{\partial t}(x,t) \mathrm{d}S + \langle \sigma, y_0(x,t) \rangle, \end{aligned} \tag{1.17}$$

where

$$\begin{aligned} \langle \sigma, y_0(x,t) \rangle = \int_\Omega \frac{\partial W}{\partial F}(x, F, \theta) . \nabla \frac{\partial \tilde{y}_0}{\partial t}(x,t) \mathrm{d}x - \int_\Omega f(x,t) \frac{\partial \tilde{y}_0}{\partial t}(x,t) \mathrm{d}x \\ - \int_{\Gamma_N} g(x,t) \frac{\partial \tilde{y}_0}{\partial t}(x,t) \mathrm{d}S. \end{aligned} \tag{1.18}$$

Comparing this result (1.17) with equation (1.11) where the entropy production is set to zero leads us to the fact that for the cases in which the Helmholtz free energy ψ does not depend on time it may be identified with the stored energy of a hyper-elastic material. Moreover the weak formulation of eq.(1.3) for quasi-static processes and hyper-elastic materials is, provided all functions are sufficiently smooth, equivalent to the minimization of the functional

$$\int_\Omega W(x, F, \theta) \mathrm{d}x - \int_\Omega f(x,t) y(x,t) - \int_{\Gamma_N} g(x,t) y(x,t) \mathrm{d}x, \tag{1.19}$$

in almost all times on the set of all admissible deformations. We see that the minimized functional is exactly the Gibbs free energy and therefore for hyper-elastic materials and quasi-static, non-dissipative processes every deformation satisfying Newton's second law is a stable state and vice versa.

1.3 Microstructure

Having established the framework of continuum mechanics needed for modelling let us investigate the link between crystalline structures described in the previous section and continuum mechanics. Assume that in the reference configuration the atoms of the body are organized in a lattice $L(e_a^0)$. If these atoms are rearranged to a lattice $L(e_a)$ either by loading or by change of temperature we may assume that the effect is the same as if a homogeneous deformation, the deformation gradient of which satisfies $Fe_a^0 = e_a$, had been applied. This assumption is backed by the so-called *Cauchy-Born hypothesis* (cf. [9, pages 34-37]).

This allows for an identification of crystalline structures with deformation gradients. A natural way is to identify the austenitic phase with the identity matrix and martensitic crystalline structures with deformation gradients of deformations that allow forming the martensitic structure out of austenite. However, depending on symmetry of both austenite and martensite there might be more independent ways to form the martensite. To see why more deformations may lead to the martensitic lattice let us consider the following example of a shape memory alloy having a cubic crystalline structure in austenite and tetragonal in martensite. For simplicity suppose the coordinate system of the problem to be such that each axis is identical with one edge of the cube. Then we can form a cuboid by stretching the cube along one arbitrary axis of the coordinate system. The deformations describing these stretches are naturally different, but all of them realize the transformation to a tetragonal lattice and all of them are admissible.

Deformation gradients of possible deformations forming martensite from austenite are called *variants* of martensite and moreover deformation gradient F_1,F_2 such that there exists a $Q \in \mathrm{SO}(3)$ and $F_1 = QF_2$ form the same variant. The existence of multiple variants is important to give rise to the so called microstructure described in this section.

In the end of Section 1.2 we saw that at least for hyper-elastic materials and non-dissipative processes it is enough to give the stored energy density to be able to compute the behaviour of the material. Therefore we shall give a typical stored energy density (see for example [53, page 184]) for a shape memory alloy in the following way

$$\forall\ \theta \geq \theta_c \begin{cases} W(Q\mathbb{I}, \theta) = 0 & \forall Q\ \in \mathrm{SO}(3), \\ W(F, \theta) > 0 & \forall F\ \neq Q\mathbb{I},\ \forall Q\ \in \mathrm{SO}(3), \end{cases} \tag{1.20}$$

$$\forall\ \theta \leq \theta_c \begin{cases} W(QU_i, \theta) + \delta(\theta) = 0 & \forall i = 1 \dots M, \quad \forall Q\ \in \mathrm{SO}(3), \\ W(F, \theta) > 0 & \forall F\ \neq QU_i\ \ \forall i = 1 \dots M, \quad \forall Q\ \in \mathrm{SO}(3), \end{cases} \tag{1.21}$$

where $\mathbb{I}$ denotes the distortion matrix of the austenite, i.e. the identity matrix

and $U_1 \dots U_M$ denote the distortion matrices of the M variants of martensite. In addition, θ_c is the transformation temperature and δ is some offset.

We see that at temperatures lower than θ_c the energy in eq. (1.19) with zero forces is minimized not only by a constant distortion U_i for any $i = 1 \dots M$, but also by a combination of these distortion, e.g.

$$F = \begin{cases} U_i & \text{if } x \in \Omega_1, \\ U_j & \text{if } x \in \Omega_2, \end{cases}$$

such that $\Omega_1 \cup \Omega_2 \cup N = \Omega$ where N is a set with zero measure and $\Omega_1 \cap \Omega_2 = \emptyset$ is also a minimizer of (1.19) disregarding the boundary condition.

However the situation is different if boundary conditions are also taken into account. We may for example demand the distortion to be identity on some part of the boundary. Yet, if no variant of the martensite has a distortion matrix equal to identity (which is the most common case) then the energy cannot be zero - we still assume having no forces acting on the material - and the boundary condition satisfied at the same time. To minimize the energy and to satisfy the boundary condition at the same time the material has to develop a fine mixture of variants, which is called *microstructure*. To study the situation in more detail we shall investigate the following example:

Example 1.1. Let the crystalline structure of martensite be tetragonal and let variants 1 and 2 have the distortion matrices U_1 and U_2 respectively. Assume that these distortion matrices are rank-1 connected, meaning that there exist vectors $\mathbf{a}$ and $\mathbf{n}$ and a rotation Q such that

$$U_1 - QU_2 = \mathbf{a} \otimes \mathbf{n}. \tag{1.22}$$

Moreover assume that the material forms a cube which is fixed i.e. $u(x) = 0$ for any x lying on the boundary of the cube. For the sake of simplicity let $\mathbf{n}$ in eq. (1.22) be $(0, 0, 1)^{\mathrm{T}}$ and $Q = \mathbb{I}$. In addition let U_1 and U_2 be such that $1/2U_1 + 1/2U_2 = \mathbb{I}$, which together with (1.22) implies neither U_1 nor U_2 can be identity matrices; hence none variant satisfies the boundary condition (we assume that $U_3 \neq \mathbb{I}$). However if U_1 and U_2 are arranged in narrow stripes like in Figure 1.1 the boundary condition is satisfied and the energy is positive only on the grey triangles. By making the stripes finer the energy is even lowered, thus a sequence of these stripes is an infimizing sequence, but a minimum does not exist.

When taking into account this stripe arrangement we see why we need to impose condition (1.22). This is because only in this case the tangential component of the deformation is continuous at the interfacial planes, which is a natural physical requirement.

The stripes in Figure 1.1 always have in reality finite length-scales. This however is not handled within the mesoscopic model, since it disregards the interfacial energy between the stripes and also continuum mechanics is not applicable for small length-scales (cf. [9, pages 102-103]).

The microstructure showed in Figure 1.1 is called a *laminate of the first order* and even more complicated microstructures can be observed. Some of them will be part of these thesis for others we refer to e.g. [9], [53].

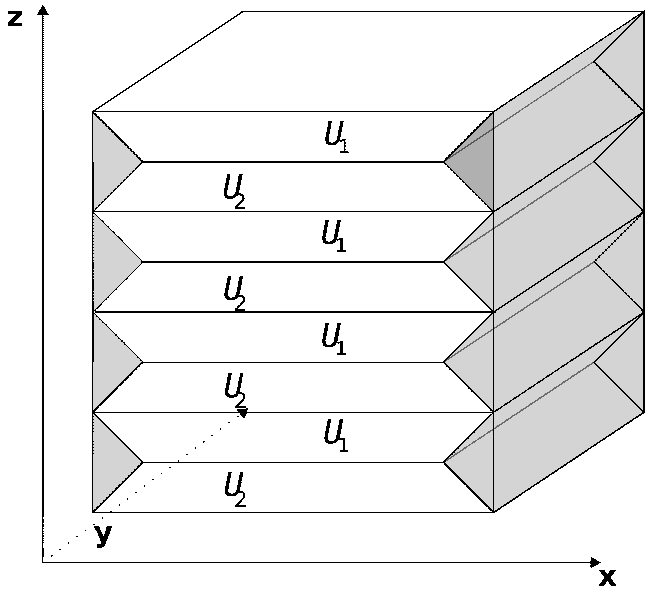

Figure 1.1: Twinning of two variants characterized by U_1, U_2 in martensite. In the grey triangles the deformation gradient tends continuously to identity to satisfy the boundary condition.

Having the knowledge about the microstructure of martensite we can explain the special effects of shape memory alloys that were mentioned in the beginning of this chapter.

To explain the *shape memory effect* suppose that the material is in martensite having initially, in stress-free configuration, the same shape as in austenite. When being deformed by a small enough loading the deformation can be compensated by rearrangement of variants and a change in microstructure (cf. [9, pages 143-150]). On heating a phase transition to austenite occurs, but since there is only one variant of austenite there is only one possible shape it can have in a stress free configuration. Therefore the material will recover exactly this shape.

Pseudoelasticity is explained as follows. The material is deformed while being in austenite and because of the applied loads it transits to martensite and creates a microstructure. Loads that are bigger than those that induce the phase transition lead to a change in microstructure as described in the case of the shape memory effect. After removing all loads the only stable stress free configuration at the given temperature is the austenitic one and therefore the material recovers its original shape, which reminds of an elastic response. (see also [25])

Quasiplasticity is an effect that occurs if the material is in martensite and is deformed. Similarly to the previous cases the deformation leads to a rearrangement of variants. When all loads are released the new microstructure is stable as well, so the shape of the material is unchanged. So, the behaviour of the material seems to be plastic.

1.4 Dissipation and process stability

It was observed that the transformation from austenite to martensite is a dissipative process, which does not start unless a threshold in loading has been overcome (see e.g. the papers [1], [36], [55] and references therein). This behaviour, however, is not taken into account if we would rely in our modelling only on eq. (1.13).

In what follows the term "phase" will be used not only for the martensitic or austenitic phase, but also all martensitic variants will be referred to as *phases*. Therefore a material which is tetragonal in martensite (having three variants) is from now said to have four different phases in each of which as well as in a mixture of these it can be observed. This nomenclature is very typical of mathematical literature.

An integration of dissipation into the current model can be done only in the framework of thermodynamics, which was already introduced in Section 1.2 and will here be used once again. We shall partly follow the work [45], but this work contains mostly only information on the case of pure phases whereas here we take into account also mixtures of phases.

In the following we shall assume that each material point can be in a mixture of phases. This is an abstraction of the laminates mentioned before, as we assume that the lamination is so narrow that more that one phase are defined at each point. Let us therefore introduce a phase distribution function defined at each point as $c_x = \sum_{\text{All Phases}} \lambda_i(x) e_i$, where e_i indicates the i-th phase, $\lambda_i(x) \in [0,1]$ are called *volume fractions*. The vector of all volume fractions will be denoted λ. We shall furthermore introduce the overall phase distribution function $c = \{c_x\}_{x\in\Omega}$ which is a collection of the phase distribution functions in any point of the domain Ω, but itself does not explicitly depend on x.

We suppose that the material dissipates an energy $D(c^1, c^2)$ if the overall phase distribution changes from c^1 to c^2. Furthermore let us assume (as in [55], [58], [43] or [44]) that there exists a non-negative function d such that $D(c^1, c^2) = \int_\Omega d(\lambda^2(x) - \lambda^1(x))\mathrm{d}x$, where $\lambda^1(x), \lambda^2(x)$ are the volume fractions vectors of the phases c^1, c^2 respectively. Physically this means that the dissipated energy is dependent only on the change of the fractions of each phase and but on the initial or final phase distribution.

From above it follows that the energy dissipated during the time interval $[t_1, t_2]$ is equal to

$$\mathrm{Diss}_{[t_1,t_2]} = \int_\Omega \mathrm{Var}_{[t_1,t_2]} d(\lambda(t)). \tag{1.23}$$

Here the variation[3] of the function $d(\cdot)$ is evaluated because we assume that during each bounded time interval only a finite number of phase transitions can occur. Furthermore assuming that the Gibbs free energy as defined in (1.12) depends

[3]Recall that by a variation of a function $d : [t_1, t_2] \to \mathbb{R}$ we understand

$$\mathrm{Var}_{[t_1,t_2]} d(\lambda(t)) = \sup \left\{ \sum_i d(\lambda(t^i) - \lambda(t^{i-1})); \text{of all partitions } t_1 \le t^1 \le t^2 \ldots \le t^n \le t_2 \right\}.$$

also on the phase distribution c, we may rewrite eq. (1.11) as

$$G(t_2, c(t_2)) - G(t_1, c(t_1)) + \mathrm{Diss}_{[t_1,t_2]} = -\int_{t_1}^{t_2} \left(\int_\Omega y(x)\dot{f}\,\mathrm{d}x + \int_\Gamma y(x)\dot{g}\,\mathrm{d}S \right) \mathrm{d}t + \int_{t_1}^{t_2} \langle \sigma, y_0(x,t) \rangle \,\mathrm{d}t, \tag{1.24}$$

where we used the postulate (cf. [45]) that the dissipated energy has to equal to the entropy production multiplied by temperature. The derived law (1.24) gives us the *conservation of energy* during the process, but is itself not sufficient to describe the process.

We shall use the postulate of realizability similarly as in Section 1.2 to derive conditions of stability for a process. Namely we shall see that a state characterized by $(y(t), c(t))$, a deformation and a phase distribution function, is stable if and only if

$$G(t, y, c) - G(t, \tilde{y}, \tilde{c}) \leq D(c, \tilde{c}), \tag{1.25}$$

for any other state characterized by $(\tilde{y}, \tilde{c})$. To prove this condition suppose that (y, c) is a stable state within the small time increment Δt but (1.25) does not hold. Choose $(y(t+\tau), c(t+\tau)) = (\tilde{y}, \tilde{c})$ for which (1.25) is not satisfied. Then as (y, c) is a stable state this state cannot be reachable by a physically admissible process and so

$$-(G(t+\tau, c(t+\tau)) - G(t, c(t))) - \int_t^{t+\tau} \left(\int_\Omega y(x)\dot{f}\,\mathrm{d}x + \int_\Gamma y(x)\dot{g}\,\mathrm{d}S \right) \mathrm{d}t + \int_t^{t+\tau} \langle \sigma, y_0(x,t) \rangle \,\mathrm{d}t < \mathrm{Diss}_{[t,t+\tau]}, \tag{1.26}$$

has to hold for any τ smaller than the time increment Δt. This condition is a clear corollary of the postulate of realizability, since if a process from (y, c) to $(\tilde{y}, \tilde{c})$ was admissible it would happen immediately and $c(x)$ could not characterize a stable state. As eq. (1.26) holds for any τ this gives a contradiction.

The conservation of energy and the definition of the stable states will be the key ingredients to define solutions of the problem when loading a shape memory alloy specimen as we shall see in Chapter 3.

Chapter 2

Mathematical Background

Let us recall Example 1.1 on lamination given in previous chapter. Essentially the problem posed there was

$$\text{Minimize } I(y) = \int_\Omega W(\nabla y, \theta)\mathrm{d}x \text{ on } V = \{y \in W^{1,p}(\Omega, \mathbb{R}^m); y = y_0 \text{ on } \Gamma_{\mathrm{D}} \subset \partial\Omega\}, \tag{2.1}$$

if the deformation is placed into appropriate function spaces and the boundary condition is formulated in a more general way. In this particular example we have seen that a minimizer may not exist for some kinds of boundary conditions. Namely, if the material was required to satisfy that $u(x) = 0$ for almost all x lying on the boundary than we observed that no minimizers exists. This was caused by the fact that the gradient of the minimizer would be required to be U_1 or U_2 a.e. in Ω and at the same time its trace on a part of the boundary had to be x (if we imagined $y_0(x) = x$), which is impossible for a function in $W^{1,p}(\Omega, \mathbb{R}^m)$.

In this chapter we shall therefore give mathematical concepts that allow to treat this problem basically by extending (relaxing) the studied functional in such a way that a minimizer for this extended functional exists and its minimum has the same value as the infimum of the original problem. Moreover we would like to be able to keep some connection between infimizing sequences of the original problem and the relaxed one. At this point recall that by an infimizing sequence of the function I as in (2.1) we understand

$$\{y_k\}_{k=0}^\infty \subset V \text{ such that } I(y_k) \to \inf_{\tilde{y}\in V} I(\tilde{y}), \tag{2.2}$$

and such a sequence has always to exist. On the other hand a minimizing sequence we call

$$\{y_k\}_{k=0}^\infty \subset V \text{ such that } I(y_k) \to \min_{\tilde{y}\in V} I(\tilde{y}). \tag{2.3}$$

We will see two possibilities: either the infimizing sequence of the original problem will be also a minimizing sequence of the relaxed problem or will generate its minimizer in the sense of what follows. Moreover we would like to choose the relaxed problem somehow generally with respect to other variables and data the functional may depend on to prevent the need to relax to a different functional is these variables change. And of course, we should be able to find the relaxed functional without previous knowledge if the infimum or infimizing sequences of the original problem.

Most of the theorems in this chapter will be given without proofs, for proofs and more information we refer the reader to e.g. [54], [59] or [49].

2.1 Quasiconvexity

Let $I : W^{1,p}(\Omega, \mathbb{R}^m) \to \mathbb{R}$ be a functional in the form

$$I(y) = \int_\Omega \phi(x, \nabla y(x)) \mathrm{d}x, \tag{2.4}$$

where $p \in (1, \infty)$ and $\Omega \subset \mathbb{R}^n$ is a regular domain. Furthermore suppose that $\phi : \Omega \times \mathbb{R}^{m\times n} \to \mathbb{R}$ is a Carathéodory function[1] such that I is a bounded, continuous and coercive functional[2].

The easiest method to prove that the functional I has a minimum is the so called *direct method* which works as follows. Take $\{y_k\}_{k=0}^\infty$, an infimizing sequence of the functional I. As the functional is bounded from below the infimum of I has a finite value and since moreover the functional is coercive the sequence $\{y_k\}_{k=0}^\infty$ is bounded in $W^{1,p}(\Omega, \mathbb{R}^m)$. As $W^{1,p}(\Omega, \mathbb{R}^m)$ is a reflexive space[3] there is a $y \in W^{1,p}(\Omega, \mathbb{R}^m)$ being the weak limit of the infimizing sequence. This limit is then a minimizer of the functional I if it is *(sequentially) weakly lower semi-continuous.*

Clearly not for every functional of the studied type the weak limit of the infimizing sequence needs to be a minimizer. To see this, return to Example 1.1, where we already characterized one possible infimizing sequence $\{y_k\}_{k=0}^\infty$. The weak limit of this sequence is $y(x) = x$ but $I(\mathbb{I}, \theta) > I(\nabla y_k, \theta)$ for any k greater than a fixed constant, which clearly shows that the weak limit is not a minimizer.

First we shall give conditions we have to impose on the function ϕ to guarantee the functional (2.4) to be weakly lower semi-continuous which allows for the application of the direct method.

Definition 2.1. [4] We say that $\varphi : \mathbb{R}^{m\times n} \to \mathbb{R}$ is *quasiconvex* if

$$\varphi(Y) \leq \inf_{\omega \in W_0^{1,\infty}(\Omega), \mathbb{R}^m} \frac{1}{|\Omega|} \int_\Omega \varphi(Y + \nabla\omega) \mathrm{d}x, \tag{2.5}$$

for any $Y \in \mathbb{R}^{m\times n}$, and the integral in the above formula exists.

Proposition 2.2. [5] *Let $\phi : \mathbb{R}^n \times \mathbb{R}^{m\times n} \to \mathbb{R}$ be a Carathéodory function satisfying*

$$0 \leq \phi(x, F) \leq c_2(1 + |F|^p),$$

[1] We may also assume that ϕ is also dependent on $y(x)$. However this case is not interesting when modelling the behaviour of shape memory alloys. Moreover under continuity assumptions for I this case is easily governed by the usage of compact embeddings.

[2] This can be guaranteed by e.g. by assuming that there exist constants $c_2 \geq c_1 > 0$ such that $c_1(|F|^p - 1) \leq \phi(x, F) \leq c_2(1 + |F|^p)$ for a.e. $x \in \Omega$ and every $F \in \mathbb{R}^{m\times n}$.

[3] Note that we assume that $p \in (0, \infty)$.

[4] The notion of quasiconvexity was introduced by Morrey [47], a generalized concept of $W^{1,p}$-quasiconvexity was later introduced by Ball and Murat [7].

[5] This proposition is essentially due to Morrey [47]. Actually under the growth assumed even $W^{1,p}$-quasiconvexity would suffice as shown in [7] by Ball and Murat.

for a constant $c_2 > 0$, a.e. $x \in \Omega$, every $F \in \mathbb{R}^{m\times n}$ and $p \in (1,\infty)$. Then the functional $I(y)$ from eq. (2.4) is weakly lower semi-continuous if and only if ϕ is quasiconvex for a.e. every x in Ω.

From this characterization we see that the stored energy density in Example 1.1 is not quasiconvex as the direct method fails. To bypass the problem we shall search for the minimum of a different functional $I^*(y)$ defined by

$$I^*(y) = \int_\Omega Q\phi(x, \nabla y)\mathrm{d}x, \tag{2.6}$$

where $Q\phi$ is the quasiconvex envelope of the function ϕ defined as the supremum of quasiconvex functions lying underneath ϕ.[6]

Clearly, under appropriate growth and coercivity conditions on ϕ, a minimizer of I^* exists due to Proposition 2.2. A natural question is however whether this minimum and the infimum of the original functional have the same value. The following proposition answers the posed question positively.

Proposition 2.3. [7] *Let $\phi : \mathbb{R}^n \times \mathbb{R}^{m\times n} \to \mathbb{R}$ be a Carathéodory function, let there exist constants $c_2 \geq c_1 > 0$ and $p \in (1,\infty)$ such that*

$$c_1(|F|^p - 1) \leq \phi(x, F) \leq c_2(1 + |F|^p),$$

for a.e. $x \in \Omega$ and every $F \in \mathbb{R}^{m\times n}$. Then $\min_{y\in V} I^*(y) = \inf_{y\in V} I(y)$, where I and I^* are defined through eq. (2.4) and (2.6) respectively.

Moreover from this proposition we see that the weak limit of any infimizing sequence for the original functional is a minimizer for the new functional I^*.

Theoretically we are now at the position to find the infimum of the stored energy describing, to some extent, the static behaviour of shape memory alloys (disregarding dissipation) as the energy density can be chosen in such a way to satisfy the appropriate growth and coercivity conditions. Yet the strategy of quasi-convexification has two main drawbacks. First due to the non-local character of quasiconvexity (cf. [31]) in only very few cases we are able to decide whether a function is or is not quasiconvex. To bypass the problem of forming a quasiconvex hull one could use only the so called rank-1 convex envelope as a lower bound or a polyconvex envelope[8] as an upper bound. We give more details on this later.

Second - and from the viewpoint of physics maybe more important - is the fact that the minimizer of the quasiconvex envelope does not carry much information about the infimizing sequences themselves. To study this effect more in detail recall Example 1.1. Namely, we have already seen in this chapter that the minimizer of the functional I^*, in this particular example, is the deformation $y(x) = x$, but this deformation shows no connection with the laminate structure shown in Figure 1.1. The reason is roughly speaking the fact that due to quasi-convexification the

[6] If ϕ is a locally bounded Carathéodory function the quasiconvex envelope can also be defined as $Q\phi(Y) = \inf_{\omega\in W_0^{1,p}} \frac{1}{|\Omega|}\int_\Omega \phi(Y + \nabla\omega)\mathrm{d}x$. (see e.g. [14, Section 5.1.1.2])

[7] This is originally due to Dacorogna [14, Section 1], here taken from [54].

[8] The notion of polyconvexity was introduced by Ball [4] where the reader may find more details.

multi-well structure of the stored energy to a great extend smear out. It is therefore desirable to find a way to keep the information about microstructure (infimizing sequence) even for the minimizer of I^* by some finer extension if I. This characterization can be done by the means of *Young measures* which are subject of the next section.

2.2 Young measures

As already anticipated we would like to find a finer way to extend the functional at study to assure the existence of minimizers, but on the other hand also to track the information about infimizing sequences. An effective way is to relax the functional into so called *Young measure* introduced by Young in the connection with optimal control [67].

For further information about the broad subject of Young measures the reader is referred to e.g. [5], [27], [28],[29], [54], [59] and many others.

We shall first of all give the fundamental theorem introducing Young measures.

Theorem 2.4. [9] *Let $\{u_k\}_{k=0}^{\infty}$ be a bounded sequence in $L^p(\Omega,\mathbb{R}^m)$ for some $p \in (1,\infty)$. Then there exists a subsequence of $\{u_k\}_{k=0}^{\infty}$ (not relabelled) and a family of probability measures $\nu = \{\nu_x\}$ with the property that for any Carathéodory function $\phi : \Omega \times \mathbb{R}^m \to \mathbb{R} \cup \{+\infty\}$ such that $\{\phi(x,u_k(x))\}_{k=0}^{\infty}$ is weakly convergent in $L^1(\Omega,\mathbb{R})$ it holds*

$$\lim_{k\to\infty} \int_\Omega \xi(x)\phi(x,u_k(x))\mathrm{d}x = \int_\Omega \xi(x) \int_{\mathbb{R}^m} \phi(x,A)\mathrm{d}\nu_x(A)\mathrm{d}x, \tag{2.7}$$

for any $\xi \in L^\infty(\Omega,\mathbb{R})$.
Especially if $|\phi(x,A)| \le g(|A|)$ for some $g \in L^\infty_{\mathrm{loc}}(\mathbb{R},\mathbb{R})$ then the condition of weak convergence of ϕ in $L^1(\Omega,\mathbb{R})$ is satisfied for any bounded sequence in $L^p(\Omega)$ if $\lim_{|A|\to\infty} \frac{g(|A|)}{|A|^p} = 0$.

Definition 2.5. Let $\{u_k\}_{k=0}^{\infty}$ be a bounded sequence in $L^p(\Omega,\mathbb{R}^m)$ for some $p \in (1,\infty)$, such that there exists ν to satisfy eq. 2.7. Then ν is called the *Young measure* associated to the sequence $\{u_k\}_{k=0}^{\infty}$ On the other hand $\{u_k\}_{k=0}^{\infty}$ is in such case said to *generate* the Young measure ν.[10]

Definition 2.6. Let $\{u_k\}_{k=0}^{\infty}$ be a bounded sequence in $W^{1,p}(\Omega,\mathbb{R}^m)$ for some $p \in (1,\infty)$, $\Omega \in \mathbb{R}^n$. Then the probability measure satisfying

$$\lim_{k\to\infty} \int_\Omega \xi(x)\phi(x,\nabla u_k(x))\mathrm{d}x = \int_\Omega \xi(x) \int_{\mathbb{R}^{m\times n}} \phi(x,A)\mathrm{d}\nu_x(A)\mathrm{d}x, \tag{2.8}$$

for any Carathéodory function $\phi : \Omega\times\mathbb{R}^{m\times n} \to \mathbb{R}\cup\{+\infty\}$ such that $\{\phi(x,\nabla u_k\}_{k=0}^{\infty}$ is weakly convergent in $L^1(\Omega,\mathbb{R})$ and for any $\xi \in L^\infty(\Omega,\mathbb{R})$ is called the *gradient*

[9] This was for the first time shown by Schonbeck [61] for $p > 1$; for a proof we may refer the reader also to e.g. [3].

[10] Note that the existence of such a ν is guaranteed by the preceding theorem, but we may need to choose a subsequence. If this is the case than of course ν is associated to the subsequence chosen as different subsequences may generate different Young measures.

Young measure associated to the sequence $\{u_k\}_{k=0}^{\infty}$.
We shall further denote

$$\mathcal{G}^p_{u_D} = \{\nu \text{ is a gradient Young measure;} \\ \nabla u(x) = \int_{\mathbb{R}^{m\times n}} A \mathrm{d}\nu_x(A) \text{ for a.a } x \in \Omega \text{ and } u_{|\Gamma_D} = u_D\}$$

We shall see that defining instead of I from eq. (2.4) a new functional

$$\bar{I}(\nu) = \int_\Omega \int_{\mathbb{R}^{m\times n}} \phi(x, A) \mathrm{d}\nu_x(A) \mathrm{d}x, \tag{2.9}$$

defined on the set of gradient Young measures is a good way to extend the minimization problem in order to find a minimizer.

Proposition 2.7. [11] *Assume there exist constants $c_2 \geq c_1 > 0$ such that for a Carathéodory function ϕ it holds that*

$$c_2(|F|^p - 1) \leq \phi(x, F) \leq c_2(1 + |F|^p), \tag{2.10}$$

for some $p \in (1, \infty)$, a.e. $x \in \Omega$ and every $F \in \mathbb{R}^{m\times n}$. Moreover let the boundary condition u_D in (2.1) be in $W^{1-1/p,p}(\Gamma_D, \mathbb{R}^m)$. Then

$$\inf_{y\in V} I(y) = \min_{\nu\in\mathcal{G}^p_{u_D}} \bar{I}(\nu). \tag{2.11}$$

As this is a fundamental theorem in our discussion we shall give a proof of it. First note however, that we cannot use directly the second part of the Theorem 2.4 as the demanded growth condition does not assure that $\phi(x, \nabla z_k)$ is weakly convergent in $L^1(\Omega)$ for any sequence $\{z_k\}_{k=1}^{\infty}$ bounded in $W^{1,p}(\Omega, \mathbb{R}^m)$. Thus we shall need the following two lemmas.

Lemma 2.8. [12] *Let φ be an arbitrary non-negative Carathéodory function, $\{z_k\}_{k=1}^{\infty}$ a bounded sequence in $W^{1,p}(\Omega, \mathbb{R}^m)$ and $\nu = \{\nu_x\}$ the associated gradient Young measure. Then it holds*

$$\liminf_{k\to\infty} \int_\Omega \varphi(x, \nabla z_k) \mathrm{d}x \geq \int_\Omega \int_{\mathbb{R}^{m\times n}} \varphi(x, A) \mathrm{d}\nu_x(A) \mathrm{d}x. \tag{2.12}$$

Note that there is no demand for weak convergence in $L^1(\Omega, \mathbb{R})$ in this lemma, hence it can be used even if no information about the weak convergence is at our disposal.

Lemma 2.9. [13] *Let $\{z_k\}_{k=1}^{\infty}$ be a bounded sequence in $W^{1,p}(\Omega, \mathbb{R}^m)$ generating a gradient Young measure ν. Then there exists another bounded sequence $\{w_k\}_{k=1}^{\infty} \subset W^{1,p}(\Omega, \mathbb{R}^m)$ such that $\{|\nabla w_k|^p\}_{k=1}^{\infty}$ is weakly convergent in $L^1(\Omega, \mathbb{R})$*

[11] This proposition is taken from [54]

[12] This lemma is taken from [54] and is a consequence of Chacon's biting lemma originally proved by Brooks and Chacon [11].

[13] This lemma was originally proved by Fonseca, Müller and Pedregal [16] and independently also by Kristensen [32].

and the gradient parametrized measures associated with these sequences are same ones.
Moreover let z be the weak limit of the sequence $\{z_k\}_{k=1}^{\infty}$. Then the sequence $\{w_k\}_{k=1}^{\infty}$ can be chosen in such a way that $w_k - z \in W_0^{1,p}(\Omega)$ for all integers k.

Proof of Proposition 2.7. Let us choose $\{v_k\}_{k=1}^{\infty} \subset V$, an infimizing sequence of the functional $I(y)$. This sequence is due to the growth conditions on ϕ and because of the regularity of the boundary condition a bounded sequence in $W^{1,p}(\Omega, \mathbb{R}^m)$. If we knew that $\phi(x, z_k(x))$ was weakly convergent in $L^1(\Omega, \mathbb{R})$ we would get that $\lim_{k\to\infty} I(v_k) = \int_\Omega \int_{\mathbb{R}^{m\times n}} \phi(x, A)\mathrm{d}\nu_x^M(A)\mathrm{d}x$ for some ν^M and at least would know that $\inf_{y\in V} I(y) \leq \min_{\nu\in\mathcal{G}^p_{u_D}} \bar{I}(\nu)$.

However we do not know whether the condition of weak convergence is satisfied as the growth conditions do not assure this a-priori. Yet due to Lemma 2.9 we can find a different sequence $\{w_k\}_{k=1}^{\infty} \subset V$ such that $\{|\nabla w_k|^p\}_{k=1}^{\infty}$ is weakly convergent in $L^1(\Omega, \mathbb{R})$ generating the gradient Young measure ν^M. Due to the growth conditions assumed (2.10), $\{\phi(x, \nabla w_k(x)\}_{k=1}^{\infty}$ has to be weakly convergent in $L^1(\Omega, \mathbb{R})$, as well. Moreover, as $\{v_k\}_{k=1}^{\infty}$ is an infimizing sequence it has to hold

$$\lim_{k\to\infty} \int_\Omega \phi(x, \nabla v_k)\mathrm{d}x \leq \lim_{k\to\infty} \int_\Omega \phi(x, \nabla w_k)\mathrm{d}x = \int_\Omega \int_{\mathbb{R}^{m\times n}} \phi(x, A)\mathrm{d}\nu_x^M(A)\mathrm{d}x.$$

On the other hand, from Lemma 2.8, we have

$$\lim_{k\to\infty} \int_\Omega \phi(x, \nabla z_k)\mathrm{d}x \geq \int_\Omega \int_{\mathbb{R}^{m\times n}} \phi(x, A)\mathrm{d}\nu_x^M(A)\mathrm{d}x,$$

which implies that $\{w_k\}_{k=1}^{\infty}$ is an infimizing sequence as well and it holds that

$$\lim_{k\to\infty} \int_\Omega \phi(x, \nabla v_k)\mathrm{d}x = \int_\Omega \int_{\mathbb{R}^{m\times n}} \phi(x, A)\mathrm{d}\nu_x^M(A)\mathrm{d}x. \tag{2.13}$$

Thus we can conclude that $\inf_{y\in V} I(y) \leq \min_{\nu\in\mathcal{G}^p_{u_D}} \bar{I}(\nu)$.

To show the equality suppose that by contradiction there exists $\tilde{\nu} \in \mathcal{G}^p_{u_D}$ such that $\bar{I}(\tilde{\nu}) < \bar{I}(\nu^M)$. Then there has to exist a sequence $\{z_k\}_{k=1}^{\infty} \subset V$ generating $\tilde{\nu}$. Moreover due to Lemma 2.9 this sequence can be chosen in such a way that $\{\phi(x, \nabla z_k(x)\}_{k=1}^{\infty}$ is weakly convergent in $L^1(\Omega, \mathbb{R})$ and therefore

$$I(\tilde{\nu}) < \lim_{k\to\infty} \int_\Omega \phi(x, \nabla z_k)\mathrm{d}x,$$

which together with eq. (2.13) gives a contradiction with the fact that $\{v_k\}$ is an infimizing sequence of the functional I. □

Let us now again return to Example 1.1. For this particular example we already gave a infimizing sequence $\{v_k(x)\}_{k=1}^{\infty} \subset W^{1,p}(\Omega, \mathbb{R}^m)$, if Ω is a cube. This sequence converges weakly to $v(x) = x$ but this v is not a minimizer for I. However the Young measure associated to this infimizing sequence $\nu = 1/2\delta_{U_1} + 1/2\delta_{U_2}$, where δ denotes the Dirac mass is according to Proposition 2.7 a minimizer for the functional $\bar{I}$. We see that in the concept of Young measures the minimizing

measure gives us information on how the infimizing sequence behaves. Although the concepts of searching the minimum if $\bar{I}$ or on I^* are related, it is a good idea to include the gradient measure treatment if we want the minimizer to still carry some features of the minimizing sequence.

Let us furthermore state and prove a lemma about the convergence of Young measures, which will be important for the analysis of problems treating shape memory alloys.

Lemma 2.10. *Let there exist a constant $c_2 > 0$ such that for a Carathéodory function ϕ it holds that*

$$|\phi(x, F)| \leq c_2(1 + |F|^{p-\epsilon}),$$

for some $p \in (1, \infty)$, a.e. $x \in \Omega$ and every $F \in \mathbb{R}^{m\times n}$ and some small positive ϵ. Moreover let $\{\nu^k\}_{k=1}^{\infty}$ be a weakly converging sequence in $L^{\infty}_w(\Omega, \mathcal{M}(\mathbb{R}^{m\times n}))$, where $\mathcal{M}(\mathbb{R}^{m\times n})$ denotes the set of Radon measures on $\mathbb{R}^{m\times n}$, such that*

$$\int_\Omega \int_{\mathbb{R}^{m\times n}} |A|^p \mathrm{d}\nu_x^k(A)\mathrm{d}x \leq C, \tag{2.14}$$

for some non-negative constant C independent of k. If ν denotes the weak limit of the sequence $\{\nu^k\}_{k=1}^{\infty}$ then, for at least a subsequence*

$$\lim_{k\to\infty} \int_\Omega \int_{\mathbb{R}^{m\times n}} \phi(x, A)\mathrm{d}\nu_x^k(A)\mathrm{d}x = \int_\Omega \int_{\mathbb{R}^{m\times n}} \phi(x, A)\mathrm{d}\nu_x(A)\mathrm{d}x. \tag{2.15}$$

Proof. We need to prove that for any small ε there exists k such that

$$\int_\Omega \left| \int_{\mathbb{R}^{m\times n}} \phi(x, A)\mathrm{d}\nu_x^k(A) - \int_{\mathbb{R}^{m\times n}} \phi(x, A)\mathrm{d}\nu_x(A) \right| \mathrm{d}x \leq 2\varepsilon. \tag{2.16}$$

First of all let us verify that

$$\int_\Omega \int_{\mathbb{R}^{m\times n}} |A|^p \mathrm{d}\nu_x(A)\mathrm{d}x \leq C. \tag{2.17}$$

To see this define a cut-off function $\psi_R : \mathbb{R}^{m\times n} \to \mathbb{R}$ such that ψ_R is continuous and $\psi_R(A) = 0$ if $|A| > R$ and $\psi_R(A) = 1$ if $|A| \leq R - 1$. Then

$$\begin{aligned} \liminf_{k\to\infty} \int_\Omega \int_{\mathbb{R}^{m\times n}} |A|^p \mathrm{d}\nu_x^k(A)\mathrm{d}x &\geq \liminf_{k\to\infty} \int_\Omega \int_{\mathbb{R}^{m\times n}} \psi_R |A|^p \mathrm{d}\nu_x^k(A)\mathrm{d}x \\ &= \int_\Omega \int_{\mathbb{R}^{m\times n}} \psi_R |A|^p \mathrm{d}\nu_x(A)\mathrm{d}x \end{aligned}$$

Now note that the sequence of functions $\psi_R|\cdot|^p$ is monotone-increasing as $R \to \infty$. By the usage of Fatou's lemma we get that

$$C \geq \liminf_{k\to\infty} \int_\Omega \int_{\mathbb{R}^{m\times n}} |A|^p \mathrm{d}\nu_x^k(A)\mathrm{d}x \geq \int_\Omega \int_{\mathbb{R}^{m\times n}} |A|^p \mathrm{d}\nu_x(A)\mathrm{d}x. \tag{2.18}$$

which concludes the proof of the first assertion.

Then rewrite (2.16) as

$$\int_\Omega \left| \int_{\mathbb{R}^{m\times n}} \phi(x,A)\mathrm{d}\nu_x^k(A) - \int_{\mathbb{R}^{m\times n}} \phi(x,A)\mathrm{d}\nu_x(A) \right| \mathrm{d}x =$$
$$= \int_\Omega \left| \int_{\mathbb{R}^{m\times n}} \frac{\phi(x,A)}{|A|^{p-\epsilon}} |A|^{p-\epsilon}\mathrm{d}\nu_x^k(A) - \int_{\mathbb{R}^{m\times n}} \frac{\phi(x,A)}{|A|^{p-\epsilon}} |A|^{p-\epsilon}\mathrm{d}\nu_x(A) \right| \mathrm{d}x.$$

By the usage of the Young inequality we get

$$\int_\Omega \left| \int_{\mathbb{R}^{m\times n}} \frac{\phi(x,A)}{|A|^{p-\epsilon}} |A|^{p-\epsilon}\mathrm{d}\nu_x^k(A) - \int_{\mathbb{R}^{m\times n}} \frac{\phi(x,A)}{|A|^{p-\epsilon}} |A|^{p-\epsilon}\mathrm{d}\nu_x(A) \right| \mathrm{d}x \leq$$
$$\leq \int_\Omega \left| \int_{\mathbb{R}^{m\times n}} \left(K(\alpha) \left(\frac{\phi(x,A)}{|A|^{p-\epsilon}} \right)^{\frac{p}{\epsilon}} + \alpha |A|^p \right) (\mathrm{d}\nu_x^k(A) - \mathrm{d}\nu_x(A)) \right| \mathrm{d}x,$$

where α may be, due to the Young's inequality used, chosen as small as needed. In our case we shall choose α such that $2C\alpha$ is smaller than ε. Naturally, $K(\alpha)$, also following from the Young's inequality, is due to such a choice very big, but due to the convergence $\nu^k \overset{*}{\rightharpoonup} \nu$ we may choose k to satisfy condition (2.16), which gives the sought result. □

In the preceding theorem also gives that the weak* limit of a sequence of gradient Young measures satisfying (2.14) is again a gradient Young measure. The assertion is formulated in the following proposition.

Proposition 2.11. *Let $\{\nu^k\}_{k=0}^\infty$ be a sequence of gradient Young measures satisfying (2.14). Then ν such that $\nu^k \overset{*}{\rightharpoonup} \nu$ in $L^\infty_w(\Omega, \mathcal{M}(\mathbb{R}^{m\times n}))$ is again a gradient Young measure.*

Proof. This follows already from the previous lemma. Namely, we are to show that for $\nu = \{\nu_x\}_{x\in\Omega}$ there exists a sequence $\{u_l\}_{l=1}^\infty$ such that for all φ Carathédory with a growth strictly smaller than p

$$\lim_{l\to\infty} \int_\Omega \varphi(\nabla u_l)\mathrm{d}x = \int_\Omega \int_{\mathbb{R}^{m\times n}} \varphi(A)\mathrm{d}\nu_x(A)\mathrm{d}x.$$

But any Young measure ν^k from the considered sequence is generated by a sequence of gradients; moreover due to (2.14) all generating sequences are uniformly bounded by C. A suitably chosen diagonal sequence then generates ν due to Lemma 2.10. □

To end up this section let us now characterize the set of $\mathcal{G}^p_{u_D}$.

Theorem 2.12. [14] *Let $p \in (1,\infty)$ and let $\nu = \{\nu_x\}$ be a family of probability measures. Then $\nu = \{\nu_x\}$ is associated to some bounded sequence $\{z_k(x)\}_{k=1}^\infty \subset W^{1,p}(\Omega,\mathbb{R}^m)$ if and only if*

1. *$\nabla z(x) = \int_{\mathbb{R}^{m\times n}} A\mathrm{d}\nu_x(A)$ for a.e. $x \in \Omega$ and for some $z \in W^{1,p}(\Omega,\mathbb{R}^m)$ being the weak limit of the sequence $\{z_k(x)\}_{k=1}^\infty$,*

[14] This is a result of Kinderlehrer and Pedregal [29]; by the same authors a preceding result was proved which states the same assertion but requires $p = \infty$ [27].

2. $\psi(\nabla z(x)) \leq \int_{\mathbb{R}^{m\times n}} \psi(A)\mathrm{d}\nu_x(A)$ *for a.e.* $x \in \Omega$ *and for all* ψ *quasiconvex, continuous and bounded from below, such that* $\lim_{|A|\to\infty} \frac{\psi(A)}{1+|A|^p}$ *exists and is finite,*

3. $\int_{\mathbb{R}^{m\times n}} |A|^p \mathrm{d}\nu_x(A) < \infty$ *for a.a.* x *in* Ω.

Obviously one of drawbacks we encountered when using I^* namely the fact that we are unable to characterize the set of quasiconvex functions still persists. This can be seen from the above theorem as the decision whether a measure is or is not a gradient Young measure requires the explicit characterization of quasiconvex functions. To treat the problem somehow in numerical simulations we may restrict our attention to so called laminates being special Young measures, which will be treated in the next section.

2.3 Rank-1 convexity and laminates

We shall start by giving a definition of rank-1 convex functions:

Definition 2.13. [15] We say that $\varphi : \Omega \times \mathbb{R}^{m\times n} \to \mathbb{R}$ is rank-1 convex if

$$\varphi(x, \lambda F_1 + (1-\lambda)F_2) \leq \lambda\varphi(x, F_1) + (1-\lambda)\varphi(x, F_2). \tag{2.19}$$

for all $\lambda \in [0,1]$, a.e. $x \in \Omega$ and all F_1, F_2 such that $\mathrm{rank}(F_1 - F_2) \leq 1$

Clearly it is much easier to determine whether a function is or is not rank-1 convex than to verify whether it is quasiconvex. In general any function that is quasiconvex is also rank-1 convex, but the opposite does not hold, as Šverák's counterexample shows (see [64]). Therefore if we denoted the rank-1 convex envelope of any function ϕ, being the supremum of all rank-1 convex function lying underneath ϕ, $R\phi$ the following general identities hold

$$Q\phi \leq R\phi \leq \phi, \tag{2.20}$$

$$\min_{v\in V} \int_\Omega Q\phi(x,v)\mathrm{d}x = \inf_{v\in V} \int_\Omega R\phi(x,v)\mathrm{d}x = \inf_{v\in V} \int_\Omega \phi(x,v)\mathrm{d}x. \tag{2.21}$$

The first identity is an easy corollary of the already mentioned fact that any quasiconvex function is rank-1 convex. The second follows from the first one and Proposition 2.3.

Note that as quasiconvexity is a necessary condition for weak lower continuity we cannot assure the minimum of the rank-1 convex envelope to exist. It may therefore seem useless to speak about rank-1 convexity since our main goal when starting this chapter was to assure existence of minimizers. However the rank-1 convex envelope is related to a subset of gradient Young measures called laminates and if we have some reason to assume that the underlying measure for the minimizing sequence will be a laminate (and in modelling the behaviour of shape memory alloys this is a reasonable assumption), the construction of a rank-1 convex envelope is quite natural. We shall now give the definition of a laminate.

[15] The notion of rank-1 convexity was introduced by Morrey [48].

Definition 2.14. The set $\{\lambda_i, F_i\}_{i=1}^{2^l}$ for $\lambda_i > 0$ for all i and $\sum_{i=1}^{2^l} \lambda_i = 1$ is said to satisfy the lamination condition of the l-th order if

1. for $l = 1$ $\operatorname{rank}(F_1 - F_2) \leq 1$,
2. for $l > 1$ (after possibly rearranging indices) $\operatorname{rank}(F_1 - F_2) \leq 1, \operatorname{rank}(F_3 - F_4) \leq 1 \ldots \operatorname{rank}(F_{2^l-1} - F_{2^l}) \leq 1$ and the set $\{\tilde{\lambda}_i, \tilde{F}_i\}_{i=1}^{2^{l-1}}$ where

$$\begin{aligned} \tilde{\lambda}_1 &= \lambda_1 + \lambda_2, & \tilde{F}_1 &= \tfrac{\lambda_1}{\tilde{\lambda}_1} F_1 + \tfrac{\lambda_2}{\tilde{\lambda}_1} F_2 \\ \tilde{\lambda}_2 &= \lambda_3 + \lambda_4, & \tilde{F}_4 &= \tfrac{\lambda_3}{\tilde{\lambda}_2} F_3 + \tfrac{\lambda_4}{\tilde{\lambda}_2} F_4 \\ &\vdots & &\vdots \\ \tilde{\lambda}_{2^{l-1}} &= \lambda_{2^l-1} + \lambda_{2^l}, & \tilde{F}_{2^{l-1}} &= \tfrac{\lambda_{2^l-1}}{\tilde{\lambda}_{2^l-1}} F_{2^l-1} + \tfrac{\lambda_{2^l}}{\tilde{\lambda}_{2^l-1}} F_{2^l} \end{aligned}$$

   satisfies the lamination condition of order $l - 1$.

Definition 2.15. Let $\{\lambda_i, F_i\}_{i=1}^{2^l}$ be a set that satisfies the lamination condition of the order l. Then the gradient parametrized measure $\nu^l = \sum_{i=1}^{2^l} \lambda_i \delta_{F_i}$ where δ is the Dirac mass is called a laminate of the l-th order. The weak* limit for $l \to \infty$ in the sense of measures of laminates of the order l again a gradient parametrized measure (cf. [54, page 164]) called simply *laminate*.

Clearly a laminate of any order is also a laminate. In Example 1.1, which we should have in mind throughout this chapter, we already saw that the underlying gradient measure for the infimizing sequence considered there is $\nu = 1/2\delta_{U_1} + 1/2\delta_{U_2}$. This is, as U_1 and U_2 are rank-1 connected, a laminate of the first order. In this case therefore it is sufficient to restrict our attention to laminates only.

However in more complicated cases, for example in the cases when forces act on the investigated body we cannot be sure that the underlying Young measure will be a laminate of finite order. Nevertheless, as already mentioned, the restriction of our view to laminates of finite order is not only an acceptable restriction for modelling but also necessary for numerical implementations. Especially if we are interested in numerical treatment it is useful to have a recursive scheme to construct the rank-1 convex envelope. How this can be done is shown in the next proposition (see Kohn and Strang [30] or Dacorogna [14, Section 5.1]).

Proposition 2.16. *Let $\varphi : \mathbb{R}^{m\times n} \to \mathbb{R}$ be bounded from below. Then for any $Y \in \mathbb{R}^{m\times n}$ it holds that*

$$\begin{aligned} R\varphi(F) &= \lim_{k\to\infty} R_k\varphi(F) \quad \text{where} \\ R_0\varphi &= \varphi \quad \text{and} \\ R_{k+1}\varphi F &= \inf \{\lambda R_k\varphi(F_1) + (1-\lambda) R_k\varphi(F_2), \text{ where } \lambda \in [0,1] \\ &\qquad \text{such that } F = \lambda F_1 + (1-\lambda)F_2 \text{ and } \operatorname{rank}(F_1 - F_2) \leq 1\} \end{aligned}$$

or equivalently

$$R\varphi(F) = \inf \left\{ \int_{\mathbb{R}^{m\times n}} \varphi(A) \mathrm{d}\nu(A) \text{ where } \nu \text{ is a laminate such that } F = \int_{\mathbb{R}^{m\times n}} A \mathrm{d}\nu(A) \right\}$$

Proof. First note that the sequence $R_k\varphi(F)$ is non-increasing for any matrix F, as $R_{k+1}\varphi(F) \leq 1/2R_k\varphi(F) + 1/2R_k\varphi(F) = R_k\varphi(F)$. Since also φ is bounded from below the limit $\lim_{k\to\infty} R_k\varphi(F)$ exists and is finite for every matrix F.

Second we shall show that $\lim_{k\to\infty} R_k\varphi(F)$ is a rank-1 convex function. It follows directly from definition that

$$R_{k+1}\varphi(\lambda F_1 + (1-\lambda)F_2) \leq \lambda R_k\varphi(F_1) + (1-\lambda)R_k\varphi(F_2)$$

for any F_1, F_2 that are rank-1 connected and all λ between zero and one. As this holds for any k taking the limit for $k \to \infty$ already gives rank-1 convexity. We thus know that $\phi \geq R\varphi(F) \geq \lim_{k\to\infty} R_k\varphi(F)$.

Third as $R\varphi$ is by definition a rank-1 convex function it has to hold that $R\varphi(\lambda F_1 + (1-\lambda)F_2) \leq \lambda R\varphi(F_1) + (1-\lambda)R\varphi(F_2) \leq \lambda\varphi(F_1) + (1-\lambda)\varphi(F_2)$ for all F_1, F_2 that are rank-1 connected and all $\lambda \in [0,1]$. From this follows (by taking the infimum on both sides) that $R\varphi \leq R_1\varphi$ which proves the theorem by recursion. □

Note that a minimization on the partial envelopes R_k from the above theorem corresponds to minimizing $\bar{I}$ on laminates of the order k. We are thus able to find a numerical way to search for minima of functionals where the underlying Young measure of the infimizing sequence is a laminate of any order. However, as anticipated, not every homogeneous gradient Young measure is a laminate. However most observed microstructure in shape memory alloys are laminates and therefore the description by laminates is still useful.

Even if the minimizing gradient measure is not a laminate we still can use the laminate description. The problem is then discretized on a finite element mesh and a laminate is taken as an approximative minimizer on any element. The sequence of such laminates converges with mesh refinement (weakly*) to the minimizing measure even if this is not a laminate. We shall give more details on this in next chapter.

Chapter 3

Analysis of quasi-static evolution of a SMA specimen under loading

In this chapter we shall put results obtained in the Chapter 1 on physical background into a mathematically rigorous framework and define what we will understand to be a quasi-static evolution problem of shape memory alloy specimen subject to loads. In addition, we shall prove that a solution to such a problem does exist.

We shall follow the works of Mielke and Theil [43], [44], Mielke and Roubíček [41], Kružík, Mielke and Roubíček [34] as well as Mielke and Francfort [17] and paraphrase some of the arguments from the publications above to extend the theory also to non-zero and time-dependent boundary conditions. Such an extension is desirable as in this work (cf. Chapter 6) contrary to previous works [34] or [60] we analyse in simulations the behaviour of a specimen subject to Dirichlet and not Neumann loads. This new kind of loading allows to see effects that could not be simulated before, but are observed in experiments (e.g. [50]).

Although we mostly follow the works cited above the foundation stone for the mathematical treatment of the behaviour of shape memory alloys as presented here was already laid by Ball and James [5], [6]

3.1 Definitions of solutions

We have seen that from fundamental physical laws, namely the balance of momentum, the conservation of energy and the second law of thermodynamics the energy conservation (1.24) and the stability of the process (1.25) follow. It seems therefore natural to use these two concepts to define what a solution of the process when loading a specimen of a shape memory alloy has to satisfy.

In Chapter 2 we saw however that an energy minimizer needs not to exist, even for time-independent problems. So, it proved useful to relax the problem. As we cannot assume that in the time dependent case, which is even more complicated, a solution to the unrelaxed problem will exist, we shall therefore introduce the relaxed Helmholtz free energy as

$$\psi_R^{\mathrm{Or}}(x, u^{\mathrm{Or}}, \nu^{\mathrm{Or}}) = \int_{\mathbb{R}^{3\times 3}} \psi(x, u^{\mathrm{Or}}(x) + x, \mathbb{I} + A)\mathrm{d}\nu(A). \tag{3.1}$$

Here we introduced a new notation, namely the superscript "Or" which is an abbreviation for *original* and was introduced here to indicate that the Young measure, the displacement and the Helmholtz free energy were not shifted by the Dirichlet boundary condition. This shift will be introduced later and we shall see that it will be useful for the analysis.

After relaxation the Young measure ν must also be taken in account as a variable describing the process. Moreover the phase distribution function, represented by the vector of volume fractions, is another important description parameter which is needed to calculate the dissipation during the process and needs therefore to be considered as a variable describing the process. As already mentioned the Young measure ν, at least if it has the form of a laminate, can be interpreted as an indicator of the phase distribution. Therefore it is not surprising that we shall define the following general relation between the Young measure and the phase distribution function, represented by the vector of volume fractions (see for example [34])

$$\lambda^{\mathrm{Or}}(x) = \int_{\mathbb{R}^{3\times 3}} L^{\mathrm{Or}}(A)\mathrm{d}\nu^{\mathrm{Or}}(A). \tag{3.2}$$

Here $L^{\mathrm{Or}} : \mathbb{R}^{3\times 3} \to \mathbb{R}^{M+1}$ is a phase indicator function and M is the number of martensitic variants.

Let us now define the space Q^{Or} in which we shall search for solution of the loading problem:

$$\begin{aligned} Q^{\mathrm{Or}} = \{&(u^{\mathrm{Or}}, \nu^{\mathrm{Or}}, \lambda^{\mathrm{Or}}) \in W^{1,p}(\Omega, \mathbb{R}^3) \times \mathcal{G}^p_{u_D} \times W^{\alpha,r}(\Omega, \mathbb{R}^{M+1}) \text{ such that} \\ &u^{\mathrm{Or}}_{|\Gamma_D} = u_D;\ \nabla u^{\mathrm{Or}}(x) = \int_{\mathbb{R}^{3\times 3}} A\mathrm{d}\nu^{\mathrm{Or}}_x(A),\ \text{and } \lambda^{\mathrm{Or}}_i(x) \geq 0 \text{ for} \\ &i = 1 \dots M+1, \sum_{i=1}^{M+1} \lambda^{\mathrm{Or}}_i = 1 \text{ for a.a. } x \in \Omega\} \end{aligned} \tag{3.3}$$

Note that we did not include condition (3.2) in the definition of the set of all admissible solutions, which allowed for the variables λ^{Or} and ν^{Or} to be independent. This is because it shall be enough to require that condition (3.2) is satisfied approximately by means of penalization.

In this definition of all admissible processes we require them to satisfy the Dirichlet boundary condition. As this condition is time dependent handling, it by requiring it through a space definition as above is rather difficult. Therefore, as anticipated, we shall apply a useful trick and shift the original problem. Take a triple $q^{\mathrm{Or}} = (u^{\mathrm{Or}}, \nu^{\mathrm{Or}}, \lambda^{\mathrm{Or}})$ be in Q^{Or} and suppose that the Dirichlet boundary condition $u_D(x,t)$ admits for any time $t \in [0,T]$ an extension $\tilde{u}_D(x,t)$ into the domain Ω satisfying $\tilde{u}_D \in W^{1,p}(\Omega, \mathbb{R}^3)$ and $\tilde{u}_{D_{|\Gamma_D}} = u_D$. Then we shall denote $q = (u, \nu, \lambda)$ a triple from the space

$$\begin{aligned} Q = \{&(u, \nu, \lambda) \in W^{1,p}(\Omega, \mathbb{R}^3) \times \mathcal{G}^p_0 \times W^{\alpha,r}(\Omega, \mathbb{R}^{M+1}) \text{ such that} \\ &u_{|\Gamma_D} = 0;\ \nabla u(x) = \int_{\mathbb{R}^{3\times 3}} A\mathrm{d}\nu_x(A),\ \text{and } \lambda_i(x) \geq 0 \text{ for} \qquad (3.4) \\ &i = 1 \dots M+1, \sum_{i=1}^{M+1} \lambda_i = 1 \text{ for a.a. } x \in \Omega\}. \qquad (3.5) \end{aligned}$$

Note that the connections between the original triple q^{Or} and the triple from the new space is $u(x) = u^{\mathrm{Or}}(x) - \tilde{u}_D(x)$ and $\lambda(x) = \lambda^{\mathrm{Or}}(x)$ for a.a. x in Ω.

According to this definition we shall shift also the Helmholtz free energy and the function L^{Or} from (3.2). Then the functions ψ_R and L are defined through the following relations

$$\psi_R(t, x, q) = \psi^{Or}(x, q^{Or}), \tag{3.6}$$

$$\lambda^{Or}(x) = \lambda(x) = \int_{\mathbb{R}^{3\times 3}} L(t, A)\mathrm{d}\nu_x, \tag{3.7}$$

which have to hold for almost all x in Ω. Note that since the Dirichlet boundary condition depends on time the new shifted function depend explicitly on time even though the unshifted functions did not.

As we have already defined the relaxed shifted Helmholtz free energy, we may also define the relaxed Gibbs free energy for any $q \in Q$

$$\begin{aligned} G_R^0(t, q(t)) = &\int_\Omega \psi_R(t, x, q)\mathrm{d}x - \int_\Omega (x + u(t, x) + \tilde{u}_D(x, t))f(t, x)\mathrm{d}x \\ &- \int_{\Gamma_N} (x + u(t, x) + \tilde{u}_D(x, t))g(t, x)\mathrm{d}S + \epsilon \left\|\lambda\right\|_{\alpha,r}^r \\ &+ K \int_\Omega \mathrm{Pen}\left(\lambda - \int_{\mathbb{R}^{3\times 3}} L(t, A)\mathrm{d}\nu_x\right)\mathrm{d}x, \end{aligned} \tag{3.8}$$

where

$$\left\|\lambda\right\|_{\alpha,r} = \left(\frac{1}{4}\int_\Omega\int_\Omega \frac{|\lambda x - \lambda\tilde{x}|^r}{|x - \tilde{x}|^{3+r\alpha}}\mathrm{d}x\mathrm{d}\tilde{x}\right)^{1/r} \tag{3.9}$$

is a regularization term, and $\mathrm{Pen}(\lambda - \int_{\mathbb{R}^{3\times 3}} L(t, A)\mathrm{d}\nu_x)$ is a penalty that assures that condition (3.2) will be satisfied approximately.

Moreover let us extend the definition of the Gibbs free energy to all $\tilde{q} \in W^{1,p}(\Omega, \mathbb{R}^3) \times \mathcal{G}_0^p \times L^1(\Omega, \mathbb{R}^{M+1})$ in the following way

$$G_R(t, \tilde{q}(t)) = \begin{cases} G_R(t, \tilde{q}(t)) & \text{if } \tilde{q}(t) \in Q, \\ +\infty & \text{otherwise.} \end{cases} \tag{3.10}$$

First of all we clarify how we may characterize the loading problem of a shape memory alloy specimen.

Definition 3.1. Assume having a quasi-static process in which we consider loading of a shape memory alloy specimen, characterized by a Gibbs free energy G_R and a dissipation D (as in (1.23)), subject to loads, characterized by the Dirichlet boundary condition u_D, the Neumann boundary condition g and a volume force f. Moreover let the process be started from an initial state q_0 then we shall denote the quasi-static evolution problem characterized by the preceding quantities briefly as the (G_R, D, u_D, g, f)-problem.

Definition 3.2. [1] The process $q : [0, T] \to Q$ will be called an energetic solution to the (G_R, D, u_D, g, f)-problem, if it satisfies

[1] The concept of energetic solutions for rate-independent processes (as the one considered here) was introduced by Mielke; from the rich bibliography published by him and collaborators considering this topic we may refer the reader to e.g. [44].

1. *the stability condition*:

$$G_R(t, q(t)) - G_R(t, \tilde{q}(t)) \leq D(q(t), \tilde{q}(t)) \tag{3.11}$$

for all $t \in [0, T]$ and all $\tilde{q} \in Q$,

2. *the energetic equality*: whenever $q(t) \in Q$ then $\partial_t G_R(t, q(t))$ exists and is continuous and moreover

$$G_R(t_2, q(t_2)) - G_R(t_1, q(t_1)) + \mathrm{Diss}_{[t_1,t_2]} = \int_{t_1}^{t_2} \partial_t G_R(t, q(t)) \mathrm{d}t, \tag{3.12}$$

It may not be obvious at first sight how the energy equality formulated here relates to the balance of energy (1.24) derived from physical first principles. To see the relation between these two equations suppose that the Helmholtz free energy depends on the position and the deformation gradient only i.e. $\psi^{\mathrm{Or}} = \psi^{\mathrm{Or}}(x, \nabla u)$. Moreover suppose that it is continuously differentiable with respect to its second argument and satisfies an appropriate growth condition (A1) from the next section. In addition, assume that the external forces f and g and the extension of the boundary condition $\tilde{u}_D$ are continuously differentiable in time. Then by using Lebesgue's dominated convergence theorem we get

$$\begin{aligned}
\partial_t G_R(t, q(t)) = &- \int_\Omega \frac{\partial f}{\partial t}(x,t) u^{Or}(x,t) \mathrm{d}x - \int_{\Gamma_N} \frac{\partial g}{\partial t}(x,t) u^{Or}(x,t) \mathrm{d}S + \\
&+ \int_\Omega \int_{\mathbb{R}^{3\times 3}} \frac{\partial \psi}{\partial A}(x, A) \frac{\partial}{\partial t} \nabla \tilde{u}_D(x,t) \mathrm{d}\nu_x(A) \mathrm{d}x - \\
&- \int_\Omega f(x,t) \frac{\partial \tilde{u}_D}{\partial t}(x,t) \mathrm{d}x - \int_{\Gamma_N} g(x,t) \frac{\partial \tilde{u}_D}{\partial t}(x,t) \mathrm{d}S + \\
&+ \partial_t \int_\Omega \mathrm{Pen}\left(\lambda - \int_{\mathbb{R}^{3\times 3}} L(t, A) \mathrm{d}\nu_x \mathrm{d}x\right)
\end{aligned} \tag{3.13}$$

Plugging this relation into (3.12) we see the correspondence with the energy balance (1.24) except for the last term coming from the penalty. Naturally we cannot see any correspondence to this "penalization force" as we did not include it in the physical formulation.

3.2 Data qualifications and time discretization

In this section we shall formalize the assumptions on the Helmholtz free energy the Dirichlet boundary condition and the outer forces. To do so let us first establish the notion of convergence on the space Q.

Definition 3.3. We say that $q^k = (u^k, \nu^k, \lambda^k) \in W^{1,p}(\Omega, \mathbb{R}^3) \times \mathcal{G}_0^p \times W^{\alpha,r}(\Omega, \mathbb{R}^{M+1})$ converges weak* to a $q = (u, \nu, \lambda) \in W^{1,p}(\Omega, \mathbb{R}^3) \times L^\infty_w(\Omega, \mathcal{M}(\mathbb{R}^{3\times 3})) \times W^{\alpha,r}(\Omega, \mathbb{R}^{M+1})$ and denote it as $q^k \overset{*}{\rightharpoonup} q$ if $u_k \rightharpoonup u \in W^{1,p}((\Omega, \mathbb{R}^3)$, $\nu^k \overset{*}{\rightharpoonup} \nu \in L^\infty_w(\Omega, \mathcal{M}(\mathbb{R}^{3\times 3}))$ and $\lambda_k \rightharpoonup \lambda \in W^{\alpha,r}(\Omega, \mathbb{R}^{M+1})$

Remark 3.4. Note that, unless we can assure that $\{\nu^k\}$ above satisfy (2.14) we cannot know that the limiting ν indeed is a gradient Young measure. However, since in what follows we will always be able to assure this condition we shall sometimes shortly write that $q^k \overset{*}{\rightharpoonup} q$ in Q if the above convergences are satisfied.

Further we shall list data qualifications that will be of need throughout the whole chapter.

(A1) *Helmholtz free energy*: Let ψ^{Or} be Carathéodory function and let moreover $\psi^{\mathrm{Or}}(x,\cdot) \in C^1(\mathbb{R}^{3\times 3})$ for a.a. $x \in \Omega$. Further assume that there exist non-negative constants c_0, c_1, c_3 such that

$$c_0|A|^p - c_1 \leq \psi^{\mathrm{Or}}(x,A) \leq c_1(1+|A|^p), \tag{3.14}$$

$$\left|\frac{\partial \psi^{\mathrm{Or}}}{\partial A}(x,A)\right| \leq c_3(1+|A|^{p-1}), \tag{3.15}$$

are satisfied for a.a. x in Ω and p corresponds to the definition of the state space Q in (3.4).

(A2) *Dissipation*: We assume that the dissipation is a (not necessarily symmetric) pseudo-metric on the space Q, i.e. it holds

$$D(q_1,q_2) \geq 0 \quad \forall q \in Q, \quad \lambda_1 = \lambda_2 \Leftrightarrow D(q_1,q_2) = 0, \tag{3.16}$$

$$D(q_1,q_3) \leq D(q_1,q_2) + D(q_2,q_3) \quad \forall q \in Q. \tag{3.17}$$

In addition we require the dissipation to be weakly* continuous, meaning that whenever $q_1^k \overset{*}{\rightharpoonup} q_1$ and $q_2^k \overset{*}{\rightharpoonup} q_2$ in Q then $D(q_1^k,q_2^k) \to D(q_1,q_2)$, and the following bound

$$C_{D1}\left\|\lambda_1-\lambda_2\right\|_{L^1(\Omega,\mathbb{R}^{M+1})} \leq D(q_1,q_2) \leq C_{D2}\left\|\lambda_1-\lambda_2\right\|_{L^1(\Omega,\mathbb{R}^{M+1})}, \tag{3.18}$$

for some non-negative constants C_{D1} and C_{D2} to be satisfied.

(A3) *Volume force*: Let

$$f \in C^1([0,T], L^{p^{*'}}(\Omega,\mathbb{R}^3)), \tag{3.19}$$

where p corresponds to (3.4) and $[0,T]$ is the time interval on which the time dependent problem is solved.

(A4) *Surface force*: Let

$$g \in C^1([0,T], L^{p^{\sharp'}}(\Gamma_N,\mathbb{R}^3)), \tag{3.20}$$

(A5) *Boundary Condition*: Let

$$u_D \in C^1([0,T], W^{1-\frac{1}{p},p}(\Gamma_D,\mathbb{R}^3)), \tag{3.21}$$

which assures that there exists an extension of this boundary condition $\tilde{u}_D$ such that $\tilde{u}_{D_{|\Gamma_D}} = u_D$ and $\tilde{u}_D \in C^1([0,T], W^{1,p}(\Omega,\mathbb{R}^3))$.

(A6) *Phase Distribution Function*: Let the function $L(t) : \mathbb{R}^{3\times 3} \to \mathbb{R}^{M+1}$ satisfy the growth condition $|L(t, A)| \leq C(1 + |A|^{p-\epsilon})$ for all t, a non-negative constant C and some small positive ϵ.

Moreover we require that $L(t, A)$ is continuously differentiable in time and that $|\partial_t L(t, A)| \leq C(1 + |A|^{p-\epsilon})$.

(A7) *Penalization function*: Let $\mathrm{Pen} : \mathrm{R}^{M+1} \to [0, \infty]$ be an increasing[2] continuously differentiable function, such that

$$\left|\frac{\mathrm{dPen}}{\mathrm{d}r}\right| \leq C_1(1 + \mathrm{Pen}(r)), \tag{3.22}$$

for some constant C_1. Moreover we require the following growth conditions to be satisfied

$$\mathrm{Pen}(r) \leq C_2(1 + |r|^q), \tag{3.23}$$

where q is chosen to satisfy both $q \leq \tilde{r} - \delta$ and $q(p - \epsilon) < p$. Here ϵ refers to the growth of the phase distribution function, $\tilde{r}$ refers to the embedding $W^{\alpha,r}(\Omega, \mathbb{R}^{M+1}) \hookrightarrow L^{\tilde{r}}(\Omega, \mathbb{R}^{M+1})$ and δ is some small positive number. Note that at least for q=1 this condition can be satisfied.

If these assumptions are satisfied it holds that whenever we have a q in Q there exists a continuous derivative of the Gibbs free energy with respect to time as is demanded in Definition 3.2.

Let us at this point prove a lemma that shall be of use at several points later.

Lemma 3.5. *Let* $(\lambda^k, \nu^k) \overset{*}{\rightharpoonup} (\lambda, \nu)$ *in* $W^{\alpha,r}(\Omega, \mathbb{R}^{M+1}) \times L^\infty_w(\Omega, \mathcal{M}(\mathbb{R}^{3\times 3}))$ *such that (2.14)*[3] *holds true. Moreover assume (A6)-(A7) above to be satisfied. Then*

$$\int_\Omega \mathrm{Pen}\left(\lambda_k - \int_{\mathbb{R}^{3\times 3}} L(t, A)\mathrm{d}\nu^k_x(A)\right)\mathrm{d}x \to \int_\Omega \mathrm{Pen}\left(\lambda - \int_{\mathbb{R}^{3\times 3}} L(t, A)\mathrm{d}\nu_x(A)\right)\mathrm{d}x. \tag{3.24}$$

Proof. In view of assumption (A7), namely the growth condition (3.23), it suffices to show that both $\lambda^k \to \lambda$ and $\int_{\mathbb{R}^{3\times 3}} L(t, A)\mathrm{d}\nu^k_x \to \int_{\mathbb{R}^{3\times 3}} L(t, A)\mathrm{d}\nu^k_x$ in $L^q(\Omega, \mathbb{R}^{M+1})$[4]. As $W^{\alpha,r}(\Omega, \mathbb{R}^{M+1})$ is compactly embedded into $L^q(\Omega, \mathbb{R}^{M+1})$ for the sequence $\{\lambda^k\}_{k=1}^\infty$ this will surely hold.

Let us therefore turn our attention to the convergence of $\int_{\mathbb{R}^{3\times 3}} L(t, A)\mathrm{d}\nu^k_x$ and estimate

$$\int_\Omega \left|\int_{\mathbb{R}^{3\times 3}} L(t, A)\mathrm{d}\nu^k_x\right|^q \mathrm{d}x \leq C \int_\Omega \int_{\mathbb{R}^{3\times 3}} |L(t, A)|^q \mathrm{d}\nu^k_x \mathrm{d}x. \tag{3.25}$$

As $|L(t, A)|^q$ has still a growth that is strictly less than p we may use Lemma 2.10 to show the desired convergence. □

[2]Here we mean increasing in the sense that if $|r_1| > |r_2|$ for some r_1, r_2 in $\mathbb{R}^{M+1}$ then $\mathrm{Pen}(r_1) > \mathrm{Pen}(r_1)$.

[3]Recall that (2.14) demanded that

$$\int_\Omega \int_{\mathbb{R}^{m\times n}} |A|^p \mathrm{d}\nu^k_x(A)\mathrm{d}x \leq C,$$

is satisfied for some positive constant C.

[4]Here we think of the map $x \to \int_{\mathbb{R}^{3\times 3}} L(t, A)\mathrm{d}\nu^k_x$ as to be in $L^q(\Omega, \mathbb{R}^{M+1})$.

When searching for an energetic solution we shall use Rothe's method of time discretization and divide the interval $[0,T]$ into N time-steps and for the sake simplicity of notation assume that the partitions we choose are equi-distant. However we shall not need this assumption at any point of the proof below[5]. First we shall search for solutions of the following time-incremental minimization problem

Definition 3.6. Let q_0 be the initial condition of the energetic process. Then when denoting $q_N^0 = q_0$ we shall call q_N^k the solution of

$$\begin{aligned} \text{Minimize} \quad & G_R(t_k, \tilde{q}) + D(q_N^{k-1}, \tilde{q}) \\ \text{s.t. } & \tilde{q} \in Q. \end{aligned} \tag{3.26}$$

where $0 = t_0 \leq t_1 \leq t_2 \ldots \leq t_{N-1} \leq t_N = T$ is some partition of the interval $[0,T]$ such that $\min_{k=1\ldots N} t_k - t_{k-1} = \tau$.

We shall first show the existence of solutions for this minimization problem and the way this solution can be found.

Proposition 3.7. [6] *Let the assumptions (A1)-(A7) be satisfied. Then there exists a solution q_τ^k to the problem (3.26).*

Proof. Let us take a sequence q^l such that

$$G_R(t_k, q^l) + D(q_\tau^{k-1}, q^l) \to \inf_{\tilde{q}\in Q} G_R(t_k, \tilde{q}) + D(q_N^{k-1}, \tilde{q}).$$

As the space Q is non-empty we know that $G_R(t_k, q^l) + D(q_N^{k-1}, q^l) \leq C$ for some positive constant C. Because moreover $D(q_N^{k-1}, q^l)$ as well as the penalization function are non-negative due to assumption (3.16) and (A7) we may estimate

$$\begin{aligned} G_R(t_k, q^l) &\geq c_0 \int_\Omega \int_{\mathbb{R}^{3\times 3}} |A + \nabla u_D(t_k, x)|^p \mathrm{d}\nu_x^k(A)\mathrm{d}x - c_1|\Omega| - \left\langle l(t_k), u^l \right\rangle + \left\|\lambda^l\right\|_{\alpha,r} \\ &\geq C \int_\Omega \int_{\mathbb{R}^{3\times 3}} |A|^p \mathrm{d}\nu_x^k(A)\mathrm{d}x - c^* \int_\Omega |\nabla u_D|^p \mathrm{d}x - c_1|\Omega| - C^* \left\|l(t)\right\|_{(W^{1,p}(\Omega))^*}^{p'} \\ &- \epsilon \left\|u^l\right\|_{W^{1,p}(\Omega)}^p + \left\|\lambda^l\right\|_{\alpha,r} \\ &\geq \tilde{c} \left\|u^l\right\|_{W^{1,p}} - c^* \int_\Omega |\nabla u_D|^p \mathrm{d}x - c_1|\Omega| + \left\|\lambda^l\right\|_{\alpha,r} - C^* \left\|l(t)\right\|_{(W^{1,p}(\Omega))^*}^{p'}, \end{aligned}$$

where we used (3.14), Theorem 2.12, the Friedrichs' inequality and denoted

$$\langle l(t), u\rangle = \int_\Omega f(x,t)(x + u_D(x,t) + u)\mathrm{d}x + \int_{\Gamma_N} g(x,t)(x + u_D(x,t) + u)\mathrm{d}S, \tag{3.27}$$

$$\left\|l(t)\right\|_{W^{1,p}(\Omega,\mathbb{R}^3)^*} = \left\|f\right\|_{L^{p^{*\prime}}(\Omega,\mathbb{R}^3)} + \left\|g\right\|_{L^{p^{\sharp\prime}}(\Gamma_N,\mathbb{R}^3)}. \tag{3.28}$$

[5] Quite on the contrary we will assume that the partition can be chosen arbitrarily.

[6] Note that this is, in principle, a corollary of Proposition 2.7, as it is this Proposition that assures minimizers for the Young measure part. The proof given here however is different.

We conclude that $q^l \overset{*}{\rightharpoonup} q$ for some q in $W^{1,p}(\Omega,\mathbb{R}^3)\times L^\infty_w(\Omega,\mathcal{M}(\mathbb{R}^{3\times 3}))\times W^{\alpha,r}(\Omega,\mathbb{R}^{M+1})$. Finally, from the properties of the convergence of Young measures and the weak lower semi-continuity of norms, the weak continuity of the dissipation and Lemma 3.5 above, we conclude that

$$G_R(t_k,q)+D(q_N^{k-1},q)\leq \liminf_{l\to\infty} G_R(t_k,q^l)+D(q_N^{k-1},q^l)=\inf_{\tilde{q}\in Q} G_R(t_k,\tilde{q})+D(q_N^{k-1},\tilde{q}_N).$$

Moreover from Proposition 2.11 ν is a gradient Young measure and by exploiting also Lemma 2.10 we get that truly $q\in Q$. Therefore q is the searched minimizer of the problem (3.26). □

Of course, when recalling previous chapter, this result is not satisfactory as we are not able to describe the minimizer q_N^k which applies especially to the Young measure part. In the following proposition however we shall give a method how the solution of the problem (3.26) can be found numerically.

Proposition 3.8. [7] *Let Ω be a tetrahedral domain and let τ_h be a regular triangulation of the domain such that τ_m for $m<h$ is a refinement of the mesh τ_h. Let*

$$\begin{aligned} Q_h=\{q\in Q; u\in C(\Omega,\mathbb{R}^3), u_{|K}\in P_1\ \forall K\in\tau_h,\\ \lambda\in L^\infty(\Omega,\mathbb{R}^3), \lambda_{|K}\in P_0\ \forall K\in\tau_h, \nu=\delta_{\nabla u}\}. \end{aligned} \tag{3.29}$$

Then there exists a minimizer to the problem $\inf_{\tilde{q}\in Q_h} G_R(t_k,\tilde{q})+D(q_N^{k-1},\tilde{q})$ denoted $q_N^{h,k}$. Moreover as h tends to zero this sequence converges weakly to q_N^k which is a solution to the problem (3.26).*

Proof. As the space Q_h is finite-dimensional and $G_R(t_k,\tilde{q})+D(q_N^{k-1},\tilde{q}_N)$ is continuous and coercive there exists a minimizer to this problem $q_N^{h,k}$. Moreover as we can choose the mesh τ_m for $m<h$ to be a refinement of the mesh τ_h it holds that

$$G_R(t_k,q_N^{m,k})+D(q_N^{k-1},q_N^{m,k})\leq G_R(t_k,q_N^{h,k})+D(q_N^{k-1},q_N^{h,k}),$$

and the bound $G_R(t_k,q_N^{h,k})+D(q_N^{k-1},q_N^{h,k})\leq C$ holds uniformly in h. From the coercivity assumptions (see also the proof of Proposition 3.7) we therefore conclude that $q_N^{m,k}\overset{*}{\rightharpoonup}\tilde{q}_N^k$ in $W^{1,p}(\Omega,\mathbb{R}^3)\times L^\infty_w(\Omega,\mathcal{M}(\mathbb{R}^{3\times 3}))\times W^{\alpha,r}(\Omega,\mathbb{R}^{M+1})$.

As the triangulation is regular we know that for any $\lambda\in W^{\alpha,r}(\Omega,\mathbb{R}^{M+1})$ there exists a sequence $\{\lambda_h\}_{h>0}$ such that λ_h is in $W^{\alpha,r}(\Omega,\mathbb{R}^{M+1})$ piecewise constant and $\lambda_h\to\lambda$ strongly. Similarly for any $u\in W^{1,p}(\Omega,\mathbb{R}^3)$ there exists a sequence $\{u_h\}_{h>0}$ such that u_h is in $C(\Omega,\mathbb{R}^{M+1})$ piecewise linear such that $u_h\to u$.

We now have to show that $\tilde{q}_N^k$ is a solution to (3.26). Due to Proposition 3.7 we may choose q_N^k a minimizer of the time incremental problem. Moreover let choose $\{u_m\}_{m=0}^\infty$ the underlying sequence for the Young measure ν_N^k. Using the above said

[7] Note that this is, as can be seen from the proof, a corollary of Theorem 2.4 and the well known fact that functions from Sobolev spaces may be approximated continuous piecewise linear function (see e.g. [23]).

let us choose sequences $\{u_m^h\}_{h>0}$ converging to u_m and $\{\lambda^h\}_{h>0}$ converging to λ_N^k. Then the triple $q^{m,h} = (u_m^h, \delta_{\nabla u_m^h}, \lambda^h)$ is in Q_h and therefore

$$\begin{aligned} G_R(t_k, \tilde{q}_N^k) + D(q_N^{k-1}, \tilde{q}_N^k) &\leq \liminf_{h\to 0} G_R(t_k, q_N^{h,k}) + D(q_N^{k-1}, q_N^{h,k}) \\ &\leq \liminf_{h\to 0} G_R(t_k, q_N^{m,h}) + D(q_N^{k-1}, q_N^{m,h}) \\ &= G_R(t_k, q_N^k) + D(q_N^{k-1}, q_N^k) + \\ &+ \left(\int_\Omega \psi(t, \nabla u_m) \mathrm{d}x - \int_\Omega \int_{\mathbb{R}^{3\times 3}} \psi(t, A) \mathrm{d}\nu_x^k(A) \mathrm{d}x \right) \\ &+ \int_\Omega \mathrm{Pen}(\lambda - L(t, \nabla u_m)) - \mathrm{Pen}\left(\lambda - \int_{\mathbb{R}^{3\times 3}} L(t, A) \mathrm{d}\nu_x^k \right) \mathrm{d}x \end{aligned}$$

which follows from the growth condition (3.14) and continuity properties. Moreover taking the limit for m tending to infinity makes the last two terms (in brackets) vanish and gives the sought result. □

3.3 A-priori estimates

According to previous section a solution to the minimization problem (3.26) denoted q_N^k exists. Let us introduce a function q_N defined on $[0, T]$ as follows

$$q_N(t) = \begin{cases} q_0 & \text{for } t = 0, \\ q_N^k & \text{for } t \in (t_{k-1}, t_k]. \end{cases} \tag{3.30}$$

Our goal throughout the next sections will be to show that as N tends to ∞ this q_N converges to an energetic solution. In this section however we shall concentrate on a preliminary step - the a-priori estimates as formulated in the next proposition.

Proposition 3.9. [8] *Let the assumptions (A1)-(A7) be satisfied. Then there exist positive constants C_1 and C_2 such that the following bounds hold true*

$$\|u_N\|_{L^\infty([0,T], W^{1,p}(\Omega, \mathbb{R}^3))} \leq C_0, \tag{3.31}$$

$$\|\lambda_N\|_{BV([0,T], L^1(\Omega, \mathbb{R}^{M+1})) \cap L^\infty([0,T], W^{\alpha,r}(\Omega, \mathbb{R}^{M+1}) \cap L^\infty(\Omega, \mathbb{R}^{M+1}))} \leq C_1. \tag{3.32}$$

Moreover a discrete stability condition

$$G_R(t_k, q_N(t_k)) \leq G_R(t_k, \tilde{q}) + D(q_N(t_k), \tilde{q}) \quad \forall\ \tilde{q} \in Q, \tag{3.33}$$

and the discrete two-sided energy inequality

$$\begin{aligned} \int_{t_{k-1}}^{t_k} \partial_t G_R(s, q_N(t_k)) \mathrm{d}s &\leq G_R(t_k, q_N(t_k)) + \mathrm{Diss}_{[t_{k-1}, t_k]} - G_R(t_{k-1}, q_N(t_{k-1})) \\ &\leq \int_{t_{k-1}}^{t_k} \partial_t G_R(s, q_N(t_{k-1})) \mathrm{d}s, \end{aligned} \tag{3.34}$$

are satisfied for all $k = 0, 1 \ldots N$.

[8] This partly paraphrases the arguments of e.g. [34] or [17].

Proof. Let us begin by proving the second part of the theorem. First of all as $q_N(t_k)$ solves (3.26) we know that for all $\tilde{q}$ in Q

$$G_R(t_k, q_N(t_k)) + D(q_N(t_{k-1}), q_N(t_k)) \leq G_R(t_k, \tilde{q}) + D(q_N(t_{k-1}), \tilde{q}), \tag{3.35}$$

which together with (3.17) gives

$$\begin{aligned} G_R(t_k, q_N(t_k)) &\leq G_R(t_k, \tilde{q}) + D(q_N(t_{k-1}), \tilde{q}) - D(q_N(t_{k-1}), q_N(t_k)) \\ &\leq G_R(t_k, \tilde{q}) + D(q_N(t_k), \tilde{q}), \end{aligned}$$

being the desired stability condition.

We shall now turn to the discrete energy inequality. Choosing in (3.35) for $\tilde{q} = q_N(t_{k-1})$ we get

$$\begin{aligned} &G_R(t_k, q_N(t_k)) + D(q_N(t_{k-1}), q_N(t_k)) \leq G_R(t_k, q_N(t_{k-1})) \\ &= G_R(t_k, q_N(t_{k-1})) - G_R(t_{k-1}, q_N(t_{k-1})) + G_R(t_{k-1}, q_N(t_{k-1})) \\ &= G_R(t_{k-1}, q_N(t_{k-1})) + \int_{t_k}^{t_{k-1}} \partial_t G_R(s, q_N(t_{k-1}))\mathrm{d}s. \end{aligned}$$

Moreover as we already know that $q_N(t_{k-1})$ satisfies the discrete stability condition (3.33)

$$\begin{aligned} &G_R(t_{k-1}, q_N(t_{k-1})) \leq G_R(t_{k-1}, q_N(t_k)) + D(q_N(t_{k-1}), q_N(t_k)) \\ &= G_R(t_{k-1}, q_N(t_k)) + D(q_N(t_{k-1}), q_N(t_k)) + G_R(t_k, q_N(t_k)) - G_R(t_k, q_N(t_k)) \\ &= G_R(t_k, q_N(t_k)) + D(q_N(t_{k-1}), q_N(t_k)) - \int_{t_k}^{t_{k-1}} \partial_t G_R(s, q_N(t_k)\mathrm{d}s, \end{aligned}$$

which gives exactly the first part of the discrete energy inequality.

Next turn our attention to the estimates on q_N. Choosing $\tilde{q} = 0$ in (3.35) leads to

$$\begin{aligned} &G_R(t_k, q_N(t_k)) + D(q_N(t_{k-1}), q_N(t_k)) \leq G_R(t_k, 0) + D(q_N(t_{k-1}), 0) \leq \\ &\leq c_1|\Omega| + \|\nabla \tilde{u}_D\|^p_{W^{1,p}(\Omega,\mathbb{R}^3)} + c_2\|\dot{f}(x,t_k)\|_{L^{p^{*\prime}}(\Omega,\mathbb{R}^3)} + \\ &+ c_3\left\|\dot{g}(x,t_k)\right\|_{L^{p^{\sharp\prime}}(\Gamma_N,\mathbb{R}^3)} + c_4\left\|u_D(x,t)\right\|_{W^{1,p}(\Omega,\mathbb{R}^3)} \leq C, \end{aligned}$$

where we used (3.18) and the fact that $\lambda_N(t_k) \in Q$. Therefore

$$\begin{aligned} &\|u_N\|_{L^\infty([0,T],W^{1,p}(\Omega,\mathbb{R}^3))} \leq C_0, \\ &\|\lambda_N\|_{L^\infty([0,T],W^{\alpha,r}(\Omega,\mathbb{R}^{M+1})\cap L^\infty(\Omega,\mathbb{R}^{M+1}))} \leq C_1, \end{aligned}$$

and it only remains to prove that λ_N is of bounded variation. To see this note that because of the growth condition (3.15) and (A7) and the uniform bounds already established $\partial_t G_R(t, q_{t_k}) \leq C$ is bounded uniformly in time and k. From this and the second part of the two-sided energy estimate and the growth condition (3.18) estimate already follows. □

Note that during this proof we have shown even more than anticipated in the proposition namely we established that the Gibbs free energy as well as its time derivative are uniformly bounded which means that

$$G_R(t, q_N(t)) \leq C_1, \tag{3.36}$$
$$|\partial_t G_R(t, q_N(t))| \leq C_2, \tag{3.37}$$

where C_1, C_2 are some constants and $t = t_k$, but independently of k and N. Together with the coercivity conditions this also implies that $\int_\Omega \int_{\mathbb{R}^3} |A|^p \mathrm{d}\nu_N(A)\mathrm{d}x$ remains uniformly bounded with refinement of the division of the interval $[0, T]$.

3.4 Convergence

We are now at the point to prove our main theorem, namely to show that the solutions of the time incremental minimization problem (3.26) converge in a weak sense to an energetic solution of the loading problem of a shape memory alloy.

Theorem 3.10. *Let q_N be the solutions of the time incremental minimization problem (3.26) and let q_0 be a stable initial state. Then there exist a finer net $\{q_{N_\xi}\}_{\xi\in\Xi}$ and $q : [0, T] \to Q$ such that $q_{N_\xi}(t) \overset{*}{\rightharpoonup} q(t)$ for all t in $[0, T]$. Moreover $q(t)$ is an energetic solution satisfying the conditions required in Definition 3.2 and $q(0) = q_0$.*

Proof. [9] We shall divide the proof into several steps. In the first we shall choose the subsequences of q_N, or to be more rigorous finer nets, and by using the a-priori estimates we will see that they do weakly converge to a q in Q. In the second step we shall see that the limiting q is a stable state and in the third and fourth step we will see that it even more satisfies the energetic equality.

Step 1: Choice of subsequences

First of all note that due to the bound of λ_N we may choose by an application of the Helly's selection principle in a generalized form (cf. [38]) a subsequence of λ_N (not relabelled) such that $\lambda_N(t) \rightharpoonup \lambda(t)$ in $W^{\alpha,r}(\Omega, \mathbb{R}^{M+1})$ and $\lambda \in BV([0, T], L^1(\Omega, \mathbb{R}^{M+1})) \cap L^\infty([0, T], W^{\alpha,r}(\Omega, \mathbb{R}^{M+1}) \cap L^\infty(\Omega, \mathbb{R}^{M+1}))$.

Moreover, the set $L^\infty_w(\Omega, \mathcal{M}(\mathbb{R}^{3\times3}))$ is metrizable and compact, henceforth the set $L^\infty_w(\Omega, \mathcal{M}(\mathbb{R}^{3\times3}))^{[0,T]}$ is compact as well by exploiting the Tikhonov theorem ([65]; note that the German spelling for "Tikhonov" is "Tychonoff"). Therefore we may choose a finer $\{q_{N_\xi}\}_{\xi\in\Xi}$ (such that the convergence above is not destroyed) to assure that ν_{N_ξ} converges weakly* to some $\nu = \{\nu(t)\}_{t\in[0,T]}$ in $L^\infty_w(\Omega, \mathcal{M}(\mathbb{R}^{3\times3}))^{[0,T]}$.

If we can moreover assure that the limit $q(t)$ is in Q we will already establish the convergence in the theorem.

Step 2: Stability of the limit function and it belonging to Q

Let us fix t arbitrary. As already noted, $L^\infty_w(\Omega, \mathcal{M}(\mathbb{R}^{3\times3}))$ is metrizable hence we may choose a sequence $\{q_{N_l}\}$ converging to $q(t)$.

[9] In the proof we shall follow the structure suggested in [17], however some arguments are modified for the situation investigated here.

Due to the note after the proof of Proposition 3.9 the function

$$\mathrm{DG}_N(t) = \begin{cases} \partial G_R(t_k, q_N(t_k)) & \text{if } t \in (t_{k-1}, t_k] \\ \partial G_R(\tau, q_0) & \text{if } t = 0 \end{cases}$$

is bounded in $L^\infty([0,T])$ and therefore there exists $\mathrm{DG}_\infty(t)$ such that at least for a subsequence $\mathrm{DG}_N \overset{*}{\rightharpoonup} \mathrm{DG}_\infty$. Moreover for the current time t we define $\mathrm{DG}_{pt}(t) = \limsup_{N\to\infty} DG(t)$. Clearly we may choose a subsequence of the indexes N_l denoted again N_l[10] such that $\mathrm{DG}_{pt}(t) = \lim_{N_{l(t)}\to\infty} \mathrm{DG}$. When using Fatou's lemma we get that

$$\int_0^t \mathrm{DG}_\infty(s)\mathrm{d}s = \limsup_{N\to\infty} \int_0^t \mathrm{DG}(s)\mathrm{d}s \le \int_0^t \limsup_{N\to\infty} \mathrm{DG}(s)\mathrm{d}s = \int_0^t \mathrm{DG}_{pt}(s)\mathrm{d}s.$$

We now want to show that the above defined $q(t)$ is stable. Let us denote t_{N_l} the points of the respective partitions N_l (as chosen above) such that $t_{N_l} \to t$[11]. Then we shall first examine the convergence of the penalization function. Surely $\lambda_{N_l}(t) \to \lambda(t)$ in $L^q(\Omega, \mathbb{R}^{M+1})$ where q correspond to (A7). As far as the penalization function is concerned we have that

$$\begin{aligned}\int_{\mathbb{R}^{3\times3}} L(t_{N_l}, A)\mathrm{d}\nu_{N_l}(t)(A) = &\left(\int_{\mathbb{R}^{3\times3}} L(t_{N_l}, A)\mathrm{d}\nu_{N_l}(t)(A) - \int_{\mathbb{R}^{3\times3}} L(t, A)\mathrm{d}\nu_{N_l}(t)(A)\right) \\ &+ \int_{\mathbb{R}^{3\times3}} L(t, A)\mathrm{d}\nu_{N_l}(t)(A).\end{aligned}$$

Now note that due to Lemma 3.5 and also due to the continuity of L in time $\int_{\mathbb{R}^{3\times3}} L(t_{N_l}, A)\mathrm{d}\nu_{N_l}(t)(A) \to \int_{\mathbb{R}^{3\times3}} L(t, A)\mathrm{d}\nu(t)(A)$ in $L^q(\Omega, \mathbb{R}^{M+1})$. Therefore

$$\begin{aligned}&\int_\Omega \mathrm{Pen}\left(\lambda_{N_l}(t) - \int_{\mathbb{R}^{3\times3}} L(t_{N_l}, A)\mathrm{d}\nu_{N_l}(t)(A)\right)\mathrm{d}x \to \\ &\to \int_\Omega \mathrm{Pen}\left(\lambda(t) - \int_{\mathbb{R}^{3\times3}} L(t, A)\mathrm{d}\nu(t)(A)\right)\mathrm{d}x. \end{aligned} \tag{3.38}$$

By similar arguments we establish that[12]

$$\partial_t \int_\Omega \int_{\mathbb{R}^{3\times3}} \psi(t_{N_l}, A)\mathrm{d}\nu_{N_{l(t)}}(t)(A)\mathrm{d}x \to \partial_t \int_\Omega \int_{\mathbb{R}^{3\times3}} \psi(t, A)\mathrm{d}\nu(x)(A)\mathrm{d}x, \tag{3.39}$$

$$\begin{aligned}&\partial_t \int_\Omega \mathrm{Pen}\left(\lambda_{N_l}(t) - \int_{\mathbb{R}^{3\times3}} L(t_{N_l}, A)\mathrm{d}\nu_{N_l}(t)(A)\right)\mathrm{d}x \to \\ &\to \partial_t \int_\Omega \mathrm{Pen}\left(\lambda(t) - \int_{\mathbb{R}^{3\times3}} L(t, A)\mathrm{d}\nu(t)(A)\right). \end{aligned} \tag{3.40}$$

As the Helmholtz free energy ψ has a p-growth we are not entitled to use Lemma 2.10 directly. However we may establish that

$$\liminf_{N_l\to\infty} \int_\Omega \int_{\mathbb{R}^{3\times3}} \psi(t_{N_l}, A)\mathrm{d}\nu_{N_{l(t)}}(t)(A)\mathrm{d}x \le \int_\Omega \int_{\mathbb{R}^{3\times3}} \psi(t, A)\mathrm{d}\nu(x)(A)\mathrm{d}x, \tag{3.41}$$

[10] But note that this further subsequence may depend on the choice on the fixed time t.

[11] Of course the points have to exist as $N_l \to \infty$

[12] Realize that $\partial_t\psi$ has due to (3.14) a growth that is strictly lower than p and also due to the continuity assumed in (A5) $\partial_t\nabla\tilde{u}_D(t_{N_l}) \to \partial_t\nabla\tilde{u}_D(t)$ in $L^p(\Omega, \mathbb{R}^{3\times3})$.

which follows similarly as above by using the continuity of ψ with respect to time; in addition as ψ is bounded from below (guaranteed by (3.14)) we can establish that

$$\liminf_{N_l\to\infty}\int_\Omega\int_{\mathbb{R}^{3\times 3}}\psi(t,A)\mathrm{d}\nu_{N_{l(t)}}(t)(A)\mathrm{d}x\le\int_\Omega\int_{\mathbb{R}^{3\times 3}}\psi(t,A)\mathrm{d}\nu(x)(A)\mathrm{d}x. \tag{3.42}$$

Using the above results and the discrete stability condition we get that

$$\begin{aligned}G_R(t,q(t))&\le\liminf_{N_{l(t)}\to\infty}G(t_{N_l},q_{N_l}(t))\\&\le\liminf_{N_l\to\infty}G(t_{N_l},\tilde q)+D(q_{N_l}(t),\tilde q)=G(t,\tilde q)+D(q(t),\tilde q),\end{aligned}$$

for any $\tilde q\in Q$. This in particular implies that ν is a gradient Young measure (by the usage of Proposition 2.11) and by using also Proposition 2.10 $q\in Q$. Therefore we may set $\tilde q=q$ and obtain

$$\lim_{N_l\to\infty}\int_\Omega\int_{\mathbb{R}^{3\times 3}}\psi(t_{N_l},A)\mathrm{d}\nu_{N_{l(t)}}(t)(A)\mathrm{d}x=\int_\Omega\int_{\mathbb{R}^{3\times 3}}\psi(t,A)\mathrm{d}\nu(x)(A)\mathrm{d}x. \tag{3.43}$$

Step 3: Upper energy estimate From the above said and condition (A7) we may deduce that

$$\partial_t G_R(t_{N_l},q_{N_l}(t)\to\partial_t G_R(t,q(t))$$

as $N_l\to\infty$ and therefore $\mathrm{DG}_{pt}(t)=\partial_t G_R(t,q(t))$ for all t in $[0,T]$. When using the two sided energy inequality (3.34) and calculating the limit we get that

$$\begin{aligned}&G_R(t,q(t))+\mathrm{Diss}_{[0,t]}-G(0,q_0)\le\liminf_{N_l\to\infty}G_R(t_{N_l},q_{N_l})+\mathrm{Diss}_{[0,t]}-G(0,q_0)\\&\le\liminf_{N_l\to\infty}\left(\int_0^t\partial_t G_R(t_{N_l+1},q_{N_l}(s))\mathrm{d}s-\int_{t_{N_l}}^t\partial_t G_R(t_{N_l+1},q_{N_l}(s)\mathrm{d}\right)\\&\le\int_0^t\partial_s G_R(s,q(s))\mathrm{d}s,\end{aligned}$$

where we used the fact that that under restriction (A2) the total variation is weakly lower semi-continuous. This already gives the upper energy estimate.

Step 4: Lower energy estimate Let us use the already established discrete lower energy inequality in the form

$$G_R(t_{k+1},q_N(t_{k+1}))-G_R(t_k,q_N(t_k))+D(q_N(t_k,q_N(t_{k+1}))\ge\int_{t_k}^{t_{k+1}}\partial_t G_R(s,q_N(t_k))\mathrm{d}s,$$

where $0=t_1\le t_2\dots t_{K-1}\le t_N=t$ is some division of the interval $[0,T]$[13] and $t\in[0,T]$. When summing the above relation we get that

$$G_R(t,q_N(t))-G_R(0,q_0)+\mathrm{Diss}_{[0,T]}\ge\sum_{k=0}^N\int_{t_k}^{t_{k+1}}\partial_t G_R(s,q_N(t_k))\mathrm{d}s,$$

[13]Here we exploit that the arguments above were nowhere dependent of the partition of the interval $[0,T]$.

when $t = t_k$ for some k in $[0, N]$. Then we shall rewrite the sum in the upper relation as

$$\sum_{k=0}^{N} \int_{t_k}^{t_{k+1}} \partial_t G_R(s, q_N(t_k)) \mathrm{d}s = \sum_{k=0}^{N} (t_{k+1} - t_k) \partial_t G_R(t_k, q_N(t_k)) \mathrm{d}s + \sum_{k=0}^{N} \int_{t_k}^{t_{k+1}} \partial_t G_R(s, q_N(t_k)) - \partial_t G_R(t_k, q_N(t_k)) \mathrm{d}s.$$

However when recalling that

$$\begin{aligned} \partial_t G_R(s, q(t_k)) = &- \int_\Omega \frac{\partial f}{\partial t}(x, s) u^{Or}(x, t_k) \mathrm{d}x - \int_{\Gamma_N} \frac{\partial g}{\partial s}(x, t) u^{Or}(x, t_k) \mathrm{d}S + \\ &+ \int_\Omega \int_{\mathbb{R}^{3\times 3}} \frac{\partial \psi}{\partial A}(x, A) \frac{\partial}{\partial t} \nabla \tilde{u}_D(x, s) \mathrm{d}\nu_x(A) \mathrm{d}x - \\ &- \int_\Omega f(x, s) \frac{\partial \tilde{u}_D}{\partial t}(x, s) \mathrm{d}x - \int_{\Gamma_N} g(x, s) \frac{\partial \tilde{u}_D}{\partial t}(x, s) \mathrm{d}S \\ &+ \partial_t \int_\Omega \mathrm{Pen} \left(\lambda - \int_{\mathbb{R}^{3\times 3}} L(s, A) \mathrm{d}\nu_x \right) \mathrm{d}x \end{aligned}$$

and using the assumption on continuous differentiability in time (A3)-(A7) and by using furthermore integral mean value theorem we get that

$$\begin{aligned} \left| \int_{t_k}^{t_{k+1}} \partial_t G_R(s, q_N) - \partial_t G_R(t_k, q_N) \mathrm{d}s \right| &\leq (t_{k+1} - t_k) \left| \partial_t G_R(s_k, q_\tau) - \partial_t G_R(t_k, q_\tau) \right| \\ &\leq (t_{k+1} - t_k) \epsilon \end{aligned}$$

when ϵ tends to zero with the refinement of the division of the time interval. We therefore conclude that the term $|\sum_{k=0}^{N} \int_{t_k}^{t_{k+1}} \partial_t G_R(s, q_\tau(t_k)) - \partial_t G_R(t_k, q_\tau(t_k)) \mathrm{d}s| \leq T\epsilon$ and therefore converges to zero if the division of the time interval is further refined. The proof of the proposition is finalized by using the Theorem 3.11 below and choosing the partition of the interval in a special way. □

Theorem 3.11. [14] *Let X be a Banach space and $f \in L^1((0, t), X)$. Then there exists a sequence of partitions of the interval $(0, t)$ $0 = t_0^n \leq t_1^n \leq \ldots \leq t_{N(n))}^n = t$ satisfying that $\max_{k=1\ldots N(n)} t_k^n - t_{k-1}^n$ tends to zero with n going to infinity*

$$\lim_{n\to\infty} \sum_{k=1}^{N(n)} \left\| (t_k^n - t_{k-1}^n) f(t_{k-1}^n) - \int_{t_{k-1}^n}^{t_k^n} f(s) \mathrm{d}s \right\| = 0. \tag{3.44}$$

[14] This theorem is due to Dal Maso, Francfort and Toader, see [15, Lemma 4.12] following an idea of Hahn [21].

Chapter 4

Numerical Implementation

In Chapter 3 we gave a proof of existence of energetic solution for quasi-static evolution of a shape memory alloy specimen. The proof given is not only useful from the viewpoint of analysis, but also suggests a kind of recipe how to design an algorithm that would compute the behaviour of a shape memory alloy specimen subject to loads in the quasi-static approximation. Therefore we shall build-up this section similarly as the last one, here however emphasizing the implementational point of view.

A great effort has been undertaken in the past decades to design algorithm that would be capable of computing the quasi-static behaviour of a shape memory alloy specimen. We should mention the pioneer works of Ball and James [5], [6] that came up with the idea to model shape memory alloys in the way presented here and after them a rich number of papers considering this subject can be found e.g. [33], [2], [1], [35], [34], [60].

First of all let us recall that in simulations we may choose the concrete form of the Gibbs free energy, dissipation distance and boundary conditions for the displacement as well as forces acting on the body. The choice of the first two is a constitutive choice we always have to make in modelling to give a description of the material in question. The choice of the latter two reflects the loads we want the material to be exposed to. The choice of these quantities is restricted only by the the fact that assumptions (A1)-(A7) from previous chapter ought to be satisfied.

Let us moreover recall that we are solving the problem on the time interval $[0, T]$ and the domain Ω. Haven chosen the necessary quantities we have to discretize the problem to allow for numerical solutions.

The discretization in time follows exactly the ideas from previous chapter meaning that we choose a division $\{t_k\}_{k=0}^N$ of the interval $[0, T]$. For each time-step k we choose a triangulation of the domain Ω which denotes the domain that is occupied by the material in reference configuration. Note that - as is usual in modelling of solids - although the body may be deformed, the domain Ω remains unchanged as we perform the calculations in reference configuration. Though it is possible to choose a different triangulation for different time-steps in the code developed by the author, mostly the same triangulation for all time-steps is used.

As soon as the loads and the Gibbs free energy as well as the dissipation distance are chosen, the computing variables for the code in a specific time-step k

are the values of the displacement in each vertex as well as the values of the Young measure on each element. However the discretization of the Young measure may not be obvious at first sight and we shall come back to the question how to approximate it in what follows.

4.1 Discretization of displacements

Let us denote $\tau_{k,h}$ the triangulation of the domain in the k-th time-step and let $\{K_i\}_{i=1}^{L}$ be the collection of tetrahedra forming the triangulation. In the specific time-step k we then search for the numerical approximation of the displacement denoted $u_{k,h}$ in the space

$$U_{k,h} = \left\{ u \in C(\bar{\Omega}, \mathbb{R}^3), \text{ s.t. } u_{|K_i} \text{ is affine, } \forall k = 1 \dots M \right\}. \tag{4.1}$$

Moreover we require that $u_{k,h}(x_B) = u_D(t_k, x_B)$ where x_B are all such vertices of the triangulation $\tau_{k,h}$ that $\Gamma_D \cap x_B \neq \emptyset$.

In this definition we see that the discretized displacement enjoys a greater regularity, namely the spatial continuity, than the continuous one. It is therefore not surprising that we have to suppose that the Dirichlet boundary condition is continuous not only in time (which is already assured by assumption (A5) stated in previous chapter) but also in space. This is necessary to allow us to speak about values of the boundary condition in vertices and to satisfy that they are equal to values of the discretized displacement.[1]

Note that the shift of the whole problem with respect to the Dirichlet boundary condition, that was very helpful for mathematical analysis, brings no benefits for numerical solving or implementation. Hence we shall abandon this shift and work with the original problem, as already the definition of the space in which we search for solutions (4.1) suggests.

Note that as the displacement is piecewise affine the displacement gradient, which is the crucial quantity we are interested in, is piecewise constant.

4.2 Discretization of Young measures

The approximation of the Young measure is more complicated and relies on its approximation by a finite-order laminate (cf. e.g [2], [35]) given in Definition 2.14. On every tetrahedron of the triangulation we approximate

$$\nu_{k,h} = \sum_{k=1}^{2^l} \lambda_k \delta_{F_k}, \tag{4.2}$$

such that $\sum_{k=1}^{2^l} \lambda_k = 1$ and the matrices F_k satisfy the the lamination condition (2.19) of the l-th order and moreover $\sum_{k=1}^{2^l} \lambda_k F_k = F = \mathbb{I} + \nabla u$. The last condition assures that the average of the Young measure $\nu_{k,h}$ is exactly the deformation

[1] Note that no such requirement has to be put on the Neumann data, as those occur in the definition of the numerical Gibbs free energy (see (4.6) below) only in integrals.

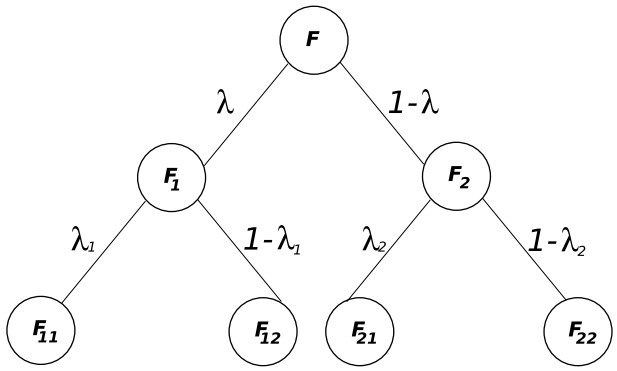

Figure 4.1: The scheme of the rank-1-partition of the deformation in case of a second order laminate.

gradient F. Theoretically any lamination order may be used in the code developed by the author, in practise however second order laminates are used at most.[2] The concrete form of the Young measure as soon as the order of the laminates is fixed can be read from the diagram given in Figure 4.1. Note that the matrices F_1 and F_2 forming the rank-1-partition of the deformation gradient of the first order are fully determined by the deformation gradient itself, a weight λ and two vectors for which it holds

$$F_1 = F + (1-\lambda)\mathbf{a} \otimes \mathbf{n},$$
$$F_2 = F - \lambda \mathbf{a} \otimes \mathbf{n}.$$

These relations are a direct consequence of the fact that F_1 and F_2 are rank-1 connected and moreover $\sum_{k=1}^{2^l} \lambda_k F_k = F$. Similar relations hold also for the matrices $F_{12} \dots F_{22}$ following Figure 4.1.

In the algorithm these vectors and weights are taken as degrees of freedom which assure all compatibility conditions to be satisfied. Geometrically the vector $\mathbf{n}$ represents the normal of the lamination as is shown in Figure 4.2 whereas the vector $\mathbf{a}$ has no obvious geometrical interpretation.

Obviously the approximation of the Young measure by a laminate of a finite order is not exact as we have already seen that not every Young measure is of the form of a laminate. However Proposition 3.8 guarantees that with mesh refinement this approximation will converge weakly* to an energetic solution (of course also the division of the time interval has to be further refined).

4.3 Definition of volume fractions

In the continuous setting presented as above we had to give up our wish to satisfy condition (3.2) exactly and had to be satisfied with a penalization function that guaranteed that this condition shall be satisfied at least approximately. This

[2]This is due to the fact that laminates observed in nature are mostly of the second order (see e.g. [9] or [52]); some new observations suggest that special forms of a laminate of the third order might also be possible [62].

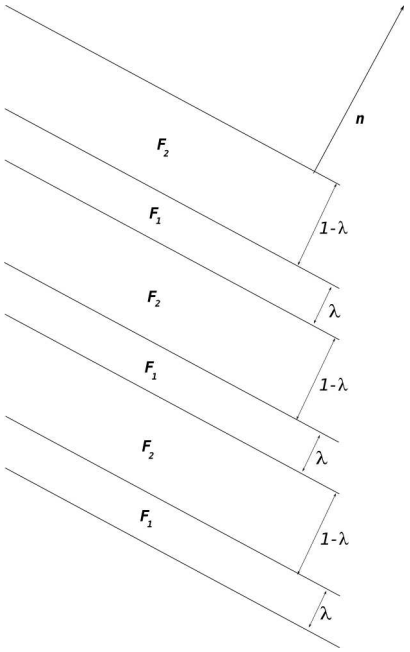

Figure 4.2: First order laminate with a weight λ and a normal $\mathbf{n}$

compromise had to be made due to technical reasons as we would not be able to prove existence of solution in case we insisted on requiring (3.2). These technical difficulties arose mainly due to the shift by the time-dependent Dirichlet boundary conditions, however this shift was necessary too.

In the discrete setting we return to the original problem in the sense, that we do not shift the problem. Therefore there is no necessity for a penalization function to be added to the Gibbs free energy. Hence in every time-step volume fractions are directly calculated by

$$\lambda_{k,h} = \int_{\mathbb{R}^{3\times 3}} \tilde{L}(A)\mathrm{d}\nu_{k,h}, \tag{4.3}$$

where the function $\tilde{L}$ is independent of time[3] and is chosen in the specific form (following e.g. [60])

$$\tilde{L}(A) = \left\{ \frac{d(|FF^{\mathrm{T}} - U_l U_l^{\mathrm{T}}|)}{\sum_{k=1}^{M+1} d(|FF^{\mathrm{T}} - U_k U_k^{\mathrm{T}}|)} \right\}_{l=1}^{M+1}, \tag{4.4}$$

where we used the notation from Chapter 1. For the readers convenience let us shortly repeat that we denote $U_1 \dots U_M$ deformation matrices, each of which corresponds to one variant of martensite. As U_{M+1} we denoted the deformation matrix corresponding to the austenite phase, a natural choice is to consider $U_{M+1} = \mathbb{I}$.

[3]Realize that the only reason why the function L in previous chapter is time dependent is the shift due to the time dependent Dirichlet boundary condition.

The function d, which was not defined yet, is a continuous function $\mathbb{R} \to \mathbb{R}$ such that outside an sufficiently small interval $[-\epsilon, \epsilon]$ it is equal some very small number. The norm $|\cdot|$ is the Frobenius norm[4] defined on matrices.

Such a definition of the function $\tilde{L}$ ensures roughly speaking that as soon as the deformation gradient - or only the matrices forming its rank-1 decomposition in the sense of the laminate chosen - are near to the well of a variant, volume fractions are assigned to this well. However such a definition cannot handle cases when the material has to stay in one phase during a possibly large deformation as no other variant would be more advantageous for the material.

To end up with let us note that determining volume fractions (although they are not degrees of freedom for the code) is not only important for the program output, but also for the computation of the energy dissipated. This can be easily seen in the context of what was said previously in Chapter 1, namely the dissipation is connected to a change of the phase distribution function which may be represented by the vector of volume fractions.

4.4 Discrete problem

First of all denote $Q_{k,h}$ the space of the pairs $(u_{k,h}, \nu_{k,h})$ which satisfy the requirements stated in previous sections. To be more specific

$$\begin{aligned} Q_{k,h} = \{&(u_{k,h}, \nu_{k,h}) \in C(\bar{\Omega}, \mathbb{R}^3) \times \mathcal{G}^p_{u_D} \text{ s.t. } \nu_{k,h} \text{ is a laminate of finite order and} \\ &u_{|K_i} \text{ is affine, } \forall k = 1 \dots M \text{ and } u_{k,h}(x_B) = u_D(t_k, x_B),\ x_B \text{ are vertices s.t.} \\ &\Gamma_D \cap x_B \neq \emptyset\}, \end{aligned} \tag{4.5}$$

where $\tau_{k,h}$ is a regular triangulation of the domain Ω. Let us moreover have an initial condition $(u^0_{k,h}, \nu^0_{k,h})$ that is stable.

In previous section we stated that the penalization term in the Gibbs free energy introduced for the reasons of mathematical analysis is not necessary in the discrete case. Similarly we may drop the regularization term for volume fractions and so return to the original physical Gibbs free energy, however relaxed to Young measures. We therefore define the Gibbs free energy for numerical reasons as

$$G^N(t, q(t)) = \int_\Omega \psi_R^{\mathrm{Or}}(t, x, q)\mathrm{d}x - \int_\Omega (x + u(t,x)) f(t,x)\mathrm{d}x - \int_{\Gamma_N} (x + u(t,x)) g(t,x)\mathrm{d}S, \tag{4.6}$$

where $q = (u, \nu)$ is from the space $Q_{k,h}$, which turns the integrals to summations over the the particular tetrahedra of the triangulation:

$$\begin{aligned} G^N(t_k, q_{k,h}) = &\sum_{K_i \in \tau_h} |K_i| \psi_R(t_k, \nu_{k,h}(K_i), \nabla u_{k,h}(K_i)) - \\ &- \sum_{K_i \in \tau_h} \frac{|K_i|}{4} \sum_{j=1}^{4} (x^j_{K_i} + u(t_k, x^j_{K_i})) f(t_k, x^j_{K_i}) - \sum_{\Gamma_i} \frac{|\Gamma_i|}{3} \sum_{j=1}^{3} (x^j_{\Gamma_i} + u(t_k, x^j_{\Gamma_i})) g(t_k, x^j_{\Gamma_i}) \end{aligned} \tag{4.7}$$

[4]Recall that for a matrix $A \in \mathbb{R}^{3\times 3}$ the Frobenius norm is $|A| = \sqrt{\sum_{i,j=1}^3 a_{ij}^2}$ where $\{a_{ij}\}_{i,j=1}^3$ are the elements of the matrix A.

Here t_k denotes the time in k-th time-step, K_i the tetrahedra of the triangulation, $x^j_{K_i}$ the vertices of the i-th tetrahedron, Γ_i the triangles that lie on the Neumann boundary and $x^j_{\Gamma_i}$ the vertices of these triangles. Moreover by the notation $\nu_{k,h}(K_i)$ we mean the Young measure on the i-th element, as Young measures are constant on each element but have no good meaning in vertices as they might exhibit jumps.

The integration over the boundary is the least advantageous part of this calculation but it is possible to give an easier formula in case the domain of the material is a prism or a cylinder and a constant surface force acts only the the base side (i.e. the one which is perpendicular to all other sides). Let $\mathbf{n}$ be the unit normal of this side. Then we may rewrite

$$g(x + u(t, x)) = (g \otimes \mathbf{n})\mathbf{n}(x + u(t, x)),$$

which gives by the usage of the divergence theorem

$$\int_{\Gamma_N} (x + u(t, x))g\mathrm{d}S = \int_\Omega \mathrm{div}(\mathbf{n} \otimes g(x + u(t, x)))\mathrm{d}x = \int_\Omega (\mathbf{n} \otimes g).(\mathbb{I} + \nabla u(t, x))\mathrm{d}x.$$

In the discrete form then

$$\int_{\Gamma_N} (x + u(t, x))g\mathrm{d}S = \sum_{K_i \in \tau^k} |K_i|(\mathbf{n} \otimes g).(\mathbb{I} + \nabla u(t_k, K_i)), \tag{4.8}$$

where we denoted $\nabla u(t_k, K_i)$ the value of the displacement gradient on the i-th element as it constant element-wise. The implementation of such a formula is much easier and although it may seem that the restriction we had to require are quite strong it covers the most commonly used case of tension experiments.

The dissipation shall be chosen in the same way as it was in physical context or in the framework of mathematical analysis.

Having a stable initial condition, compatible boundary conditions and a time discretization $\{t_k\}_{k=1}^N$ we are solving the problem

$$\begin{aligned} \text{Minimize} \quad & G^n(t_k, \tilde{q}) + D(q^{k-1}_{k,h}, \tilde{q}) \\ \text{s.t.} \quad & \tilde{q} \in Q_{k,h}. \end{aligned} \tag{4.9}$$

This problem is solved by the means of a gradient method with respect to the degrees of freedom.[5] Taking into account that the problem is non-convex and non-smooth as well as the number of degrees of freedom is in the order of thousands for even tens of elements used in the mesh gives us an insight into how complicated the minimization is.

4.5 Two-sided energy inequality

In previous section we noted that the minimization problem we have to calculate in order to simulate the quasi-static behaviour of a shape memory alloy specimen

[5] Recall that these are the three components of the displacement vector in each vertex (besides the vertices on the Dirichlet boundary) and the weights as well as vectors characterizing the Young measure on each element.

in some time-step is a difficult one. Difficult especially in the sense, that due to the dimensions of the problem (thousands of degrees of freedom) and non-convexity of the minimized function a great number of local minima exists. However the algorithm is demanded to choose the global minimum, as only the global minimizer corresponds to a physical state. Hence we have to develop a strategy for global optimization as a gradient method algorithm itself is not capable to do so.

There exist several strategies to search for global optima (see e.g. [24]), but clearly none of them can truly assure that the global minimum is found. In case of problems where the concept of energetic solutions is applicable the verification of the two-sided energy inequality (3.34) has proved to be useful tool for searching of global optima (see [42]). Naturally, when recalling the proof of Proposition 3.9, the two-sided energy inequality is only a necessary condition for the global optimum, it has however the ability to intercept effects described below.

For the readers convenience let us here recall the two-sided energy inequality (3.34) rewritten into the currently used notation

$$\begin{aligned}\int_{t_{k-1}}^{t_k} \partial_t G^N(s, q_{k,h}^k)\mathrm{d}s &\leq G^N(t_k, q_{k,h}^k) + \mathrm{Diss}_{[t_{k-1},t_k]} - G^N(t_{k-1}, q_{k,h}^{k-1}) \\ &\leq \int_{t_{k-1}}^{t_k} \partial_t G^N(s, q_{k,h}^{k-1})\mathrm{d}s. \end{aligned} \tag{4.10}$$

To analyse the selectivity of this two-sided energy inequality we shall treat the upper and lower bound separately.

Let us start with the upper bound which, as we shall see, has nearly no selectivity. Namely, recall that the upper bound of (4.10) verifies (when also taking into account the proof of Proposition 3.9) whether the optimum found by the algorithm in the current time-step has a lower energy than the optimum found in the former step, with a change on the boundary if necessary. However it is quite natural, and therefore implemented in the code presented here, to take exactly the optimum from the previous step as an initial guess for optimization for the current step. Therefore the upper sided inequality verifies only whether the optimum found has a lower than the initial guess, which is naturally satisfied for all good algorithms.

The lower energy inequality on the other hand has some selectivity, because it verifies whether a state found as optimal in the k-th step of the algorithm would not achieve a smaller energy in the $(k-1)$-th step (of course after a change in boundary conditions if necessary) than the optimum found there. To see when the lower energy inequality helps in minimization let us consider the following simplified example.

Example 4.1. Let us suppose that we have to minimize the energy (or more generally the energy plus dissipation) in four steps, which follow after one each other. Of course in every step the shape of the energy distribution changes; we shall suppose that first it is a convex function with one global minimum. In the next step a further local minimum evolves, however the original minimum is still the global minimum. Then in step three and four their positions change in the sense that the new minimum starts to be the global one. The situation is shown

in Figure 4.3, where due to simplicity the energy function is shown only in one dimension. The black dot in this figure denotes the state in which would typically be selected to be optimal by a gradient method algorithm. We see that in step one as well as step two the guess of the algorithm is right, however in step three it stays in the original minimum. Only in step four the algorithm "recognizes" that a deeper local minimum has evolved. However this minimum would have been optimal also in step three and this is exactly what the lower energy inequality verifies. This means that in step four the lower energy inequality would not be satisfied.

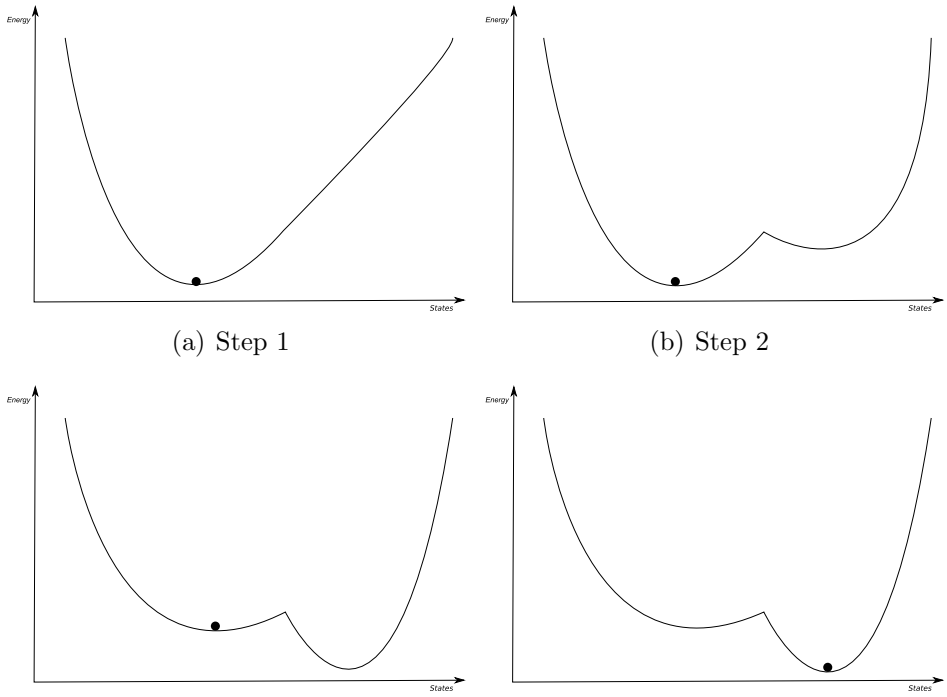

(a) Step 1 (b) Step 2

(c) Step 3 (d) Step 4

Figure 4.3: Example of an evolution of the energy when the two sided energy inequality will not be satisfied. The black dot denotes the state evaluated as optimal by the algorithm

If the two-sided energy inequality is not satisfied the following strategy will be used. As we know that in the previous step there exists a lower local minimum than the one found by the algorithm (namely the one found in the current step), the algorithm returns to the previous time-step and the current state $q^k_{k,h}$ is given to the algorithm as an initial guess. Of course the current step $q^k_{k,h}$ has to be modified in boundary conditions if time varying Dirichlet boundary conditions are used. Then, due to the change in initial guess the algorithm founds a different optimizer and of course for this optimizer the two-sided energy inequality is again verified, which may lead to a further return. The algorithm may return to some time-step even repeatedly, however the number of returns should be finite.

Of course by the usage of this method we can never assure that there is no other local minimum (not "seen" by the algorithm) which might be even better than the found ones.

Nevertheless the practical implementation of this algorithm can give good results as we shall see further in Chapter 6.

4.6 Notes on implementation

In this section we shall give only brief notes on the code, developed by the author, implemented to simulate the behaviour of a specimen of a shape memory alloy when being loaded.

The code has been written in C++ using the concept of object-oriented programming. It is therefore satisfactory to describe the main classes used in the code,which are the following ones, to give some insight into the function of the code.

- *Mesh*: The class *Mesh* uses smaller classes *Vertex*, *Edge*, *Face* and *Element* the meaning of which is straightforward, namely they store and handle the original positions and displacements. Moreover they have built-in functions to return the displacement gradient on each element or to return their area and volume. The class *Mesh* itself handles a mesh file given to the code. It is able to read this file to save it to appropriate variables and pre-processes the mesh in the sense that it calculates the volumes of all elements and also pre-calculates some variables for later use.

  The constructor for the class *Mesh* can be called either without attributes to create an empty mesh or it can be given a mesh file to read in a mesh. Unfortunately the code is not able to do any meshing by itself and needs to be given a mesh file. However in every step a different mesh file may be used although the code has no built-in procedure to select from several mesh files - this selection needs to be done by the user.

- *Material*: The class *Material* stores all information about the current material, namely the distortion matrices of each variant, elastic constants and offsets due to temperature. It is able to read this information from a data file and save it to appropriate variables. Moreover it pre-calculates some matrices that will be useful in energy evaluation. The built-in functions of this class are mostly only functions to return the matrices that might be of need.

- *Model*: The class *Model* is the main class in the code and it includes built-in functions to calculate the energy as soon as it has rank-1 decomposed the deformation gradient, as well as to minimize the energy. Therefore the two classes mentioned before are variables of this class and it is exactly this class that runs their constructors. Moreover the class *Model* is able to load or use default initial conditions, boundary conditions as well as forces. After calculation the class writes the results to appropriate files in VTK-format so that they may be used for visualisation in open source programs such as *ParaView* (more information `www.paraview.org`) or *MayAvi* (see also `mayavi.sourceforge.net`). For verification of the results the class may inform the main program whether the two-sided energy inequality was satisfied.

It may be stressed that most of the built-in functions as well as variables of the class *Model* are set to be *private* which disables the user to alter them (for variables) or call them (for functions) in the main program. This is done to allow inexperienced users for easier orientation as there is only one function *MinimizeEnergy()* that needs to be called after running the constructor to perform the computation. It moreover assures security as it prevents users from changing accidentally some computing variables during evaluation.

Besides these main classes the code uses also some helping classes such as *Polygon* for creating files to visualize the microstructure or *Vector* or *Matrix* for handling vectors or matrices.

As already said the key part of the program is the class *Model* which initializes the model and calculates the discrete Gibbs free energy (4.6). The calculation is quite straightforward, the only interesting part is the way how the laminate of finite order is implemented. When recalling Figure 4.1 we already see that the decomposition of the deformation gradient is in the form of a binary tree. Therefore this algorithmic structure is used also implemented in the code. The relaxed Gibbs free energy density is then evaluated recursively when using the scheme from Lemma 2.16. This recursive implementation is very advantageous, since it allows for usage of laminates of any order with only little change in the code, namely the order of lamination is chosen during initialization of the binary tree in question and may be (with a little change in the code not needed so far) read from a file. Moreover for the program it does not matter whether the binary tree used is symmetric or non-symmetric. The only restriction is that the order and structure of the lamination binary tree needs to be chosen before calculation. At the moment it is not possible to choose the lamination binary tree differently for each step of the calculation, but if this change was desired it could be added with little effort.[6] After having calculated the relaxed discrete Gibbs free energy (4.6) the program performs minimization (4.9). For minimization it uses the external routine *L-BFSG-B* which is a gradient method minimization allowing for bounds on variables subject to minimization (downloadable at `www.ece.northwestern.edu/~nocedal/lbfgsb.html`; a reader interested in computational methods is also referred to articles [12], [69]). As an input for the gradient method the energy gradient with respect to the degrees of freedom must be given. Due to the complexity of the problem the easiest way to evaluate this is to use a library for automatic differentiation. In the code an external library ADOL-C (see further `http://www.math.tu-dresden.de/~adol-c/` or sources [18], [19]) which evaluates the derivatives by operator overloading in C++ is called.

As far as boundary conditions are concerned the program is able to take Dirichlet and Neumann boundary condition into account, however with the restriction that only homogeneous Neumann conditions are considered so far. For both types of boundary conditions the program is able to calculate stress-strain diagrams which are important for comparison with experiment. We may shortly note how

[6] Although it is possible to perform the minimization - thanks to the recursion used - with a laminate of any order the same is not true for visualisation. So far only a non-symmetric laminate of the second order can be visualized.

these stress-strain diagrams are computed. In the case of Neumann conditions the calculation is straightforward as these Neumann conditions themselves represent the stress acting on the body. In the case of Dirichlet boundary conditions (and zero forces acting on the body) $\partial_F \psi_R^{\mathrm{Or}}(\nu_{k,h}, F)$ evaluated at the current deformation gradient is in accord with (1.18) assumed to be the stress.

Simulations calculated with this program can be found in Chapter 6.

Chapter 5

R-phase of NiTi

The alloy $NiTi$ is the shape memory alloy used mostly in industry as well as in experiments. It may be observed in three phases: the cubic austenite phase, the monoclinic martensite phase and the rhombohedric R-phase. While the austenitic and martensitic phases are fairly well known and often used in industry, the R-phase is not used that much. One reason might be that it exists only in a small range of temperatures. On the other hand, not still enough is known about the R-phase, but as it offers interesting features like small dissipation at phase transition or small transformation strains a great effort has been undertaken in the past few years to study it. The R-phase has been studied experimentally explicitly in e.g. [26], [46], [63], [66], theoretically in e.g. [22] or as a part of the overall behaviour of $NiTi$ in e.g. [10], [56], [68] or the review article [52].

In this chapter we shall give properties of the R-phase in $NiTi$ that shall be of importance in numerical modelling as collected from the above sources by the author in previous work [8].

5.1 Crystalline structure

As already pointed out the crystalline structure of $NiTi$ in austenite is cubic and we shall identify (following Section 1.3) it with the identity matrix. The four rhombohedric variants of the R-phase may be identified with the following matrices

$$U_1 = \begin{pmatrix} \eta_1 & \eta_2 & \eta_2 \\ \eta_2 & \eta_1 & \eta_2 \\ \eta_2 & \eta_2 & \eta_1 \end{pmatrix}, \qquad U_2 = \begin{pmatrix} \eta_1 & -\eta_2 & \eta_2 \\ -\eta_2 & \eta_1 & -\eta_2 \\ \eta_2 & -\eta_2 & \eta_1 \end{pmatrix},$$
$$U_3 = \begin{pmatrix} \eta_1 & \eta_2 & -\eta_2 \\ \eta_2 & \eta_1 & -\eta_2 \\ -\eta_2 & -\eta_2 & \eta_1 \end{pmatrix}, \qquad U_4 = \begin{pmatrix} \eta_1 & -\eta_2 & -\eta_2 \\ -\eta_2 & \eta_1 & \eta_2 \\ -\eta_2 & \eta_2 & \eta_1 \end{pmatrix}, \tag{5.1}$$

where

$$\eta_1 = \frac{1}{3}\left(\sqrt{1+2\cos\alpha} + 2\sqrt{1-\cos\alpha}\right),$$
$$\eta_2 = \frac{1}{3}\left(\sqrt{1+2\cos\alpha} - \sqrt{1-\cos\alpha}\right). \tag{5.2}$$

Table 5.1: Lattice parameters for the austenitic phase and the R-phase. Here a_0 denotes the length of one cubic side, b denotes the length of one side of the rhombohedron.

Type	Symmetry	Temperatures	Lattice parameters
Austenite	cubic	300 K	a_0=3.0125 Å
R-phase	rhombohedric	292 K	b=3.0134 Å α=89.57°
R-phase	rhombohedric	285 K	b=3.0115 Å α=89.44°
R-phase	rhombohedric	272 K	b=3.0105 Å α=89.32°

Here α denotes the angle formed by two attaching sides of the rhombohedron; for clarity see also Figure 5.1.

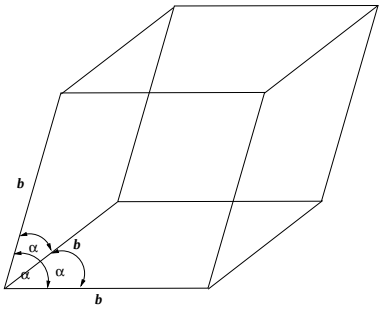

Figure 5.1: One variant of the rhombohedric martensite in *NiTi*. Here the most important parameter to describe the rhombohedron namely the angle α is shown.

A special property of R-phase of *NiTi* is the fact that the angle α does not stay constant after the phase transition to the R-phase, but varies further. This property can, to the authors knowledge, be found in no other shape memory alloy and shows that after the phase transition to the R-phase another phase transition of the second order is going on. This behaviour is very interesting, but could not be implemented in the current model as this model does not reflect temperature dependence. Experimental values (as found in [63]) for this angle are given in the Table 5.1.

Each of the variants of martensite represents a stretch of the original austenitic cube along one space diagonal. So, the variants of martensite are related to each other by symmetry relations and rotations but there exists no rotation R such that $RU_i = U_j$ for some i, j not equal to each other. To see the situation in more detail the reader is referred to Figure 5.2

5.2 Energetics

Throughout this thesis we have seen that choosing the form of the (unrelaxed) Helmholtz free energy, and hence also the Gibbs free energy, is one of the most important modelling assumptions.

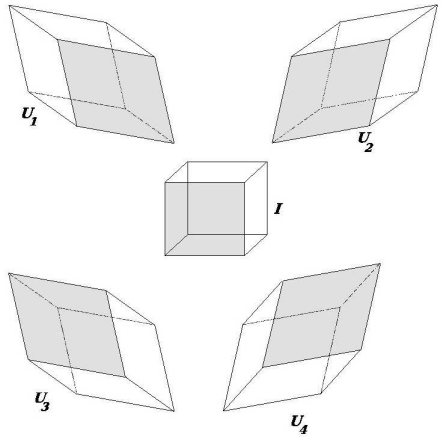

Figure 5.2: All variants of the R-phase. The front side is depicted darker.

One requirement, the Helmholtz free energy is supposed to satisfy, was the multi-well character already noted in (1.20). Namely this is the demand for the free energy to have several local minima, each of which represents one variant of martensite or the austenitic phase at stress free configuration.

The easiest way to achieve this multi-well character is to define a "partial" Helmholtz free energy for each variant of martensite (or the austenitic phase) ψ_l and to define the overall Helmholtz free energy ψ as

$$\psi = \min_{l=1\ldots M+1} \psi_l, \tag{5.3}$$

where M is the number of martensitic variants. Physically this modelling assumption relies on the fact that the material will choose the lowest energy possible.

Still we have a lot of freedom in choosing the energetic behaviours for each martensitic variant and the austenite. The only two conditions we have to satisfy here that the partial energies have minima in the corresponding variants and that they are frame indifferent[1], which means that

$$\Psi(F,\theta) = \Psi(QF,\theta) \quad \forall Q \in \mathrm{SO}(3), \tag{5.4}$$

where SO(3) denotes the group of all rotations in three dimensions. Also here we are going to choose the simplest possible way, namely a quadratic approximation as

$$\Psi^m(F,\theta) = \frac{1}{2}\sum_{ijkl} \epsilon^m_{ij} C^m_{ijkl} \epsilon^m_{kl} + c^m_V \theta_0 \ln\left(\frac{\theta}{\theta_c}\right), \tag{5.5}$$

$$\epsilon^m = \frac{U_m^{-T} F^T F U_m^{-1} - \mathbb{I}}{2}. \tag{5.6}$$

Here C^m_{ijkl} denote the respective elastic constants whereas c^m_V denote the specific heat capacities. Recall also that θ_c is the transformation temperature. Note that

[1]Frame indifference means independence of observer in the sense that a observer in a rotated system measures the same energy as the observer in the original system, cf. [39, pages 128-140].

such a definition is in accord with assumption (A1) in Chapter 3 and represents no conflict with the existence theory presented there.

Of course more complicated forms of these partial Helmholtz free energy densities could be chosen, however as in our numerical experiments the transformation strains are very small a quadratic approximation is well applicable.

The matrix of elastic constant simplifies rapidly for the cubic symmetry to (in Voigt notation)

$$\begin{pmatrix} C_{11} & C_{12} & C_{12} & 0 & 0 & 0 \\ C_{12} & C_{11} & C_{12} & 0 & 0 & 0 \\ C_{12} & C_{12} & C_{11} & 0 & 0 & 0 \\ 0 & 0 & 0 & C_{44} & 0 & 0 \\ 0 & 0 & 0 & 0 & C_{44} & 0 \\ 0 & 0 & 0 & 0 & 0 & C_{44} \end{pmatrix}. \tag{5.7}$$

The constants C_{11}, C_{12}, C_{44} can be found in literature for the austenitic phase (here taken from [56]) in the vicinity of the phase transition as

$$\begin{aligned} C_{11} &= 160 \text{ GPa}, \\ C_{12} &= 145 \text{ GPa}, \\ C_{44} &= 35 \text{ GPa}. \end{aligned} \tag{5.8}$$

Yet, for the R-phase there is no experimental literature giving elastic constants and we shall therefore use the constants given for austenite also in the R-phase. For the specific heat capacities we have that (got by a compilation of [40], [26]; for further details see [8])

$$c_V^{\text{austenite}} = 0,32 \ \ \text{Jg}^{-1}\text{K}^{-1} = 2,1 \ \ \text{Jcm}^{-3}\text{K}^{-1}, \tag{5.9}$$

$$c_V^{\text{R-phase}} = 0,31 \ \ \text{Jg}^{-1}\text{K}^{-1} = 2,0 \ \ \text{Jcm}^{-3}\text{K}^{-1}. \tag{5.10}$$

Another important modelling parameter is the dissipation distance. Here we shall follow the idea (e.g. [55]) that the material dissipates energy if an phase transition occurs, i.e. when austenite changes to R-phase. On the other hand we assume that there is no dissipation if the variants of the R-phase transform to each other. Therefore we set the dissipation distance from (1.23)

$$d(\lambda_1, \lambda_2) = \epsilon |\lambda_1^{\text{austenite}} - \lambda_2^{\text{austenite}}|, \tag{5.11}$$

where the constant ϵ should be chosen in accordance with some experimental evidence. However, the information mostly found in literature is that the dissipation is very small, but no concrete number is given. Therefore ϵ was chosen to be 0.5 MPa, which is ten times less than the dissipation reported for *CuAlNi* (for dissipation in *CuAlNi* see e.g. [60]). Realize that such a choice of the dissipation distance satisfies assumption (A2) on Chapter 3 and fits therefore also into the concept needed for analysis.

5.3 Microstructure

Of course the most crucial cause for the effects distinguishing shape memory alloys from other materials is their ability to form microstructure. Also, as we

have already seen, which kind of microstructure will be formed is dominantly determined by the geometry of crystal lattices of the given material. If the R-phase of $NiTi$ is concerned we shall ask ourselves between which variants of martensite and austenite rank-1 connection can be established. This question has been exhaustively treated in a general setting of the cubic to trigonal transformation e.g. in [22] (see also references therein) and at this point we shall follow this work to give the connections that are of most relevance here.

First of all note that in stress free configuration there is no possibility for austenite and a single variant of martensite to form a rank-1 connection.[2] Therefore the material is forced to evaluate a laminative structure of at least two variants of martensite to establish a rank-1 connection with austenite. In the interface of R-phase and austenite a twinning system between any two variants of the R-phase is possible to establish the rank-1 connection. In this work only interfaces of austenite and R-phase via twin structures has been used since this is the most common way to do so. In fact, for a long time it was even believed that twin structures are the only way to connect austenite and martensite, but recent experiments [62] in $CuAlNi$ have shown that the interface might also be constituted by a special kind of structure, namely the parallelogram microstructure, which can also be formed by four variants of the R-phase (for parameters of the parallelogram microstructure see e.g. [22], [8]). The possibility of existence of such interfaces is very recent and therefore not included here, as it was even not investigated whether the parallelogram microstructure could be bound to austenite.

As the rank-1 connection of austenite and twins of two variants of R-phase is symmetric with respect to the choice of the two variants involved in twinning, if the loads are changed respectively, here only the interface between martensite and the variants U_1 and U_2 will be treated. To establish this connection we are to find λ_m, Q_m, Q, $\mathbf{n}_m$, $\mathbf{a}_m$, $\mathbf{n}$ and $\mathbf{a}$ such that

$$\begin{aligned} U_1 - Q_m U_2 &= \mathbf{a}_m \otimes \mathbf{n}_m \\ Q - (\lambda_m U_1 + (1-\lambda_m) Q_m U_2) &= \mathbf{a} \otimes \mathbf{n} \end{aligned} \tag{5.12}$$

is satisfied. This problem of two equations can be solved by first solving the first one and then the second one with the already obtained results. The procedure of finding the unknown parameters is described in Theorem 5.1 in [9, page 69][3] and analytical results found in [22] say that the first equation is solved by two normals $\mathbf{n}_{m1}=(0,1,0)^{\mathrm{T}}$ or $\mathbf{n}_{m2}=1/\sqrt{2}(1,0,1)^{\mathrm{T}}$. However only twins with the second normal may be used to establish a rank-1 connection with austenite.

Although algebraic expressions for the parameters we are searching for can be calculated explicitly, depending only on the lattice parameters, these expressions are very complicated (see [22] for a slightly modified problem). Therefore we shall give here only their numerical values that were really used in calculations (the angle α that characterizes the crystalline structure of the R-phase was chosen to

[2] However the simulations done here indicate that it might be possible to form a connection of deformed austenite and a deformed single variant, yet this was not confirmed by a theoretic calculation.

[3] The theorem is originally due to Ball and James [5].

be 89.44°)

$$\begin{aligned}
\mathbf{a}_m &= (-1.35\ 10^{-4}, 276.4\ 10^{-4}, -1.35\ 10^{-4})^{\mathrm{T}}, \\
\mathbf{n}_m &= 1/\sqrt{2}\ (1, 0, 1)^{\mathrm{T}}, \\
\mathbf{a} &= (-1.42\ 10^{-4}, -4.67\ 10^{-4}, 96.78\ 10^{-4})^{\mathrm{T}}, \\
\mathbf{n} &= (0.999988, 0, -0.00493514)^{\mathrm{T}},
\end{aligned}$$

and the volume fraction of the variant U_1 as well as U_2 in the laminate λ has to be $1/2$. The rotation matrices could be calculated with the data already available, but they are not important for computations. For a better picture of the configuration see Figure 5.3

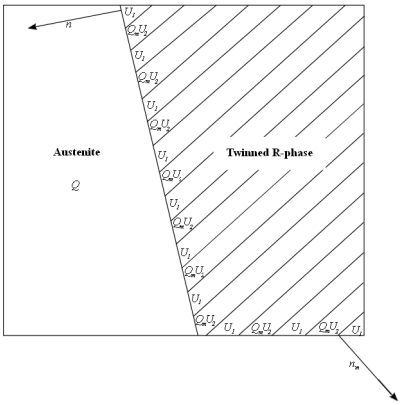

Figure 5.3: Rank-1 connection between the austenite and laminated variants U_1, U_2. Here the normals used do not correspond numerically to the calculated values

Chapter 6

Results

In this chapter the results from numerical simulations using the code described above are shown. The first two sections contain examples that are rather academic because of the complicated Dirichlet loading applied. These experiments could hardly be realized in laboratories, however due to the specific loading they verify the ability of the code to compute more difficult and more realistic experiments.

The simulations shown after these two section are far more realistic and could easily be reconstructed in laboratories if a bulk specimen of mono-crystalline $NiTi$ was at disposal.

6.1 Homogeneous loading deforming austenite martensite

This section shows simulated behaviour of a specimen of $NiTi$ under homogeneous Dirichlet loading. The simulation has been performed within the concept of the discretized problem as presented in Chapter 4, namely the time-interval on which we perform the simulation $[0, T]$[1] was divided into 100 time-steps. In each of these time-steps then we impose different affine Dirichlet boundary conditions. Affine in the sense, that we are able to represent the boundary condition imposed by a matrix, say D, such that we require $u(x) = Dx - x$ for all x lying on the boundary of the domain Ω. Recall that, Ω denotes the domain the investigated specimen occupies in reference configuration.

The simulation is designed in such a way that the the boundary condition in the 100-th time-step, denoted D_{100} corresponds to the twinned laminate structure of variants U_1 and U_2.[2] This is a test for the simulating algorithm since, if it works well, the results is predictable and should be that the material choose to deform inside the bulk in same way as on the boundary and undergo from austenite to R-phase.

As far as other physical parameters are concerned, we suppose to have mono-

[1]Here we do not give any specific time in which the experiment is performed, as specific values are not important within the concept of quasi-static evolution. We, of course, have to suppose that the process is performed "slowly", but the slowness is expressed rather by a small change in boundary conditions imposed in every time-step than by specific values of time.

[2]To be more specific $D_{100} + \mathbb{I} = 1/2U_1 + 1/2Q_mU_2$, with notation from (5.12)

crystalline $NiTi$ in $(1,0,0)$ orientation described by parameters given in Chapter 5. Initially (i.e. in time-step 0) the specimen is considered to be in austenite phase only and slightly rotated (as a whole) with respect to its reference position[3] parallel to the coordinate system axes. Therefore in time-step 0 a deformation y_0 such that

$$\nabla y_0 = \begin{pmatrix} 0.99 & 4.85\ 10^{-3} & -4.85\ 10^{-3} \\ -4.88\ 10^{-3} & 0.99 & -4.88\ 10^{-3} \\ 4.83\ 10^{-3} & 4.90\ 10^{-3} & 0.99 \end{pmatrix}, \tag{6.1}$$

is applied to the whole specimen.

Then, in every time-step a matrix A given as

$$A = \begin{pmatrix} -1415.5\ 10^{-9} & 0 & 7.0\ 10^{-9} \\ -467.2\ 10^{-9} & 0 & 2.3\ 10^{-9} \\ 96774.7\ 10^{-9} & 0 & -477.6\ 10^{-9} \end{pmatrix}. \tag{6.2}$$

is added to the Dirichlet boundary condition prescribed in the last step represented by a matrix D_{k-1}. In more clarity we demand that $u_k = D_k x - x$ for all x on the boundary and $D_k = D_{k-1} + A, D_0 = \nabla y_0 - \mathbb{I}$. Of course (except for the initial condition) the deformation inside the specimen is subject to deformation.

As already anticipated after 100 time-steps the specimen should be found solely in R-phase and the microstructure should be formed by twins of variants U_1 and U_2 with volume fraction 1/2. In case we would like the specimen to transform further to single phase variant (we choose U_1) we need to continue deforming the specimen. This further done by adding a different matrix, B, to the current boundary condition, namely $D_k = D_{k-1} + B$ if $k > 100$. The concrete form of the matrix B is

$$B = \begin{pmatrix} 4.76\ 10^{-7} & 0 & 4.76\ 10^{-7} \\ -977.35\ 10^{-7} & 0 & -977.35\ 10^{-7} \\ 4.76\ 10^{-7} & 0 & 4.76\ 10^{-7} \end{pmatrix}. \tag{6.3}$$

The following Figure 6.3 shows the evolution of the microstructure and the volume fraction of the austenite if the specimen is subject to the loading described above at transformation temperature and not taking dissipation into account.

Further we shall consider the first part of the above calculation (i.e. only the part that forces the specimen to get to the twinned martensite) and give stress-strain diagrams calculated both with and without taking dissipation into account. To do so, however we should perform the experiment above the transformation temperature. The reason is that otherwise the plateau[4] that can be seen in Figure 6.2 below would coincide with the strain-axis. In this situation the dissipation would not be visible. Namely our experiment is performed at 293.1 K which is 0.1 K[5] above the transformation temperature. In Figure 6.1 we see

[3] Physically we would consider this slightly rotated position to be the reference configuration, however numerically it is more advantageous to derive which position is taken as reference from the mesh used by the algorithm. With respect to this mesh then the specimen is rotated simply due to easier numerics.

[4] Note that the plateau corresponds to the fact that stress applied on the material can be compensated by transition of austenite to R-phase.

[5] These numbers may seem strange at first sight as it is a well known fact that temperature induced phase transition is not strict, but starts and finished at different temperatures. However here we assume, for simplicity, that the transformation has only value and follow strictly formula (5.6).

a comparison of the stress strain diagrams for calculations with and without dissipation. There the label "Forward run" corresponds to loading the specimen and therefore forcing it to transit from austenite to R-phase whereas the label "Backward run" corresponds to unloading and a return of the specimen from R-phase back to austenite.

We see that in both cases a hysteretic response occurs, however in the case when the dissipation is taken into account the dissipation is bigger. Note that the noise in the stress-strain diagram is also due to the application of the two-sided energy inequality as every return yields a sink in stress when being in the upper part of the hysteresis curve, in the lower part on the other hands it leads to a rise in stress.

If we wanted to reduce the noise we could mollify the stress strain diagrams as in Figure 6.2 by a moving average of five points. In this figure it can be seen in more clearness that the dissipation curve is broader when dissipation calculation is switched on; on average the height of the hysteresis when taking into account the dissipation is 15.7 MPa. When dissipation is not taken into account the height of the hysteresis is 11.9 MPa. This shows that when we want to have a small dissipation (as already mentioned 10 times smaller than in $CuAlNi$) it is at the level of the numerical dissipation. Therefore it is not a big mistake to drop the dissipation in some calculations, where its usage would be difficult.

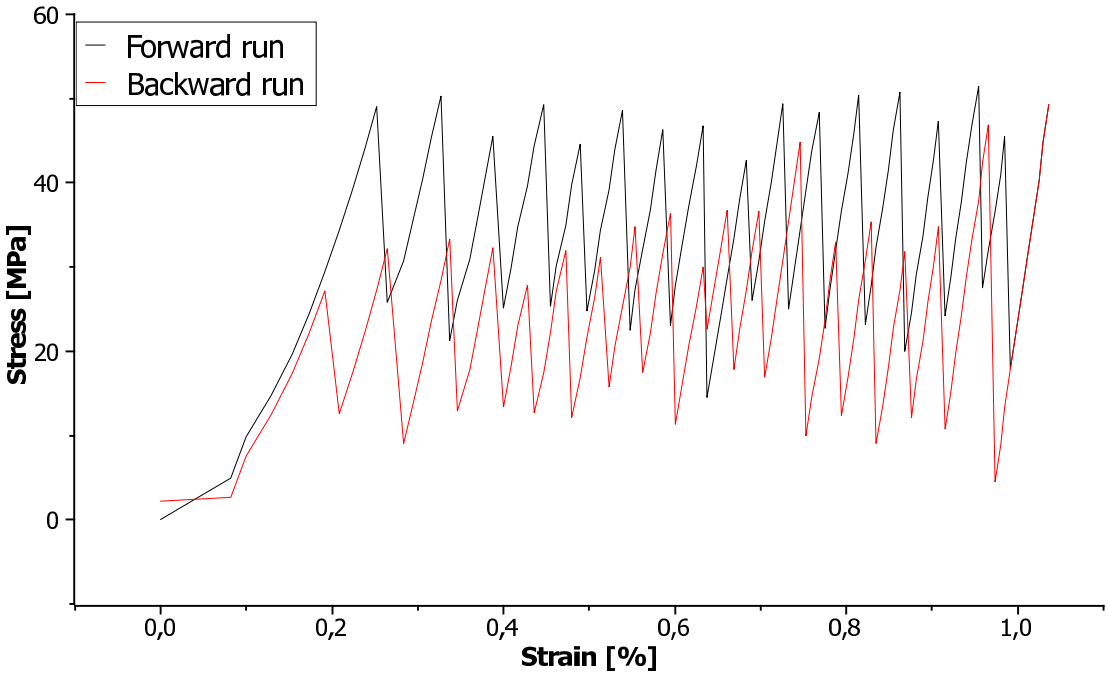

(a) Dissipation free evolution

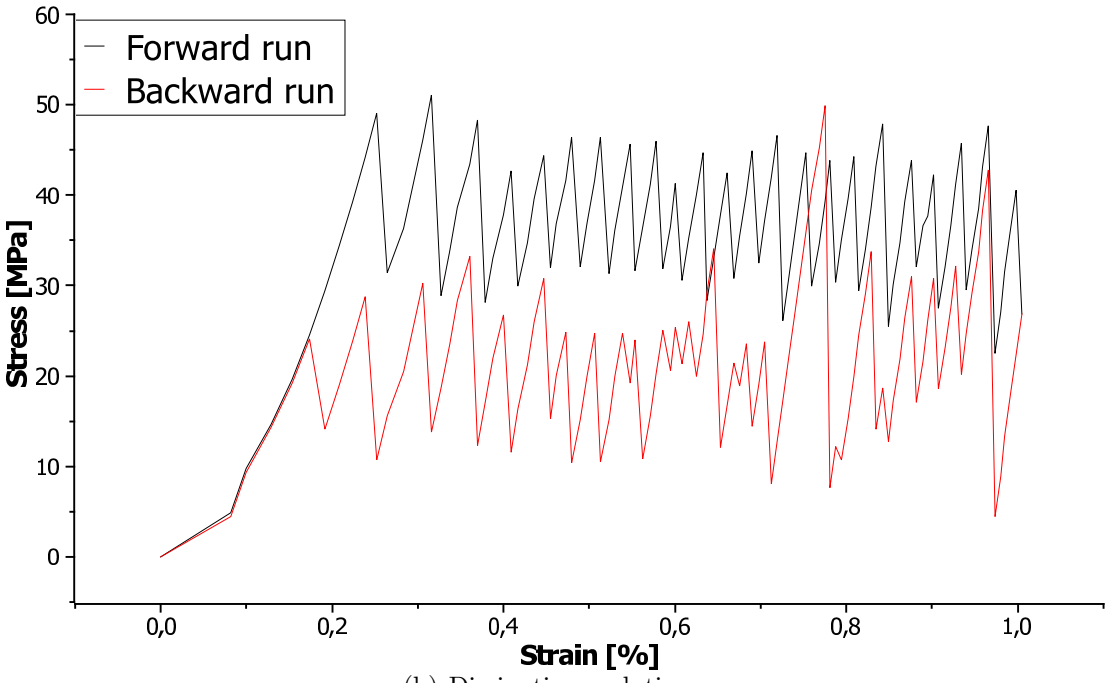

(b) Dissipative evolution

Figure 6.1: Stress-strain diagrams for the first part of the loading experiment. On the top the case without dissipation is displayed, on the bottom the evolution with dissipation. Recall also that the label "Forward run" corresponds to loading the specimen, whereas "Backward run" to unloading.

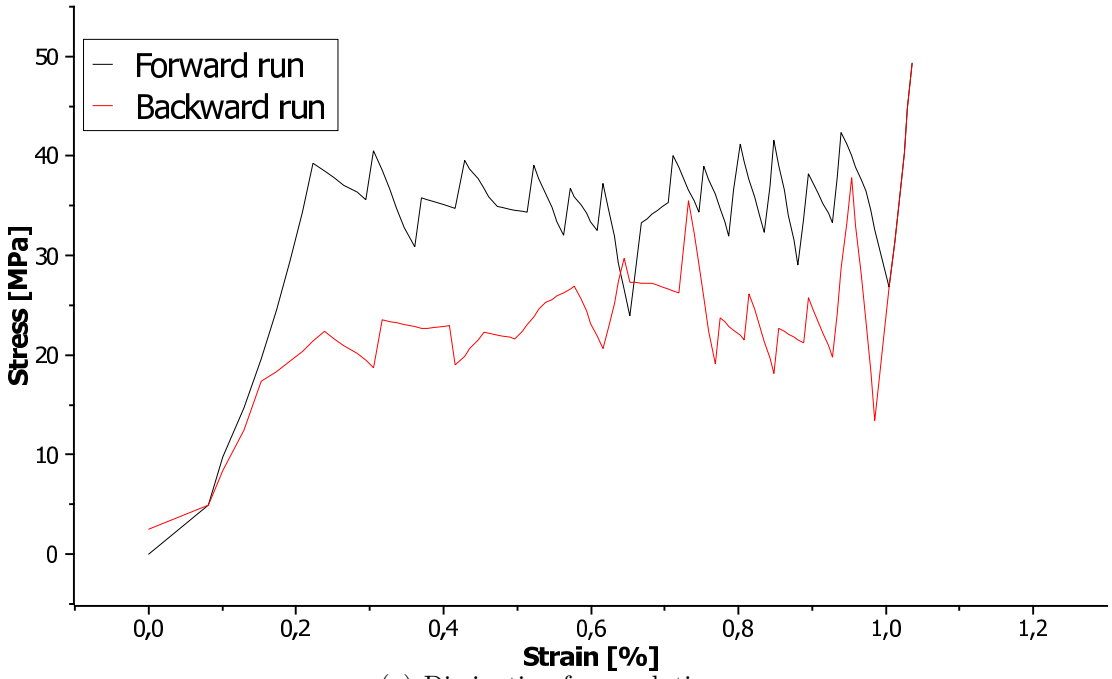

(a) Dissipation free evolution

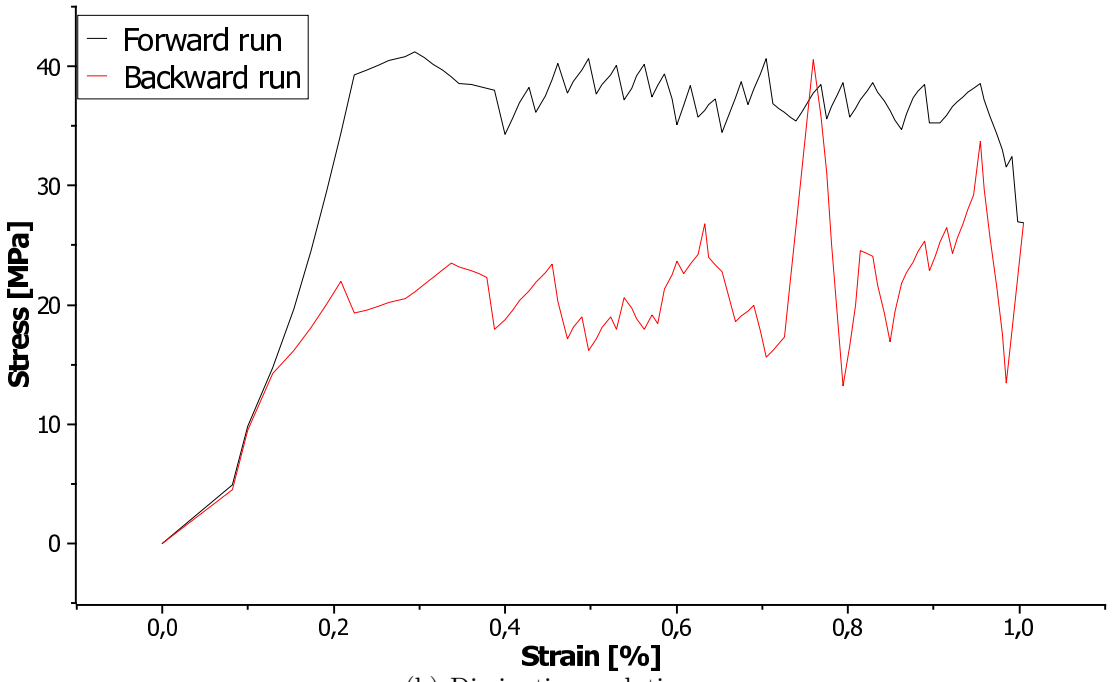

(b) Dissipative evolution

Figure 6.2: Mollified stress-strain diagrams for the first part of the loading experiment. On the top the case without dissipation is displayed, on the bottom the evolution with dissipation. Recall also that the label "Forward run" corresponds to loading the specimen, whereas "Backward run" to unloading.

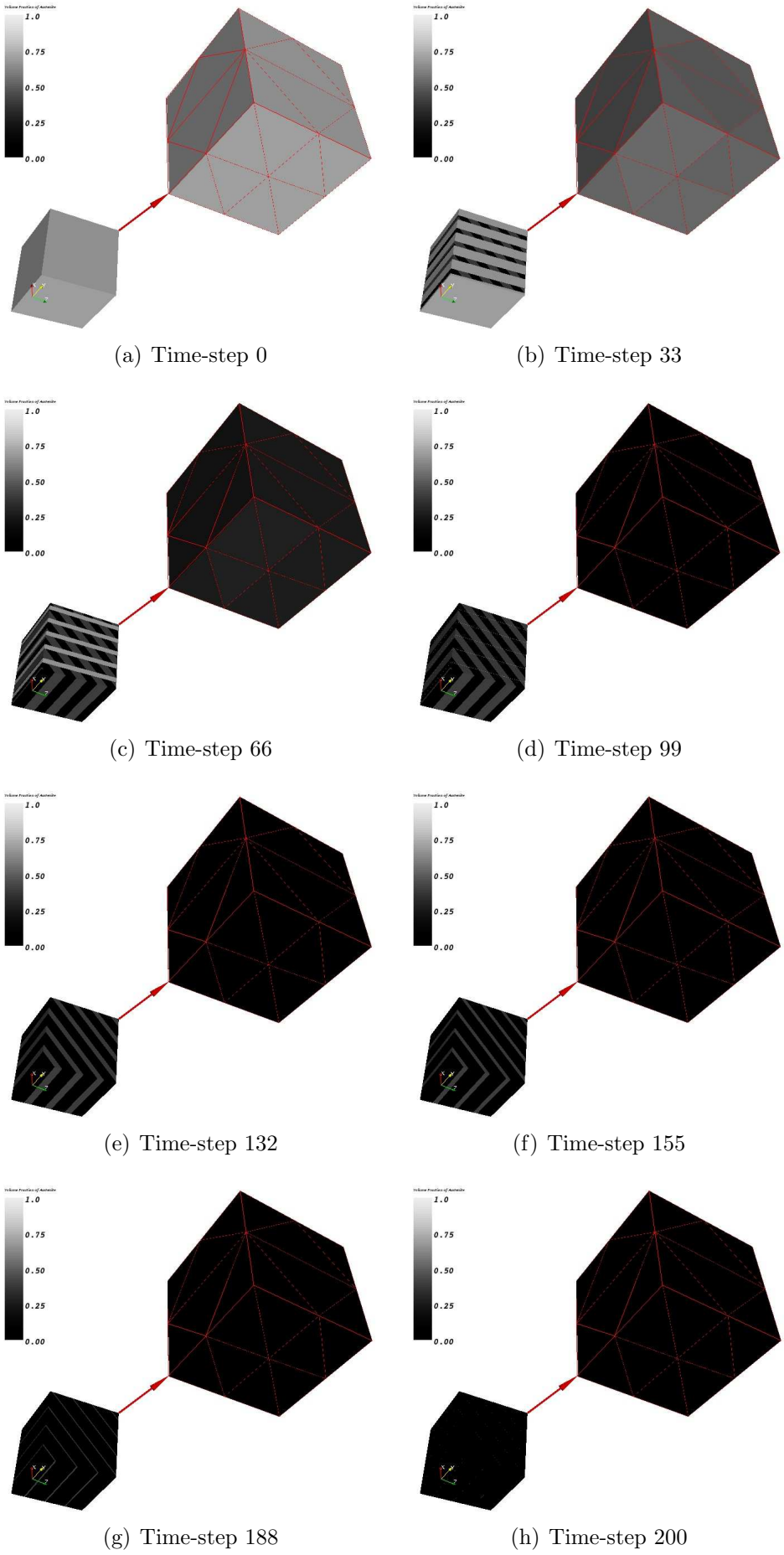

(a) Time-step 0

(b) Time-step 33

(c) Time-step 66

(d) Time-step 99

(e) Time-step 132

(f) Time-step 155

(g) Time-step 188

(h) Time-step 200

Figure 6.3: Evolution of the volume fraction of austenite as well as of microstructure when loading the specimen homogeneously as described above. Note that although the volume fraction of austenite does not change in the last steps, the microstructure does.

6.2 Non-homogeneous loading deforming austenite to twinned martensite

In this section the first part of the loading experiment from previous section is generalized in the sense that the deformation is applied only on those sides of the cube, which do not have one coordinate equal to zero.

Unfortunately, it is possible to perform only first part of the experiment in such a setting as it would be very difficult (and nearly impossible) to link a next deformation to the first one. This is due to the fact that handling the inhomogeneity is already difficult as the problem was posed. Adding more elements to the mesh could be a way out of the situation, but it would tremendously increase computation time.

The sense of this simulation is to test the algorithm in more difficult conditions, but as already anticipated we can hardly expect that this simulation could be repeated experimentally in laboratories. Again, similarly to previous section, we are able to predict simulation results. In more detail, we expect the specimen to transform fully to R-phase in one part whereas to stay totally in austenite in its other part.

The simulation was performed at transformation temperature where austenite as well as the R-phase are stable states in 100 time-steps with an $(1, 0, 0)$-oriented crystal. In these 100 steps the load the the sides of the cube that are subject to loading is linearly increased similarly as in the previous section.

The inhomogeneity in loading leads naturally to an inhomogeneous distribution of volume fractions of austenite or martensite. Results for a simulation without dissipation can be seen in in Figure 6.5 showing the microstructure and distribution of austenite volume fractions. This simulation offers natural results namely the fact that in element 0, i.e. the one which is totally surrounded by sides that are not subject of deformation no change in the microstructure occurs whereas element 47 (surrounded completely by sided that are loaded) transforms fully to R-phase. Other elements transform to R-phase only partly.

For this computation we do not give stress-strain diagrams, though they have been computed for element 47. The reason is very simple, namely these diagrams are very similar to those shown in previous section in Figure 6.1.

As in other computations the implementation of the two-sided inequality (4.10) is useful in this computation as well. However the corrections due to this inequality are not as important as in examples that shall follow. In Figure 6.4 evolution of the energy in time is shown. The drastic falls of energy indicate that the algorithm has found a better local minimum and the strategy of returning as described in Chapter 4 under example 4.1 is put into action. For this reason also the deep falls of energy are referred to as "returning points" in this thesis. For the sake of clarity only the first 40 time-steps and only the evolution of the energy and not of the lower and upper bound for the energy are shown. To see that in the deep falls the lower energy inequality is truly violated the reader is referred to Figure 6.4(b) where one such a fall or returning point is chosen and depicted in more detail. Moreover the lower and upper bound for the energy are shown and clearly, in the returning point the energy is visibly lower than its lower bound.

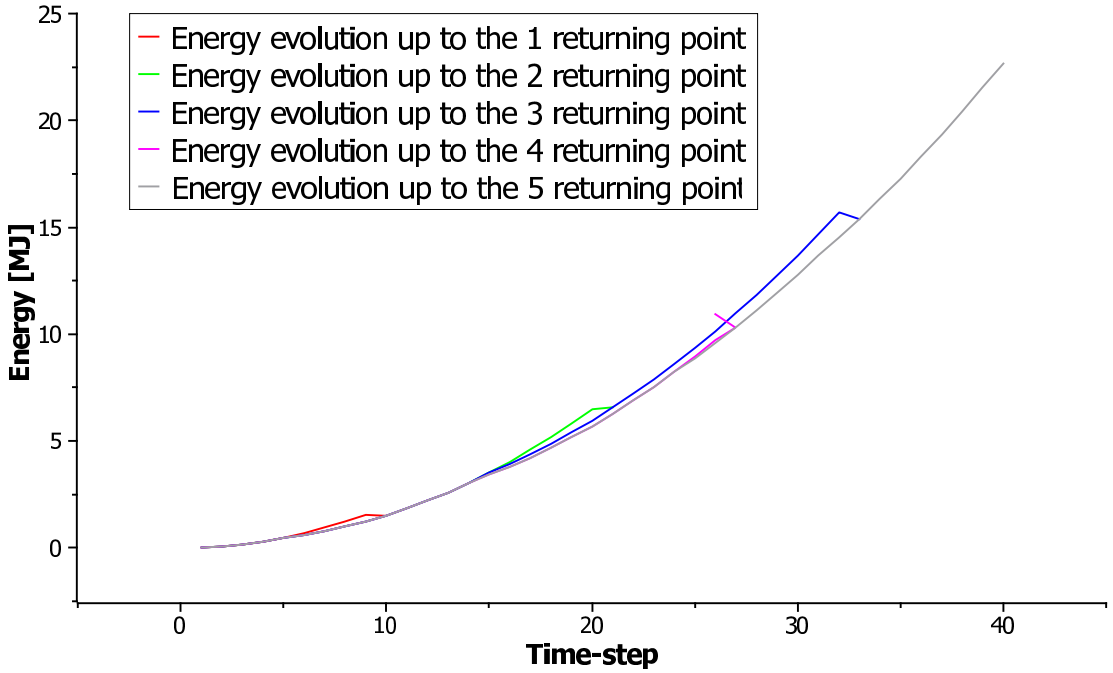

(a) Overall evolution

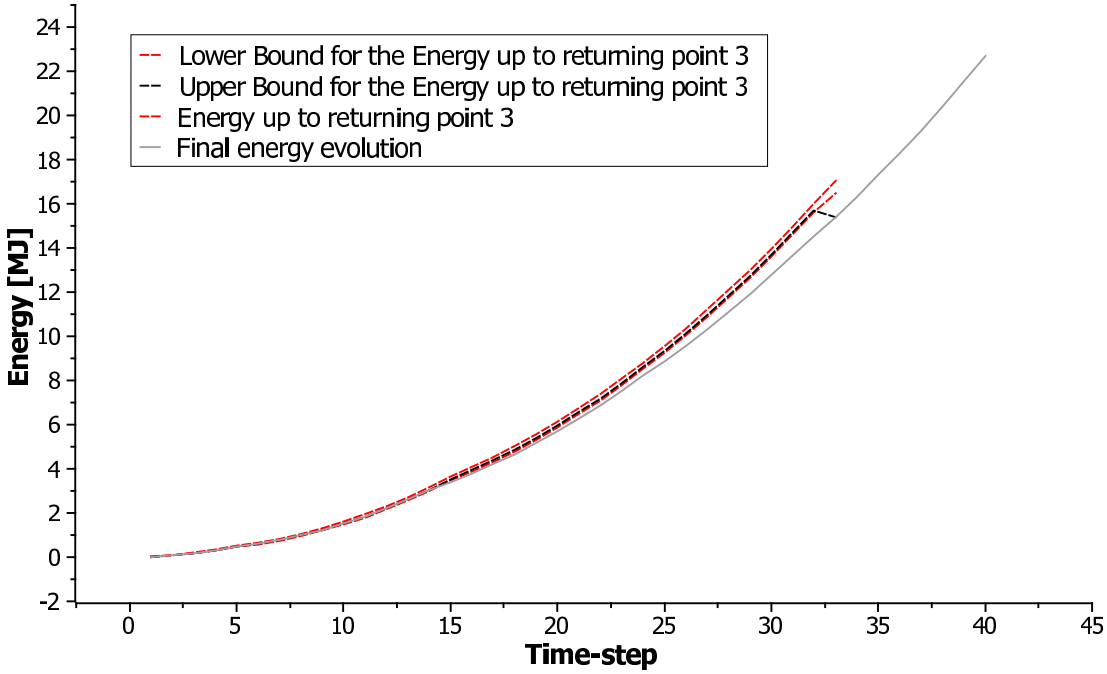

(b) Detail of one returning point including the bounds for energy.

Figure 6.4: Evolution of the energy including the returns due to violation of the two-sided energy inequality. On the top the overall evolution is shown on the bottom then a detail of one returning point.

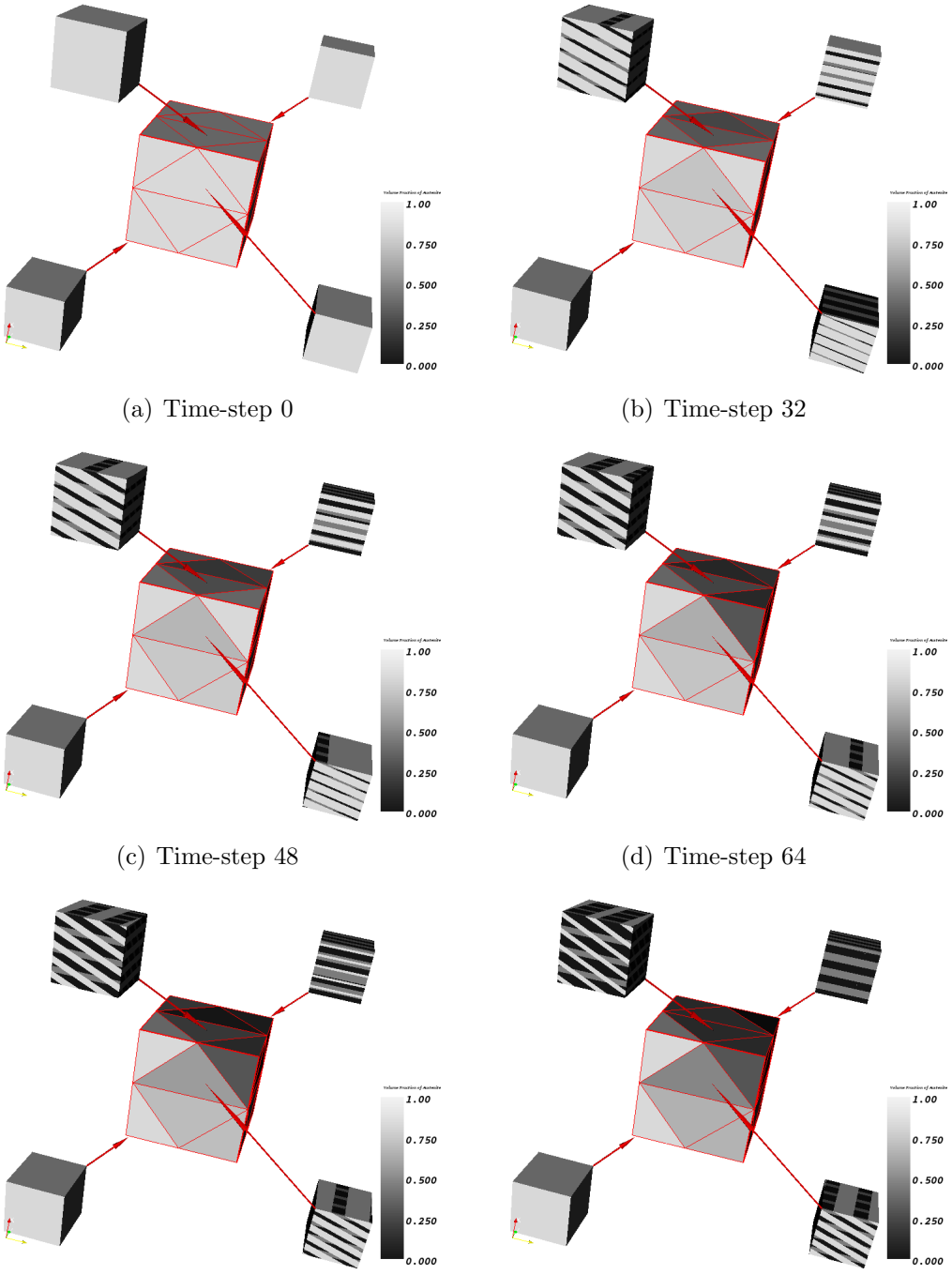

(a) Time-step 0

(b) Time-step 32

(c) Time-step 48

(d) Time-step 64

(e) Time-step 80

(f) Time-step 100

Figure 6.5: Evolution of the volume fraction of austenite as well as of microstructure when loading the alloy inhomogeneously. Namely the specimen is loaded only on those sides that do not have one coordinate equal to zero.

6.3 Homogeneous loading transforming austenite directly into variant U_1 of R-phase

The simulation described in this section is much more a "real life" experiment that the previous two and could be performed in laboratory condition to give us experimental data.

The evolution of the material is simulated to happen in 100 time-steps and in each time-step the Dirichlet boundary loading is changed homogeneously. To be more specific, in every time-step a Dirichlet load represented by the matrix $D_k = k/100U_1$ (using the same notation as in Section 6.1 above), where k is the time-step in question, is applied to the material. The load is moreover homogeneous in the sense that the same affine boundary condition is applied on the whole boundary.

Let us recall how we may imagine the formation of variants of R-phase, to see why this loading is indeed performable in laboratory conditions. Namely, this formation can be imagined to be a homogeneous tension in the direction of one space diagonal or roughly speaking by a holding the cube in two opposite corners and pulling. As the experiment presented here represents the formation of variant U_1 from austenite it is evident that the load is simple enough for experiments.

The experiment presented takes place above transformation temperature, to be concrete at 293.1 K, which is 0.1 K above transformation temperature. The results can be seen in Figure 6.7 where the evolution of the microstructure is shown, as well as in Figure 6.6 which displays the stress-strain diagram. Again two stress-strain diagrams are given, the first displaying directly computed data, the second containing their mollification by a moving average of five points.

The most interesting point about the experiment is the "turning" of microstructure as clearly seen in Figure 6.7. Namely, due to the loads applied, it is more advantageous for the material to change the normal of the plane between twinned martensite and austenite and to create a new rank-1 connection of austenite with twinned martensite, where the volume fraction of both variants of martensite involved is no longer one half. Such a microstructure would not be possible in stress free configuration. Connected with this "turning of microstructure" is the sinking stress in the stress-strain diagram shown in Figure 6.6.

Such behaviour, meaning the "turning" of microstructure and sinking of stress, can indeed be observed in laboratory experiments with shape memory alloys (see [50] for observations in *CuAlNi*). Unfortunately, the turning of microstructure is a numerically difficult and hence it was impossible to calculate this evolution with dissipation taken into account. Nevertheless, following Section 6.1 this is not a severe drawback.

Also in this experiment the implementation of the two-sided energy inequality leads to better computational results as will be illustrated in more clarity in the next section.

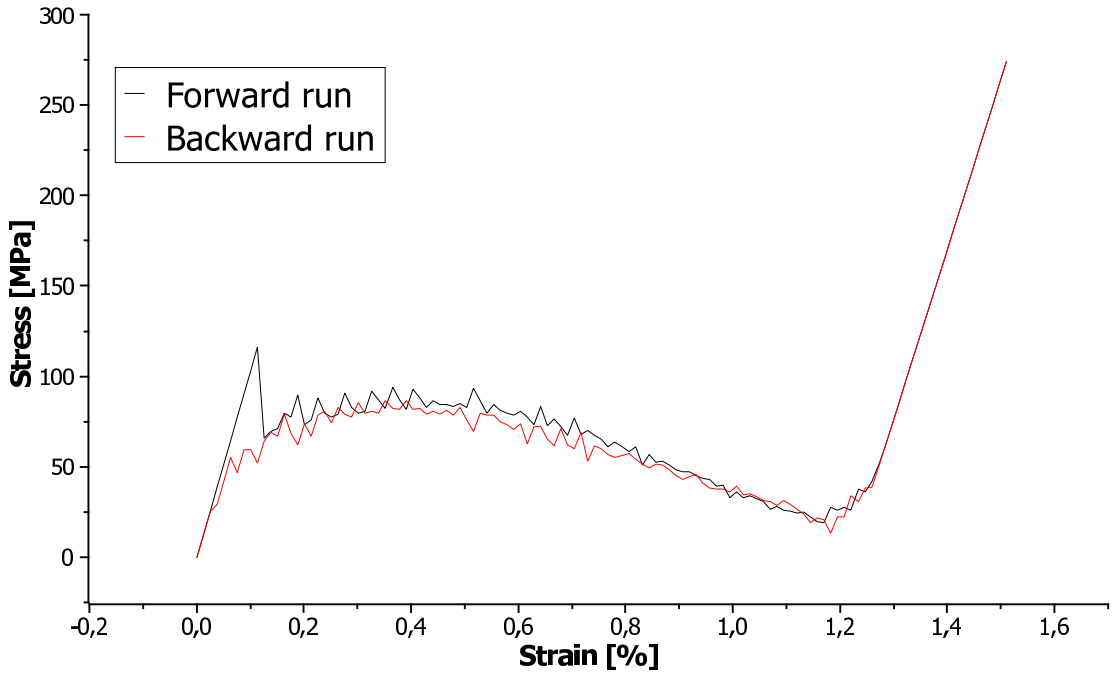

(a) Non-mollified evolution

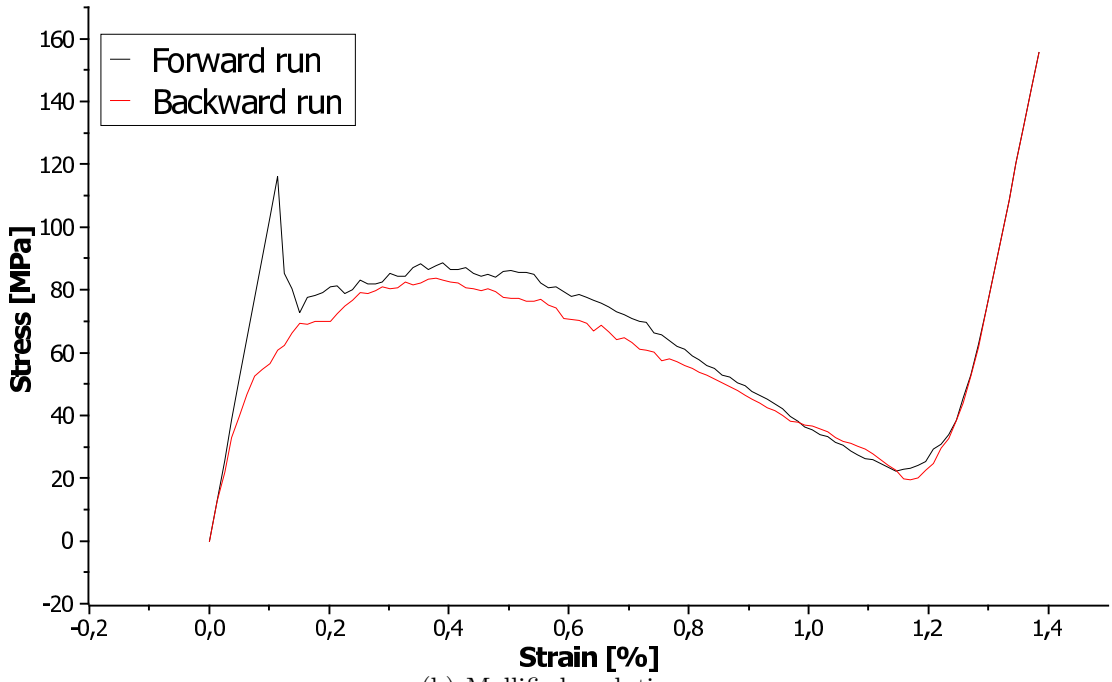

(b) Mollified evolution

Figure 6.6: Stress-strain diagrams for the loading experiment. On the top data as resulting from computation are given, on the bottom mollified data. Recall also that the label "Forward run" corresponds to loading the specimen, whereas "Backward run" to unloading.

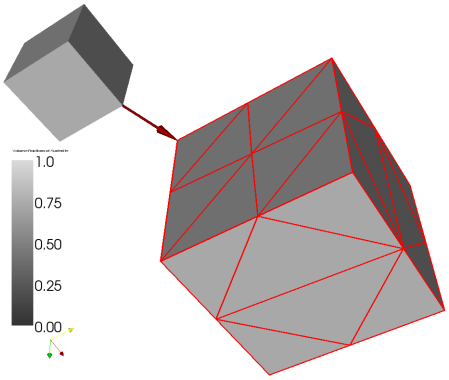

(a) Time-step 0

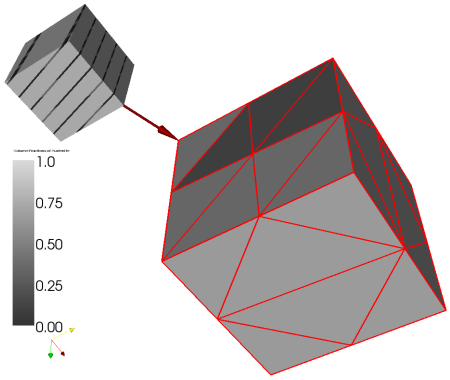

(b) Time-step 10

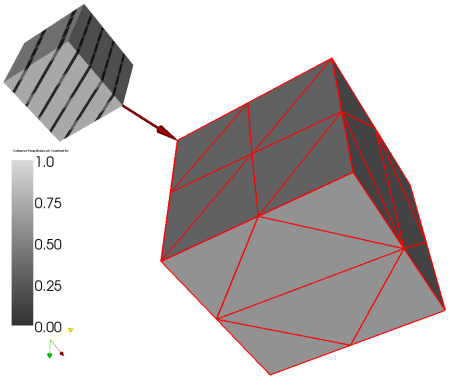

(c) Time-step 15

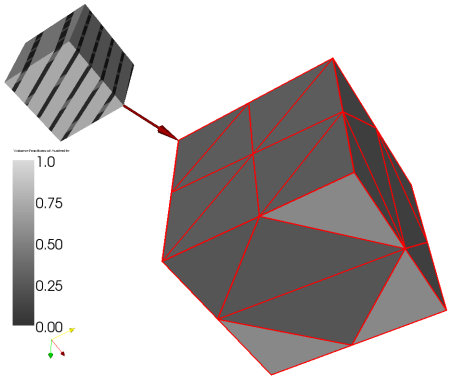

(d) Time-step 20

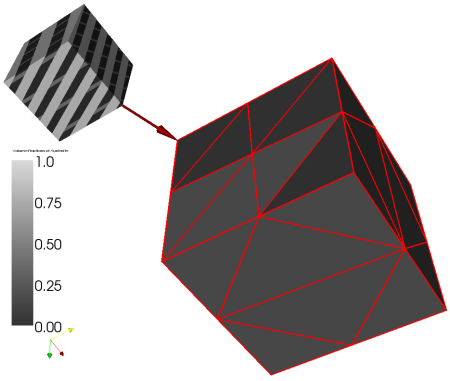

(e) Time-step 40

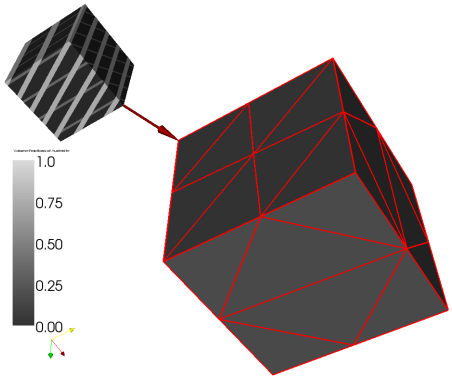

(f) Time-step 60

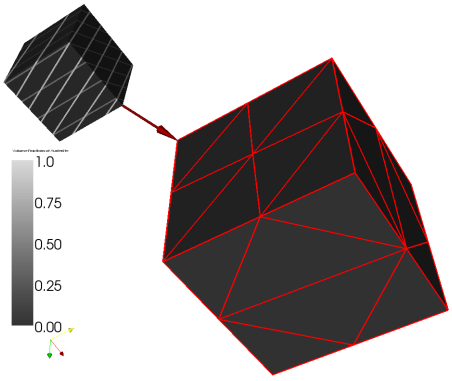

(g) Time-step 80

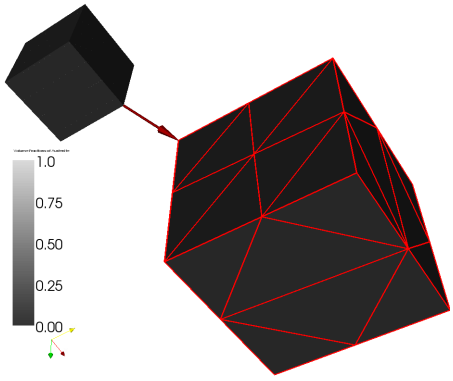

(h) Time-step 100

Figure 6.7: Evolution of the volume fraction of austenite as well as of microstructure when homogeneously in (1,1,1) direction.

6.4 Detail of homogeneous loading transforming austenite directly into variant 1 of R-phase

In this section we present an example of the usefulness of implementation the two-sided energy inequality. For the first time this energy inequality was used in calculations in [42], however in a damage problem and included only one returning point. By a returning point we understand in accord with Chapter 4 and the above said a time-step in which the energy inequality has been violated and hence the algorithm has return until this inequality will be satisfied again.

The situation presented here is much more difficult than in [42], in the sense that many returning points occur during the calculation. In this specific example we have 5 returning points, but in the experiments presented above we may have as many as 20 returning points.

The simulation that we shall present in the next few paragraphs is the behaviour of a specimen subject to the same kind of load as above, only the load is applied "slower" in the sense that to reach the full deformation, represented by U_1 of the specimen 100 time-steps were needed in previous section, but 1000 time-steps shall be needed in this section. The affine boundary condition can therefore be represented by the matrix $D_k = k/1000\, U_1$, where k denotes the current time-step.

We shall concentrate however only on approximately the first 100 time-steps, one tenth of the whole process. In is namely in this 100 time-steps when the turning of normals of the twins starts, and as the turning is difficult problem the implementation of the two-sided energy inequality eases the search for local minima.[6]

In Figure 6.8 we present a comparison of the energy evolution in the case the the two-sided energy inequality has been applied with the case when it was not. The final energy in approximately time-step 100 is 2.5 times less if the two-sided inequality is verified than if it is not, which is a huge difference. One might think that if we are interested only in evolution after time-step 100 it does not matter whether the strategy of returning is implemented or not as this strategy might change only the evolution before the two-sided energy inequality is violated. This might be a good assumption in easier cases, but here it is not true. The reason is that after the algorithm had returned it has a different initial guess and might find even lower local minima. This can be see on the detail of returning point 3 in Figure 6.9(b) where we see that the final evolution lies lower than the energy in returning point 3. This is thanks to returning pints 4 and 5 that would not be discovered if the strategy of returning would not have been implemented.

In Figure 6.9, as anticipated, details of the energy evolution up to some returning point are displayed. We clearly see that in the two specific returning points the lower energy inequality is indeed violated whereas the upper bound has no selectivity.

The fact that the algorithm chooses a false local minimum manifests itself

[6]To clarify that the problem is indeed difficult we may note that the same problem, if the load is applied inhomogeneously, leads to results that are not physical in some time-steps even though the energy inequality is included. The reason for the non-physicality is that the turning of microstructure is not identified early enough.

in this example not only in energy graphs, but also in visualization of volume fractions of austenite and microstructure. Let us turn our attention to Figure 6.10 where volume fractions and microstructure are displayed. Left the evolution with verifying the two-sided energy inequality and returning is shown, right without. If the strategy of returning is used, the turning of microstructure start earlier and the volume fraction of austenite are approximately 0.8 in all frames shown (of course constantly sinking). On the other hand if returning is not implemented the microstructure does not turn until time-step 97 but the volume fraction of austenite changes rapidly. Namely it is approximately 0.5 in time-step 95; however this value corresponds neither to the microstructure calculated nor the boundary condition imposed. Simply this value is not physical and we may conclude that not verifying the two-sided inequality might lead to non-physical results of simulations.

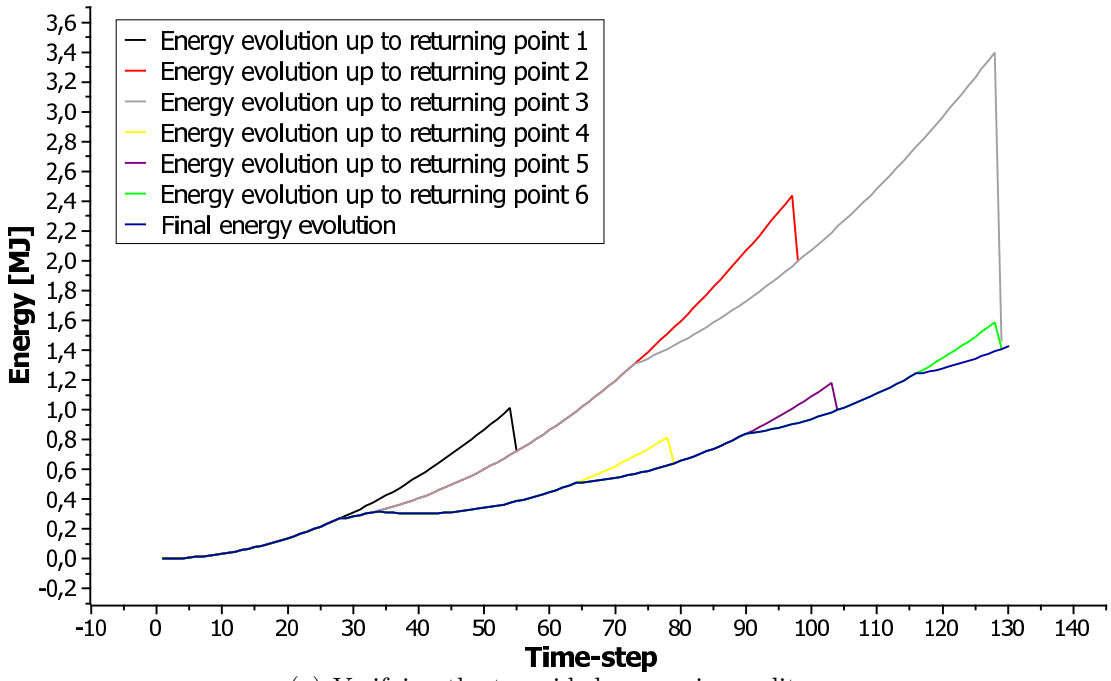

(a) Verifying the two-sided energy inequality

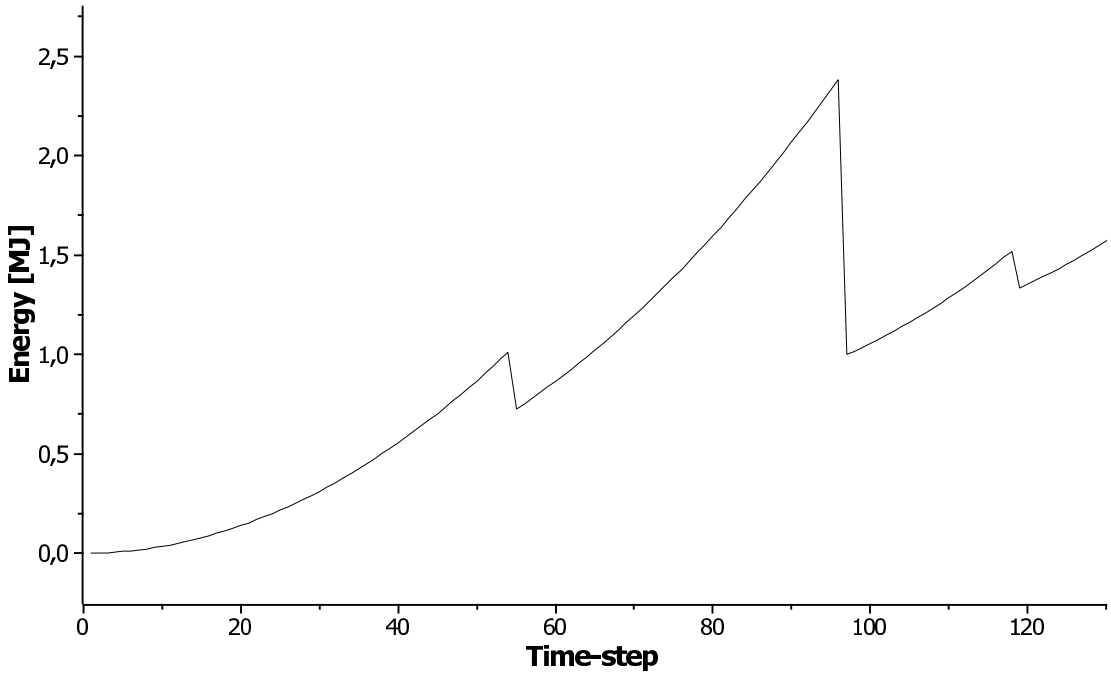

(b) Not verifying the two-sided energy inequality

Figure 6.8: Comparison of energy evolutions if the strategy of returning in case the two-sided energy inequality is violated is implemented and if it is not. On the top the evolution with returning is shown, on the bottom without.

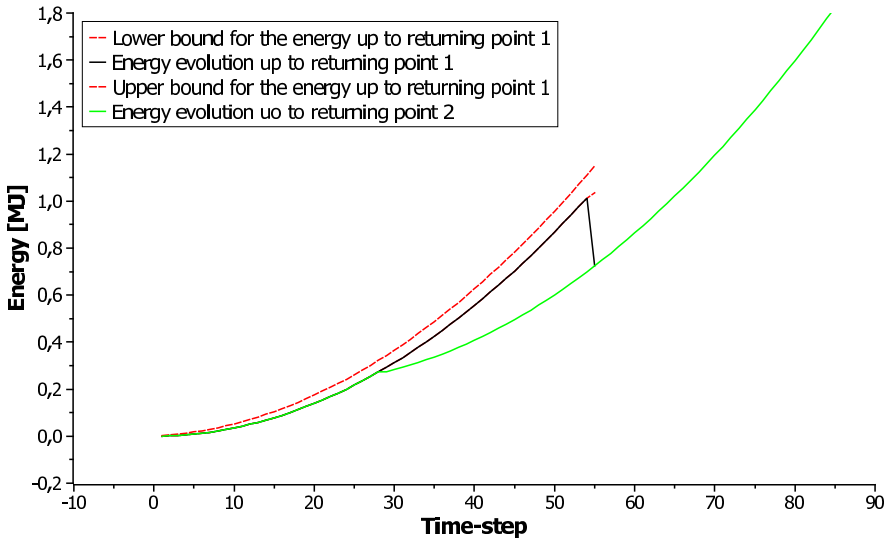

(a) Returning point 1

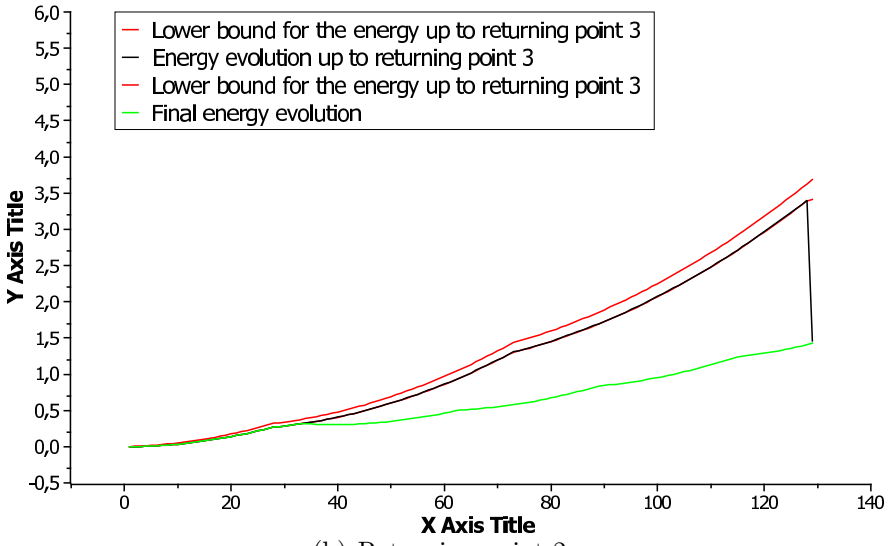

(b) Returning point 2

Figure 6.9: Detail of energy evolution. On the top the evolution up to returning point 1, on the bottom up to returning point 3 are shown. To see that lower bound is indeed violated the bounds for the energy are also depicted.

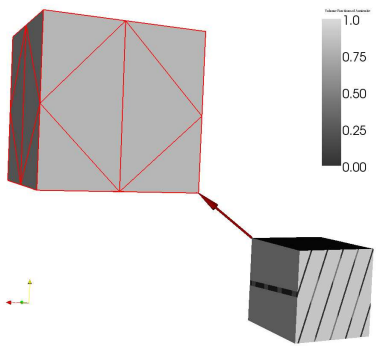

(a) Time-step 76, verifying the two-sided energy inequality

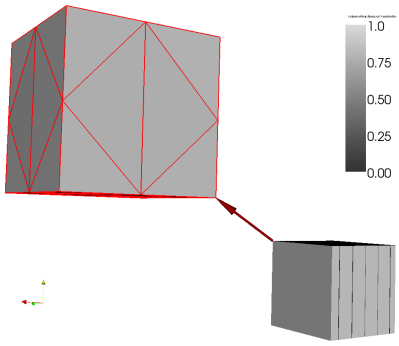

(b) Time-step 76, not verifying the two-sided energy inequality

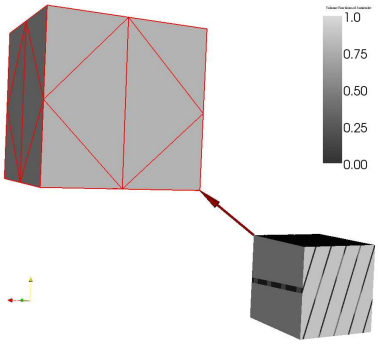

(c) Time-step 83, verifying the two-sided energy inequality

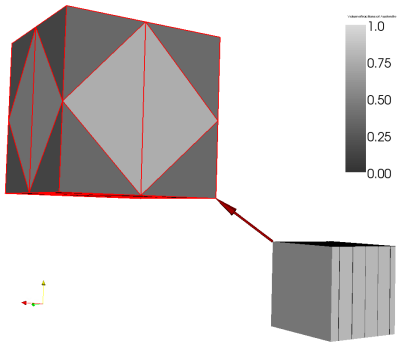

(d) Time-step 83, not verifying the two-sided energy inequality

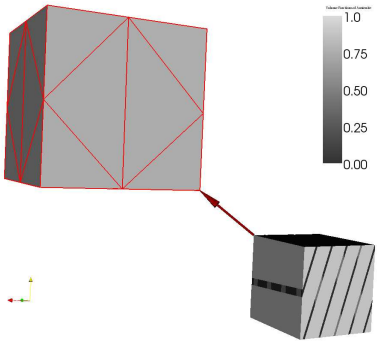

(e) Time-step 95, verifying the two-sided energy inequality

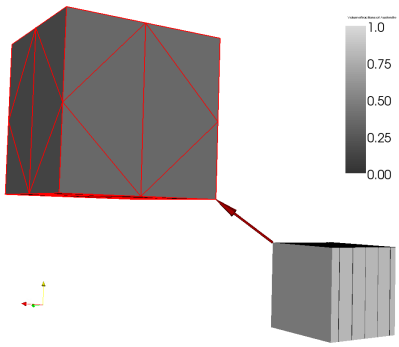

(f) Time-step 95, not verifying the two-sided energy inequality

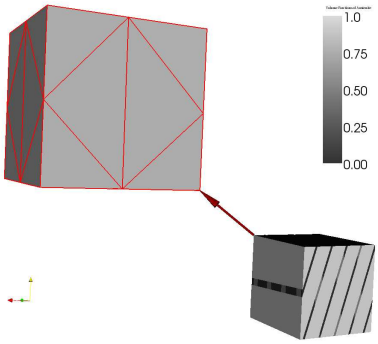

(g) Time-step 97, verifying the two-sided energy inequality

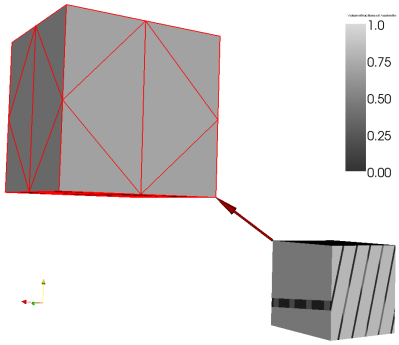

(h) Time-step 97, not verifying the two-sided energy inequality

Figure 6.10: Comparison of evolution of the volume fraction of austenite as well as of microstructure. On the left the two-sided energy has been verified and the strategy of returning implemented, on the right not.

Conclusion

Throughout this thesis we have been concerned with modelling the behaviour of a shape memory alloy specimen subject to Dirichlet loads. From the point of view of physics we have described a continuum mechanics approach to modelling this behaviour and we have seen that in such an approach the most important effects observed in shape memory alloys can be explained.

Physical considerations also led us to suppose that a quasi-static process has to fulfil the global stability condition and the energy equality to be a physically admissible process. We then took these two to the requirements to define what an energetic solution of the quasi-static evolution has to satisfy and proved the existence of energetic solutions for time-dependent Dirichlet boundary conditions. This is a small extension to the existing theory as so far only zero Dirichlet boundary condition have been supposed for simplicity.

Once the existence of energetic solutions has been proved we may turn our attention to implementation. In this work a simulation program has been developed, inspired by preceding algorithms as e.g. [60]. Extending past works the code has been written in C++ and object-oriented which is a modern form of programming and very useful in the area of question. Moreover the verification of the two-sided energy inequality as well as calculation of stresses due to Dirichlet boundary condition has been added. Especially the verification of the double-sided energy inequality brought good results and should be implemented in any future work.

The code has been tested on simulations concerning $NiTi$ and its R-phase in the hope that simulations could be compared with experiments. Unfortunately no bulk specimen of mono-crystalline specimen has been available so far, however $NiTi$ wires that are poly-crystalline but with all grains oriented the same way ar ate disposal. Yet due to lack of time, experiments on these wires could not be implemented.

Nevertheless loading by Dirichlet boundary conditions has opened new possibilities as e.g. the observation of sinking stress due to turning of microstructure. This can be also observed in experiments (cf. [50] for $CuAlNi$).

There are however a lot of open problems for the future. Maybe the main one is the absence of temperature in the model in the sense that the situations is isotermic. This is an important drawback as e.g. the shape-memory effect can not be handled theoretically nor numerically. It shall be important to add temperature dependence.

From the viewpoint of simulations many interesting problems as the connection of austenite to parallelogram structure have been observed [62] and could lead to interesting simulation results. Unfortunately, due to lack of time, they are not presented in this thesis, but remain open for future work.

Bibliography

[1] Arndt M., Griebel M., Novák V., Roubíček T., Šittner P.: *Martensitic transformation in NiMnGa single crystals: numerical simulations and experiments*, Int. J. Plasticity, **22** (2006), pp. 1943-1961.

[2] Aubry S., Fago M., Ortiz M.: *A constrained sequential-lamination algorithm for the simulation of sub-grid microstructure in martensitic materials*, Computer Methods in Applied Mechanics and Engineering, **192** (2003), pp. 823-2843(21).

[3] Ball J.M.: A version of the fundamental theorem for Young measures. In: *PDEs and Continuum Models of Phase Transitions*, Lecture Notes in Physics **344**, Springer, Berlin, (1989), pp. 207-215.

[4] Ball, J.M.:*Convexity conditions and existence theorems in nonlinear elasticity.*, Arch. Rational Mech. Anal.,**63** (1977), pp. 337–403.

[5] Ball J.M., James R.D.: *Fine phase mixtures as minimizers of energy*, Arch. Rat. Mech. Anal. **100** (1987), pp. 13-52.

[6] Ball J.M., James R.D.: *Proposed experimental tests of a theory of fine microstructure, and the two-well problem*, Phil. Trans. Roy. Soc. London A **338** (1992), pp. 389-450.

[7] Ball J.M, Murat, F.: $W^{1,p}$*-quasiconvexity and variational problems for multiple integrals*, J. Funct. Anal. **58** (1984), pp. 225-253.

[8] Benešová B.: *Mathematical modelling of shape-memory materials* (In Czech), Bachelor's thesis, Charles University in Prague, 2006.

[9] Bhattacharya K.: *Microstructure of Martensite: Why it forms and how it gives rise to the shape-memory effect*, Oxford University Press, New York, 2003.

[10] Brill T.M., Mittelbach S., Assmus W., Müllner M., Lüthi B.: *Elastic properties of NiTi* , J. Phys.: Condens. Matter **3** (1991), pp. 9621-9627.

[11] Brooks J. K., Chacon R. V.: *Continuity and compactness of measures*, Adv. in Math. **37** (1980), pp. 16-26.

[12] Byrd R. H. , Lu P., Nocedal J.: *A Limited Memory Algorithm for Bound Constrained Optimization*, SIAM Journal on Scientific and Statistical Computing, **16** (1995), pp. 1190-1208.

[13] Callen H.B.: *Thermodynamics and an introduction to thermostatistics*, Wiley, New York, 1985.

[14] Dacorogna, B.: *Direct Methods in the Calculus of Variations*, Springer, Berlin, (1989).

[15] Dal Maso G., Francfort G.A., Toader R.: *Quasistatic crack growth in nonlinear elasticity*, Arch. Ration. Mech. Anal. **176** (2005), pp. 165-225.

[16] Fonseca I., Müller S., Pedregal, P.: *Analysis of concentration and oscillation effects generated by gradients*, SIAM J. Math. Anal., **29** (1998), pp. 736-756.

[17] Francfort G., Mielke A.: *Existence results for a class of rate-independent material models with nonconvex elastic energies*, J. reine angew. Math., **595** (2006), pp. 55-91.

[18] Griewank A., Juedes D., Mitev H., Utke J., Vogel O., Walther A.: *ADOL-C: A Package for the Automatic Differentiation of Algorithms Written in C/C++*, ACM TOMS, **22** (1996), pp. 131-167, Algor. 755

[19] A. Griewank, Utke J., Walther A.: *Evaluating higher derivative tensors by forward propagation of univariate Taylor series*, Mathematics of Computation, **69** (2000), pp. 1117 - 1130.

[20] Gurtin,M.E.: *An Introduction to Continuum Mechanics*, Academic Press, San Diego, 1982.

[21] Hahn, H.: *Über Annäherung an Lebesgue'sche Integrale durch Riemann'sche Summen*, Sitzungber. Math. Phys. Kl. K. Akad. Wiss. Wien **123** (1914), pp 713–743.

[22] Hane K.F., Shield T.W.: *Microstructure in the cubic to trigonal transition*, Elsevier: Materials Science and Engineering A **291** (2000), pp. 147–159.

[23] Haslinger J.: *Metoda konečných prvků pro řešení eliptických rovnic a nerovnic Státní pedagogické nakladatelství* (In Czech), Praha, 1980.

[24] Horst R., Pardalos P.M. (eds.): *Handbook of Global Optimization*, Kluwer, Dordrecht. 1995.

[25] Huo Y., Müller I., Seelecke S. *Quasiplasticity and pseudoelasticity in shape memory alloys* In: Phase Transitions and Hysteresis, Lecture Notes in Mathematics **1584/1994**, Springer, Berlin, 1994, pp. 87-146.

[26] Khalil-Allafi J., Schmahl W.W., Reinecke T.: *Order parameter evolution and Landau free energy coefficients for the B2 -R-phase transition in a NiTi shape memory alloy*, Smart Mater.Struct. **14** (2005), pp. 192–196.

[27] Kinderlehrer D., Pedregal P.: *Characterizations of Young measures generated by gradients*, Archive Rar. Mech. Analysis **115** (1991), pp. 329-365.

[28] Kinderlehrer D., Pedregal P.: Weak convergence of integrands and the Young measure represantation, SIAM J.Math. Analysis **4** (1992,) pp. 1-19.

[29] Kinderlehrer D., Pedregal P.: *Gradient Young measure generated by sequences in Sobolev spaces*, J. of Geom. Anal **4** (1994), pp. 59-90.

[30] Kohn R., Strang G.: *Optimal Design and relaxation of variational problems II*, Comm. Pure Appl. Math. **39** (1986), pp. 189-182.

[31] Kristensen J.: *On the non-locality of quasiconvexity*, Ann. Inst. Henri Poincaré, Anal. Non Linéaire **16** (1999), pp. 1-13.

[32] Kristensen J.: *Finite functionals and Young measures generated by gradients of Sobolev functions*, Mat-report 1994-34, Mathematical Institute, Technical University of Denmark, 1994.

[33] Kružík M.: *Numerical Approach to Double Well Problems*, SIAM Journal on Numerical Analysis, **35** (1998), pp. 1833-1849.

[34] Kružík M., Mielke A., Roubíček T.: *Modelling of microstructure and its evolution in shape-memory-alloy single-crystals, in particular in CuAlNi*, Meccanica **40** (2005), pp. 389-418.

[35] Kružík M., Roubíček T.: *Mesoscopic Model of Microstructure Evolution in Shape Memory Alloys with Applications to NiMnGa*, IMA Preprint Series, November 2004.

[36] Landa M., Chlada M., Prevorovský Z., Novák V., Šittner P.: *Nondestructive evaluation of phase transformations in Cu based shape memory alloys by ultrasonics techniques.* Internat. Conference Acoustic Emission'99, June 15-17, 1999, Brno, CZ, pp. 123-130.

[37] Levitas V.I, *The postulate of realizibility: formulation and applications to postbifurcation behavior and phase transitions in elastoplastic meterials*, Int. J. Eng. Sci. **33** (1995),pp. 921-971.

[38] Mainik A., Mielke A.: *Existence results for energetic models for rate-independent systems*, Calc. Var. PDEs, **22** (2005), pp. 73-99.

[39] Maršík F.: *Termodynamika kontinua*, Academia, Praha, 1999.

[40] MatWeb: Material property data,
`http://www.matweb.com/search/SpecificMaterial.asp?bassnum=MTiNi0`

[41] Mielke A., Roubíček T.: *A rate-independent model for inelastic behavior of shape-memory alloys*, Multiscale Modeling and Simulation **1** (2003), pp. 571-597.

[42] Mielke A., Roubíček T., Zeman J.: *Complete damage in elastic and viscoelastic media and its energetics.* (Preprint No.1285, WIAS, Berlin, 2007), Computer Methods Appl. Mech. Engr., submitted.

[43] Mielke A., Theil, F.: *On rate-independent hysteresis models.* Nonl. diff. Eqns. Appl, **11** (2004), pp. 151-189.

[44] Mielke A., Theil F.: *A mathematical model for rate-independent phase transformations with hysteresis.* In H.-D. Alber, R. Balean, and R. Farwig, editors, Proceedings of the Workshop on Models of Continuum Mechanics in Analysis and Engineering, pages 117-129. Shaker-Verlag, 1999.

[45] Mielke A.,Theil F., and Levitas V.I.: *A variational formulation of rate-independent phase transformations using an extremum principle*, Arch. Rational Mech. Anal., **162** (2002), pp. 137-177.

[46] Miyazakif S., Wayman C. M.: *The R-Phase Transition and associeted Shape Memory Mechanism in Ti-Ni Single Crystals*, Acta Metall. **36** (1988), pp. 181-192.

[47] Morrey, Jr., C.B.: *Quasi-convexity and the lower semicontinuity of multiple integrals*, Pacific J. Math. **2** (1952), pp. 25-53.

[48] Morrey, Jr., C.B.: *Multiple Integrals in the Calculus of Variations*, Springer, Berlin, 1966.

[49] Müller S.: *Variational models for microstructure and phase transitions*, MPI Lecture notes **2**, Lepzig (1998).

[50] Novák V., Šittner P., Ignacová S., Černoch T.: *Transformation behavior of prism shaped shape memory alloy single crystals*, Materials Science and Engineering: A **438-440** (2006), pp. 755-762.

[51] Ogden, R. W.: *Non-linear elastic deformations*, Dover Publications, Mineola, 1997.

[52] Otsuka K., Ren X.: *Physical metallurgy of Ti–Ni-based shape memory alloys*, Progress in Materials Science **50** (2005), pp. 511–678.

[53] Pitteri M., Zanzotto G.: *Continuum Models for Phase transition and Twinning in Crystals*, Chapman & Hall/CRC, Boca Raton, 2003.

[54] Pedregal P: *Parametrized measures and variational principles*, Birkhäuser, Basel, Boston, Berlin, 1997.

[55] Rajagopal K.R., Roubíček T.: *On the effect of dissipation in shape-memory alloys.* Nonlinear Anal., Real World Applications, **4** (2003), pp. 581-597

[56] Ren X.,Miura N., Zhang J., Otsuka K., Tanaka K., Koiwa M., Suzuki T., Chumlyakov Yu.I., Asai M.: *A comparative study of elastic constants of Ti–Ni-based alloys prior to martensitic transformation* , Materials Science and Engineering A **312** (2001),pp. 196–206

[57] Roubíček T.: *Models of microstructure evolution in shape memory alloys.* In: Nonlinear Homogenization and its Appl. to Composites, Polycrystals and Smart Materials. (Eds. P.Ponte Castaneda, J.J.Telega, B.Gambin), NATO Sci. Series **II/170**, Kluwer, Dordrecht, 2004, pp. 269-304

[58] Roubíček T.: *Dissipative evolution of microstructure in shape memory alloys.* In: Lectures on Applied Mathematics (H.-J.Bungartz, R.H.W.Hoppe, C.Zenger, eds.) Springer, Berlin, 2000, pp. 45-63

[59] Roubíček T.: *Relaxation in Optimization Theory and Variational Calculus*, Walter de Gruyter, Berlin, New York, 1997.

[60] Roubíček T., Kružík M., Koutný J.: *A mesoscopical model of shape-memory alloys*, Proc. Estonian Acad. Sci. Phys. Math. **56** (2007),pp. 146-154.

[61] Schonbek M.E.: *Convergence of solutions to nonlinear dispersive equations*, Comm. Partial Differential Equations, **7** (1982), pp. 959-1000.

[62] Seiner, H., Sedlák, P., Landa, M: *Shape recovery mechanism observed in single crystals of Cu-Al-Ni shape memory alloy*, Phase Transitions, **81:6** (2008), pp. 537-551.

[63] Šittner P., Lugovyy D., Neov D., Landa M., Lukáš P., Novák V.: *On the R-phase transformation related phenomena in NiTi polycrystals subjected to thermomechanical loads*, J. Phys. IV France, **112** (2003), pp. 709-712.

[64] Šverák V.: *Rank-1 convexity does not imply quasiconvexity* Proc. R.Soc.Edinb., **120A** (1993), pp. 185-189

[65] Tychonoff A.: *Über die topologische Erweiterung von Räumen*, Math. Annalen **102** (1930), pp. 544-561.

[66] Uchil J., Mahesh K.K., Ganesh Kumara K.: *Electrical resistivity and strain recovery studies on the effect of thermal cycling under constant stress on R-phase in NiTi shape memory alloy* , Physica B **324** (2002), pp. 419–428.

[67] Young L.C.: *Generalized curves and the existence of an attained absolute minimum in the calculus of variations*, C.R. Soc. Sci. Lettres de Varsovie, Cl. III , **30** (1937), pp. 212–234

[68] Wu X.D., Fan Y.Z., Wu J.S.: *A study on the variations of the electrical resistance for NiTi shape memory alloy wires during the thermo-mechanical loading* , Elsevier: Materials and Design **21** (2000), pp. 511-515.

[69] Zhu C., Byrd R.H., Nocedal J.: *L-BFGS-B: Algorithm 778: L-BFGS-B, FORTRAN routines for large scale bound constrained optimization*, ACM Transactions on Mathematical Software, **23** (1997), pp. 550 - 560.